

NONLINEAR VIBRATION ISOLATION OF INERTIAL MEASUREMENT
UNIT

A THESIS SUBMITTED TO
THE GRADUATE SCHOOL OF NATURAL AND APPLIED SCIENCES
OF
MIDDLE EAST TECHNICAL UNIVERSITY

BY

ATA DÖNMEZ

IN PARTIAL FULFILLMENT OF THE REQUIREMENTS
FOR
THE DEGREE OF MASTER OF SCIENCE
IN
MECHANICAL ENGINEERING

JULY 2018

Approval of thesis:

**NONLINEAR VIBRATION ISOLATION OF INERTIAL MEASUREMENT
UNIT**

submitted by **Ata DÖNMEZ** in partial fulfillment of the requirements for the degree of **Master of Science in Mechanical Engineering Department, Middle East Technical University** by,

Prof. Dr. Halil Kalıpçılar
Dean, Graduate School of **Natural and Applied Sciences**

Prof. Dr. M.A. Sahir Arıkan
Head of Department, **Mechanical Engineering**

Assoc.Prof. Dr. Ender Ciğeroğlu
Supervisor, **Mechanical Engineering Dept., METU**

Assist.Prof. Dr. Gökhan O. Özgen
Co-Supervisor, **Mechanical Engineering Dept., METU**

Examining Committee Members:

Assoc. Prof. Dr. Yiğit Yazıcıoğlu
Mechanical Engineering Dept., METU

Assoc. Prof. Dr. Ender Ciğeroğlu
Mechanical Engineering Dept., METU

Assist. Prof. Dr. Gökhan O. Özgen
Mechanical Engineering Dept., METU

Assist. Prof. Dr. Bülent Özer
Mechanical Engineering Dept., METU

Assist. Prof. Dr. Selçuk Himmetoğlu
Mechanical Engineering Dept., Hacettepe University

Date: 12/07/2018

I hereby declare that all information in this document has been obtained and presented in accordance with academic rules and ethical conduct. I also declare that, as required by these rules and conduct, I have fully cited and referenced all material and results that are not original to this work.

Name, Last name:

Signature :

ABSTRACT

NONLINEAR VIBRATION ISOLATION OF INERTIAL MEASUREMENT UNIT

Dönmez, Ata

M. Sc., Department of Mechanical Engineering

Supervisor: Assoc. Prof. Dr. Ender Ciğeroğlu

Co-Supervisor: Assist. Prof. Dr. Gökhan Osman Özgen

July 2018, 155 pages

In engineering systems, dynamic parameters of systems such as acceleration, velocity, etc. are measured instantaneously to provide feedback for control systems. Since measurement equipment is sensitive to vibratory environment, performance of them is directly related to how effectively vibration is isolated. Linear vibration isolation systems have limitations due to static deflections and damping characteristic. Therefore, nonlinear elements can be used to improve isolation performance.

In this thesis, firstly the vibration isolation of the engineering systems is considered. Then the problem is narrowed to inertial measurement units (IMUs) and the specific vibration isolation issues of the IMUs are studied. Mathematical model of linear six degrees of freedom vibration isolation system containing a mechanical structure mounted on elastomeric elements is achieved. For a given isolator position and mass properties of the system, system matrices are obtained. Modal properties of the isolated system, response to harmonic, random excitations and static deflections under static loadings are considered as critical parameters to evaluate effectiveness of the isolation.

In shaker table, sine sweep and random vibration experiments are performed on an IMU suspended on commercial rubber isolators. Experiment and analysis software results are compared.

In the next step, nonlinear elements such as high-static-low-dynamic-stiffness and special version of it, quasi-zero-stiffness, geometrically nonlinear damping and dry friction are implemented to a single degree of freedom system. The nonlinear differential equations of motion of the isolation system are converted into a set of nonlinear algebraic equations by using harmonic balance method, which are solved by using Newton's method with arc-length continuation. Several case studies are performed and the effect of nonlinearities on the isolation performance is studied. Validation of the solution method is performed by both time simulations and experiments. Multi-Harmonic displacement profiles are applied to quad-lap elastomer isolator by means of servo position control. Dynamic properties of the rubber isolator under multi-harmonic displacement profile is investigated. Then, isolation performance is studied analytically for the rubber isolator whose dynamic properties are obtained experimentally.

Keywords: Nonlinear Vibration Isolation, Inertial Measurement Unit, Quasi-Zero-Stiffness, Dry Friction, Nonlinear Damping

ÖZ

ATALETSEL ÖLÇÜM BİRİMLERİNİN DOĞRUSAL OLMAYAN YÖNTEMLER KULLANILARAK TİTREŞİM İZOLASYONU

Dönmez, Ata

Yüksek Lisans., Makina Mühendisliği Bölümü

Tez Yöneticisi: Doç. Dr. Ender Cigeroğlu

Ortak Tez Yöneticisi: Dr. Öğr. Ü. Gökhan Osman Özgen

Temmuz 2018, 155 Sayfa

Mühendislik sistemlerinde, ivme, hız gibi dinamik parametreler kontrol algoritmalarına geri besleme sağlamak amacıyla anlık olarak ölçülür. Ölçüm cihazları titreşim girdilerine karşı hassas olduğundan, ölçüm sonuçları mekanik titreşimlerden etkilenmektedir. Bu nedenle, bu tip ölçüm cihazlarının performansı mekanik titreşimlerin etkin olduğu ortamdan ne kadar izole edildiği ile doğrudan ilişkilidir. Doğrusal izolasyon sistemlerinin statik yer değiştirme, sönümleme karakteristiği vb. sorunlardan performansları kısıtlıdır. Doğrusal olmayan elemanlar kullanılarak daha efektif tasarımlar elde edilebilmektedir.

Bu tez kapsamında, 6 serbestlik dereceli doğrusal sistemin matematiksel modeli oluşturulmuştur. Titreşim takozu konumları ve kütle özellikleri verilen bir izolasyon sisteminin, sistem matrisleri elde edilmiştir. Sistemin modal özellikleri, harmonik ve rastgele titreşim girdilerine cevabı, statik yükler altındaki yer değiştirme miktarları kullanılarak izolasyon sistemi değerlendirilmiştir. Piyasadan elde edilen titreşim takozları ile izole edilmiş bir ataletsel ölçüm birimi ile sarsıcı üzerinde sinüs tarama, rastgele titreşim testleri yapılmıştır. Test ve analiz program sonuçları kıyaslanmıştır.

Bir sonraki adımda ise, doğrusal olmayan direngenlik, doğrusal olmayan sönümleme ve kuru sürtünme gibi doğrusal olmayan elemanlar, tek serbestlik dereceli izolasyon sistemine entegre edilmiştir. Doğrusal olmayan diferansiyel hareket denklemleri harmonik dengeleme yöntemi kullanılarak doğrusal olmayan cebirsel denklemlere dönüştürülmüştür. Bu cebirsel denklemler Newton Metodu kullanılarak çözülmüştür. Eklenen doğrusal olmayan elemanların performansı doğrusal sistemle kıyaslanmıştır. Çözüm metodunun doğrulaması zaman simülasyonları ve deneysel çalışmalar ile gerçekleştirilmiştir. Doğrusal olmayan deplasman profilleri, servo pozisyon kontrollü deney düzeneği kullanılarak “quad-lap” kauçuk izolatöre uygulanmıştır. Kauçuk malzemenin doğrusal olmayan dinamik karakteristiği bu testler ile elde edilmiştir. Doğrusal olmayan dinamik karakteristiğe sahip kauçuk izolatörün izolasyon performansı incelenmiştir.

Anahtar kelimeler: Doğrusal Olmayan Titreşim İzolasyonu, Ataletsel Ölçer Birimleri, Kuru Sürtünme, Doğrusal Olmayan Sönümleme

Dedicated to my lovely wife, Dila Dönmez and my family

ACKNOWLEDGMENTS

First, I am grateful to my supervisor Assoc. Prof. Dr. Ender Ciğerođlu and my co-advisor Assist. Prof. Dr. Gökhan Osman Özgen for their guidance, patience, encouragement and helps on all parts of my study. Their positive perspective motivated me every time. I learned a lot and improved myself thanks to their support during this study.

I would like to thank Dr. Burcu Dönmez, Manager of the Mechatronic Design Department in Roketsan Missile Ind. For her tolerance trust and technical guidance. I would also like to state my sincere thanks to my colleagues A. Furkan Kanburođlu and Batuhan Kaygusuz for their great friendship and contributions. I always felt their support and positive energy.

I owe to my friends, Çetin Baykara, Yunus Çetinkaya and Çađlar Pınar for all things we have shared and their moral support that motivates me during this thesis study. I thank them for believing and encouraging me every time.

Finally, I would like to express my deepest gratitude to my wife, Dila Dönmez and my parents Emine and Mehmet Dönmez, my sisters, their husbands, my lovely nephews and nieces. I always feel their support and love throughout my life. I thank them for believing and encouraging me every time.

This study is supported by Turkish Undersecretariat for Defense Industries and Roketsan A.S., Grant No: 2016-03-02-32-00-18, SAYP Project.

TABLE OF CONTENTS

ABSTRACT	v
ÖZ	vii
ACKNOWLEDGMENTS.....	x
TABLE OF CONTENTS	xi
LIST OF TABLES	xiv
LIST OF FIGURES.....	xv
CHAPTERS	
1 BACKGROUND AND LITERATURE SURVEY	1
1.1 Introduction	1
1.2 Motivation	2
1.3 Thesis Layout	3
1.4 Literature Survey	4
1.4.1 Vibration Isolation Techniques	5
1.4.2 Inertial Measurement Unit.....	7
1.4.3 Classification of the Inertial Measurement Units.....	9
1.4.4 Isolator Models	13
1.4.5 System Models and Design Criteria.....	16
1.4.6 Nonlinear Isolators	18
2 LINEAR ISOLATION SYSTEMS.....	29
2.1 Mathematical Model.....	29
2.1.1 Isolator Model	29
2.1.2 Vibration Isolation System.....	31
2.1.3 Dynamics Analyses	35
2.2 Developed Vibration Isolation Analysis Software-VIASoft.....	39
2.2.1 Creating Model.....	40
2.2.2 Analysis	41
2.2.3 Results and Reporting.....	46

2.3	Verification of Developed Analysis Software	48
2.3.1	Finite Element Method	49
2.3.2	Experimental Studies	51
2.3.3	Harmonic Response Analysis Verification.....	54
2.3.4	Random Vibration Analysis Verification	60
3	NONLINEAR ISOLATION SYSTEMS	65
3.1	High Static Low Dynamic Stiffness Isolators	65
3.1.1	Stiffness Model of HSLDS isolator	66
3.1.2	Response to Base Excitation.....	70
3.1.3	Stability of steady state solutions	74
3.1.4	Validation of Taylor Series Expansion.....	75
3.1.5	Effect of QZS Isolation System.....	78
3.1.6	Load and Stiffness Deviation	79
3.2	Geometrically Nonlinear Viscous Damping.....	82
3.2.1	Geometrically Nonlinear Damping Model	82
3.2.2	Response to Base Excitation.....	84
3.2.3	Validation of Single Harmonic Solution Method.....	86
3.2.4	Conclusion	87
3.3	Dry Friction-Isolator 1	88
3.3.1	Dry Friction Model	88
3.3.2	Response to Base Excitation.....	92
3.3.3	Validation of the Solution Method	97
3.3.4	Comparison of the Proposed Isolator with QZS vibration isolation system	99
3.3.5	Effect of Slip Force Amplitude.....	100
3.3.6	Performance Comparison of Linear Viscous Damper and Dry Friction Damper.....	101
3.3.7	Conclusion	103
3.4	Dry Friction-Isolator 2	104
3.4.1	Dynamic analysis of Proposed Isolator	106
3.4.2	Response to Base Excitation.....	107

3.4.3	Isolation Performance.....	111
3.4.4	Conclusion.....	116
4	EXPERIMENTAL INVESTIGATION OF DYNAMICS OF THE GEOMETRICALLY NONLINEAR SHEAR ELASTOMER ISOLATOR....	117
4.1	Dynamic Characterization of Rubber Isolator.....	117
4.2	Geometrically and Physically Nonlinear Rubber Isolator.....	117
4.3	Mathematical Development.....	119
4.3.1	Stiffness Model.....	119
4.3.2	Damping Model.....	124
4.3.3	Base Excitation and Approximate Analytical Solution.....	125
4.4	Experimental Procedure	126
4.5	Dynamic Characterization of Elastomer	131
4.6	Isolation Performance.....	134
4.7	Performance Comparison of Proposed Isolator with QZS Isolator.	136
4.8	Conclusion.....	138
5	DISCUSSION, CONCLUSION AND FUTURE WORK	139
5.1	Discussion on the Performance of Proposed Nonlinear Isolators ...	139
5.2	Conclusion.....	141
5.3	Future Work.....	144
	REFERENCES.....	147

LIST OF TABLES

TABLES

Table 2-1 Inertial Properties.....	49
Table 2-2 Isolator Stiffness and Loss Factors	50
Table 2-3 Isolator Positions.....	50
Table 2-4 Undamped Natural Frequencies.....	51
Table 2-5 Experiment Equipment	53
Table 2-6 Experiment Matrix	53
Table 3-1 Parameter Set Used in Analyses	75
Table 3-2 Error Values of 3th Order Taylor Series Expansion.....	78
Table 3-3 Error Values of 5th Order Taylor Series Expansion.....	78
Table 3-4 Error Values of 7th Order Taylor Series Expansion.....	78
Table 3-5 Parameter Set	99
Table 3-6 Parameter Set	111
Table 4-1 Parameter Set	134
Table 4-2 Peak Absolute Transmissibility Comparison.....	137
Table 4-3 Normalized Resonance Frequency Comparison.....	137

LIST OF FIGURES

FIGURES

Figure 1-1 SDOF Vibration Isolation System.....	5
Figure 1-2 Transmissibility of SDOF Vibratory System	6
Figure 1-3 Active Vibration Isolation	7
Figure 1-4 IMU Measurement Axes	8
Figure 1-5 Classification of the Gyroscopes	10
Figure 1-6 Ring Laser Gyroscopes [25].....	11
Figure 1-7 Fiber Optic Gyroscopes [25]	12
Figure 1-8 MEMS based Gyroscope.....	12
Figure 1-9 Cost/Performance Chart for IMUs [26].....	13
Figure 1-10 (a) Voigt Model (b) Maxwell Model.....	14
Figure 1-11 Temperature and frequency dependency [9]	15
Figure 1-12 Stress Strain Curve of the Elastomer Tensile Specimen [34]	16
Figure 1-13 Mathematical Model.....	16
Figure 1-14 Jet Aircraft Vibration Exposure [36].....	18
Figure 1-15 Effect of Viscous Damping on Frequency Response Function.....	20
Figure 1-16 Nonlinear Isolator Model [40].....	21
Figure 1-17 Force Displacement Curve [40]	21
Figure 1-18 Euler beam formed negative stiffness corrector [48]	22
Figure 1-19 (a) Negative Magnetic Spring (b) Anti-spring system	24
Figure 1-20 Cubic Damping Mechanism.....	26
Figure 1-21 Dry Friction Model [77].....	27
Figure 1-22 Eddy Current Damping Mechanism [80]	27
Figure 1-23 Nonlinear Isolators	28
Figure 2-1 Isolator Model	30
Figure 2-2 Global Reference Frame [19]	30
Figure 2-3 Simulink Model for Time Simulation	39

Figure 2-4 Vibration Isolation Analysis Program VIASoft	40
Figure 2-5 Create Model	41
Figure 2-6 Modal Analysis.....	42
Figure 2-7 Harmonic Analysis	43
Figure 2-8 Static Displacement Analysis	44
Figure 2-9 Random Vibration Analysis	45
Figure 2-10 Shock Analysis	46
Figure 2-11 Results and Reports -1	47
Figure 2-12 Results and Reports-2.....	47
Figure 2-13 Analysis Report Cover Page.....	48
Figure 2-14 Rigid Body with Isolators.....	49
Figure 2-15 LORD Rubber Sandwich Isolator.....	51
Figure 2-16 Representation of Isolator Position in the Software	52
Figure 2-17 Experiment Schematic.....	52
Figure 2-18 Acceleration Time Signal	54
Figure 2-19 X Axis Response – Excitation in Y Axis	55
Figure 2-20 Y Axis Response – Excitation in Y Axis	56
Figure 2-21 Z Axis Response – Excitation in Y Axis.....	56
Figure 2-22 X Axis Response – Excitation in Z Axis.....	57
Figure 2-23 Y Axis Response – Excitation in Z Axis.....	57
Figure 2-24 Z Axis Response – Excitation in Z Axis	58
Figure 2-25 X Axis Response – Excitation in X Axis	58
Figure 2-26 Y Axis Response – Excitation in X Axis	59
Figure 2-27 Z Axis Response – Excitation in X Axis.....	59
Figure 2-28 PSD Acceleration X Axis - Excitation in X Axis.....	60
Figure 2-29 PSD Acceleration Y Axis - Excitation in X Axis.....	61
Figure 2-30 PSD Acceleration Z Axis - Excitation in X Axis	61
Figure 2-31 PSD Acceleration X Axis - Excitation in Y Axis.....	62
Figure 2-32 PSD Acceleration Y Axis - Excitation in Y Axis.....	62
Figure 2-33 PSD Acceleration Z Axis - Excitation in Y Axis	63
Figure 2-34 PSD Acceleration X Axis - Excitation in Z Axis	63

Figure 2-35 PSD Acceleration Y Axis - Excitation in Z Axis	64
Figure 2-36 PSD Acceleration Z Axis - Excitation in Z Axis	64
Figure 3-1 Nonlinear isolator with negative stiffness mechanism (a) initial unloaded state (b) equilibrium point	66
Figure 3-2 Free Body Diagram of the Mass.....	67
Figure 3-3 Effect of δ on nonlinear stiffness	68
Figure 3-4 Effect of γ on nonlinear stiffness	69
Figure 3-5 Taylor Series Expansion of QZS Isolator.....	70
Figure 3-6 Base Excitation Model	71
Figure 3-7 Comparison of Taylor Series Expansion and numerical integration ‘- - ‘:unstable solutions ‘-.-‘ Taylor Series ‘-‘ Numerical Integration, 3th order approximation	76
Figure 3-8 Comparison of Taylor Series Expansion and numerical integration ‘- - ‘:unstable solutions ‘-.-‘ Taylor Series ‘-‘ Numerical Integration, 5 th order approximation	76
Figure 3-9 Comparison of Taylor Series Expansion and numerical integration ‘- - ‘:unstable solutions ‘-.-‘ Taylor Series ‘-‘ Numerical Integration, 7 th order approximation	77
Figure 3-10 Effect of QZS Mechanism and nonlinear damping $\delta = 2, \gamma = 1, \xi v = 0.015$	79
Figure 3-11 Effect of Load Deviations- Absolute Transmissibility $\delta = 2, \gamma = 1, \xi v = 0.015, Z/a = 0.035$	80
Figure 3-12 Effect of Load Deviations Bias Term in the response $\delta = 2, \gamma = 1, \xi v = 0.015, Z/a = 0.030$	81
Figure 3-13 Effect of stiffness deviations $\delta = 2, \xi v = 0.02, Z/a = 0.035$	81
Figure 3-14 Nonlinear isolator with negative stiffness mechanism and geometrically nonlinear damping (a) initial unloaded state (b) equilibrium point	83
Figure 3-15 Non-dimensional damping force vs velocity for different sinusoidal excitation levels.....	84
Figure 3-16 Non-dimensional damping force vs position for sinusoidal excitation	84
Figure 3-17 Effect of nonlinear damping $\delta = 2, \gamma = 1, \xi v = 0.015, Z/a = 0.035$	86

Figure 3-18 Comparison of Time Domain and HBM $Za = 0.035$ $\delta = 2$, $\gamma = 1$, $\xi v = 0.015$, $\xi h = 0.05$	87
Figure 3-19 QZS Isolation system with dry friction (a) schematic drawing (b) equivalent dry friction model	89
Figure 3-20 Hysteresis loop for the proposed isolator	90
Figure 3-21 Base excitation model of the nonlinear isolator	92
Figure 3-22 Time Simulation Results, ‘- -’:unstable solutions	98
Figure 3-23 Jump down phenomena	99
Figure 3-24 Effect of QZS Mechanism and dry friction $\delta = 2$, $\gamma = 1$, $\xi v = 0.015$, ‘- -’:unstable solutions	100
Figure 3-25 Effect of slip force $\delta = 2$, $\gamma = 1$, $\xi v = 0.015$, $Za = 0.045$ ‘- -’:unstable solutions	101
Figure 3-26 Comparison with dry friction and linear viscous damping $\delta = 2$, $\gamma =$ 1 , $Za = 0.045$, ‘- -’:unstable solutions	102
Figure 3-27 Effect of viscous damping coefficient, $Za = 0.035$	103
Figure 3-28 Effect of viscous damping coefficient, $Za = 0.035$	103
Figure 3-29 HSLDS and Dry Friction Vibration Isolation System	105
Figure 3-30 Dry Friction Damper (a) schematic drawing (b) Hysteresis Loop	107
Figure 3-31 Base excitation model of the nonlinear isolator	108
Figure 3-32 Frequency Response Functions for different sliding friction force values (discrete points are time simulations)	112
Figure 3-33 Phase response of dry friction isolator-2	113
Figure 3-34 Performance plot of dry friction isolator	114
Figure 3-35 Designed isolator under different base excitation levels	115
Figure 3-36 Maximum transmissibility vs excitation level	115
Figure 4-1 Geometrically and Physically Nonlinear Rubber Isolator	120
Figure 4-2 Taylor Series Expansion of Horizontal Displacement	121
Figure 4-3 Fourier Coefficients of Horizontal Displacement Function	122
Figure 4-4 Forcing Across Elastomer	122
Figure 4-5 Effect of γstc on Normalized Force	123
Figure 4-6 Effect of γdyn on Normalized Force	124

Figure 4-7 Effect of Loss Factor on Normalized Damping Force	125
Figure 4-8 Horizontal Displacement Vector	127
Figure 4-9 Displacement Profile in time domain, $L_0 = 0.5$, $a = 0.2$, $U = 0.5$	128
Figure 4-10 Experiment Setup Block Diagram.....	128
Figure 4-11 Experiment Setup Schematic.....	129
Figure 4-12 Experiment Setup	129
Figure 4-13 Servo Position Controller Block Diagram.....	130
Figure 4-14 DC Motor Model	130
Figure 4-15 Rubber Specimen	131
Figure 4-16 Effect of Relative Displacement Amplitude on Dynamic Stiffness...	133
Figure 4-17 Effect of Relative Displacement Amplitude on Static Stiffness	133
Figure 4-18 Effect of Relative Displacement Amplitude on Loss Factor.....	134
Figure 4-19 Absolute Transmissibility for Different Excitation Levels	135
Figure 4-20 Relative Displacement Response for Different Excitation Levels	136
Figure 4-21 Quasi-Zero-Stiffness Isolator	136
Figure 5-1 Proposed Isolators (a) Proposed Isolator-1, (b) Proposed Isolator-2, (c) Proposed Isolator-3, (d) Proposed Isolator-4.....	139
Figure 5-2 Absolute Transmissibility Comparison of the Proposed Isolators	140
Figure 5-3 Phase Response of the Proposed Isolators	141

LIST OF SYMBOLS

$[M]$:	Mass Matrix
$[K]$:	Stiffness Matrix
$[H]$:	Structural Damping Matrix
m	:	Mass of the SDOF system
I_{ij}	:	Moment of Inertia Components
f_s, f_c, f_o	:	Fourier Coefficients of Nonlinear Forcing
$\{R(x, \omega)\}$:	Nonlinear Algebraic Equations Vector
a	:	Length of Nonlinear Stiffness Link
ξ_v, ξ_h	:	Vertical and Horizontal Damping Coefficients
\hat{Z}	:	Non-dimensional Base Excitation
γ, δ	:	Non-dimensional QZS parameters
Ω	:	Ratio of Excitation Frequency to Natural Frequency of the Linear System
x	:	Absolute Displacement of the Mass
k_v, k_h	:	Horizontal and Vertical Stiffness
$\theta, \dot{\theta}$:	Motor Position and velocity
u	:	Relative Displacement of the Mass
c_v, c_h	:	Vertical, Horizontal Viscous Damping Coefficient
F_s	:	Slip Force of the Dry Friction Damper
L_o	:	Free Length of the Horizontal Stiffness

LIST OF ABBREVIATIONS

IMU	:	Inertial Measurement Unit
MEMS	:	Micro Electro-Mechanical Systems
AVI	:	Active Vibration Isolation
PVI	:	Passive Vibration Isolation
HSLDS	:	High Static Low Dynamic Stiffness
RLG	:	Ring Laser Gyro
QZS	:	Quasi-Zero-Stiffness
UAV	:	Unmanned Air Vehicles
HBM	:	Harmonic Balance Method
SHBM	:	Single Harmonic Balance Method

CHAPTER 1

BACKGROUND AND LITERATURE SURVEY

1.1 Introduction

The vibration isolation is a fundamental issue for solving several engineering problems such as preventing sensitive equipment from failure, ride comfort for vehicle technology, reducing noise in measuring devices etc. The main goal of the linear isolation systems is reducing the amplitude of mechanical vibrations transmitting from harsh environment to the system to be isolated as much as possible. This can be possible by introducing elastic elements between the environment and the device. The dynamics of an isolator can be simply defined as a mechanical filter which shapes the frequency spectrum of mechanical excitation. The stop and pass frequency region of this filter is determined by natural frequency and damping properties of the system. A linear mass/spring/damper system has transmissibility that is less than unity at excitation frequencies of $\omega^2 > \frac{2k}{m}$, where k is the stiffness of the mount and m is the mass being supported [1]. While decreasing k increases the isolation region, it causes static deflection problems. With the linear passive vibration isolation techniques, it is not possible to decrease the natural frequency of the structure beyond certain limits due to the static deflection under acting of gravitational forces.

In mechanical systems, damping is another important property for the vibration isolation purposes. It is a vibration energy dissipation mechanism; hence, the resonance response depends on the damping characteristic of mechanical system

Although increasing damping in a mechanical system decreases the vibration amplitude at the resonance, it has an adverse effect in the isolation region [2].

The above considerations are the basis of the linear isolation systems. However, inertial measurement units are designed to measure accelerations. Therefore, mechanical vibrations and dynamics of the isolation system affect response of the IMU in terms of bias, noise and phase lag each of which might cause catastrophic problems in control systems fed by IMU. In other words, phase response of the isolation system also should be considered while designing isolation systems, which is usually not a basic design parameter of linear isolation systems. Although increasing damping decrease the resonance amplitudes, it may result in excessive phase lags at IMU response. Thus, vibration isolation of IMUs requires additional considerations.

1.2 Motivation

The motivation of this thesis is about the improving vibration isolation performance of inertial measurement units introducing nonlinear isolation techniques and dealing with the additional requirements of the IMU vibration isolation design problem. First, optimum linear passive isolation is obtained and then effects of nonlinear elements on this system is observed on a single degree of freedom vibratory system both analytically and experimentally.

Inertial measurement units are widely used in aerospace industry to provide control feedback to autopilot algorithms and sometimes navigate the aircraft for short range applications. Satellites, helicopters, jet aircrafts, missiles, unmanned air vehicles (UAV) and micro air vehicles can be examples of these applications [3].

IMUs consist of accelerometers and gyroscopes to provide linear acceleration and rotation rates in six degrees of freedom. Ideally, accelerometers and gyros would measure only rotational rate and accelerations. However, due to asymmetry of their mechanical design and manufacturing inaccuracies, they are sensitive to mechanical vibrations. This sensitivity results in measurement error of IMU, which is known as

Vibration Rectification Error (VRE). This error can be defined as the constant error that occurs when vibratory disturbances exist. Moreover, this error is a function of vibration amplitude. Thus, for many applications it may not be possible to use Kalman Filters to track bias drift due to VRE [4]. If an IMU is used for navigation purposes, the key importance of an IMU may be this bias drift due to the fact that navigation requires integration of IMU response [5, 6].

Other adverse effects of vibratory disturbances to IMU operation are its failure risk and the fact that harsh environment reduce reliability of IMU. Vibration and shock induced failure or structural damage of IMUs can be found in many experimental observations [3] [7] [8]. Furthermore, the reliability of IMU is crucial especially for military applications [3] [8].

Using linear vibration isolation systems, both VRE and protection of IMU from structural failure can be encountered. However, phase delays in operating frequency range of IMU and static deflections due to low stiffness of isolator, limit isolation performance. In this thesis, by utilizing nonlinear elements such as high-static-low-dynamic-stiffness (HLDS) or special version of it, quasi-zero-stiffness (QZS), dry friction and geometrically nonlinear damping, isolation performance is enhanced beyond linear system performance.

1.3 Thesis Layout

This thesis consists of five chapters. First chapter is devoted to introduction to problem and literature survey. Basis of vibration isolation, operating principles of inertial measurement units and the need of vibration isolation for different type of IMUs are explained in this chapter. Moreover, geometrically nonlinear isolators are introduced and the advantages of them are discussed.

In chapter 2, six degrees of freedom mathematical model of vibration isolation system is explained. Firstly, mass, stiffness and structural damping matrices are obtained by given mass and isolator properties. Theoretical development of analyses; modal, harmonic, random, static and shock is discussed. Vibration

analysis program and its graphical user interface are introduced. The analysis software is verified via shaker table experiments. In shaker table, sine sweep and random are performed for an IMU isolated by commercial rubber isolators. The experiment and analysis software results are compared.

Chapter 3 is based on nonlinear vibration isolators. Firstly, the effect of High-Static-Low-Dynamic-Stiffness mechanism is discussed. Nonlinear differential equation of motion is converted into nonlinear algebraic equations by utilizing single harmonic balance method. Nonlinear forcing is approximated by using Taylor Series Expansion. Fourier coefficients of nonlinear forcing are obtained analytically. Nonlinear algebraic equations are solved by Newton's Method with arc-length continuation. Using same solution approach, dry friction and geometrically nonlinear damping are studied as well. Stability of the steady state harmonic solutions is considered by Hill's method. Validation of solution method is performed by time simulations.

Chapter 4 is devoted to dynamic characterization of nonlinear elastomer having negative stiffness mechanism. Nonlinear displacement profiles for single harmonic oscillation of rigid mass is applied via servo-position-controlled motor. Force across nonlinear isolator and the displacement are measured. Physical nonlinearities and damping characteristic are investigated.

In Chapter 5, thesis study is summarized and conclusions are presented. Future improvements are suggested.

1.4 Literature Survey

In literature, there are variety of studies on vibration and shock isolation using active and passive vibration isolation techniques and recently the nonlinear isolators. In this chapter firstly, passive and active vibration isolation techniques are discussed, then the problem is narrowed to Inertial Measurement Units which is one of the sensitive measurement unit widely used in the aerospace industry.

1.4.1 Vibration Isolation Techniques

In the passive vibration isolation problem, system is isolated from the vibratory environment by means of “isolators”, which are generally made up of a rubber like materials (Figure 1-1). Considering the cost and compactness, the passive vibration isolation is widely used method in the industry [9] [10] [11]. Furthermore, passive vibration isolation system does not require any power supply and electronics [8] [12]. This also reduces the maintenance cost and increase the reliability of the system. However, the isolation performance is highly depended on the environmental conditions such as temperature and the frequency content of the input [13] [14] [15] [16].

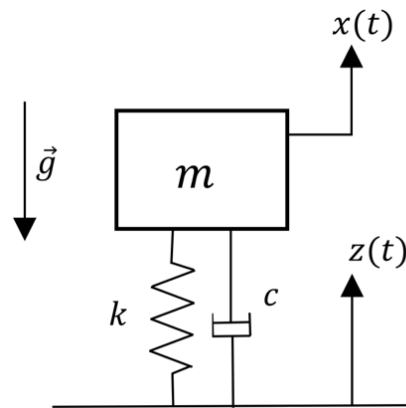


Figure 1-1 SDOF Vibration Isolation System

Passive vibration isolation technique is based on the mechanically filtering the input vibrations over a frequency range. This frequency range is determined by the natural frequencies and damping characteristic of the isolated system [17]. Considering the frequency response function of a single degree of freedom system shown in Figure 1-2, vibrations coming from the environment is filtered out at the isolation region. Around the resonance region, however, excitation is amplified and this may cause issues especially for the sensitive measurement devices.

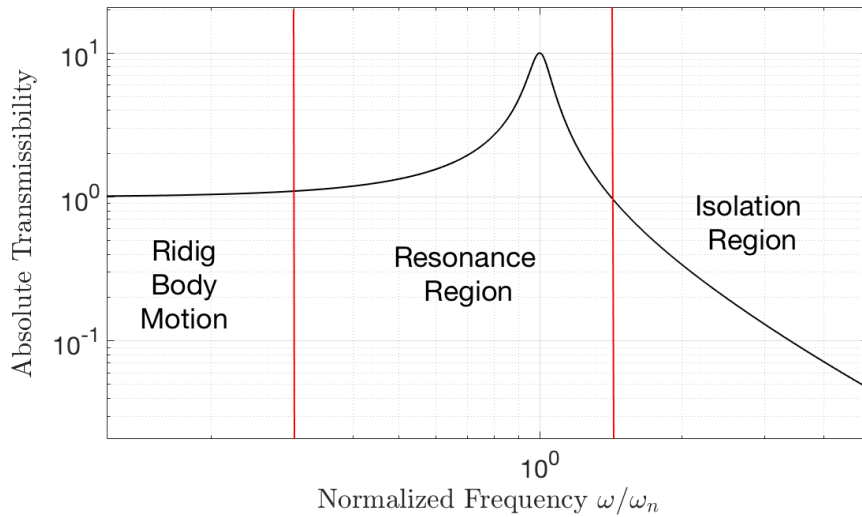


Figure 1-2 Transmissibility of SDOF Vibratory System

In literature, there are variety of study on passive vibration isolation systems and their design procedure. Yoon, studied on the vibration isolation of the micro electro mechanical systems (MEMS) and indicated the importance of the isolation especially for the measurement devices [7]. Yoon mentioned that vibration causes unpredictable false outputs that cannot be compensated by electronic filters and these errors may generate critical and systemic problems. Baytemir developed a software that performs static, modal, random and harmonic response analyses and optimization on selection of the vibration isolators for a given system in MATLAB® environment [18] [19]. Moreover, in his study, Baytemir tabulated the current studies and their capabilities. For instance, Song studied on MSC ADAMS based vibration isolation design software. This program is specialized for the design of the engine vibration isolation system (engine mount system) [55]. In addition, there are many studies based on commercial software such as ANSYS, LS-DYNA and ProE/Mechanica [20] [21] [22]. In their studies, analysis is performed in the commercial analysis software. Thesis study of the Çınarel focused on the vibration isolation of the inertial measurement devices. In addition to response characteristics, Çınarel also considered the elastic center of the system which is an important measure for an IMU [8] [12].

Active vibration isolation is another isolation technique for reducing transmissibility of the system to be isolated. In passive isolation systems, control force is dependent on the natural dynamics of the isolator. Hence, this force cannot be adjusted once the system is designed. The system responses, however, are sensed and control actions are applied to the system according to desired control values in active vibration isolation [23]. On the other hand, this system requires sensors, actuators, control algorithms and power supply, which makes the system complicated [24]. Basic schematic of an AVI system can be seen in Figure 1-3. Its main advantage over the passive isolation system is performance at the resonance region. It doesn't have resonance problems unlike the passive vibration isolation systems. However, because of the complexity of the system, the reliability of the system is reduced. Moreover, AVI increases the cost of the design and requires power, which may be a disadvantage for the aerospace applications [23].

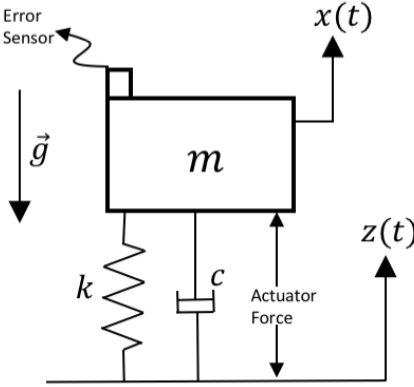


Figure 1-3 Active Vibration Isolation

1.4.2 Inertial Measurement Unit

Inertial measurement units are basically defined as a measurement device which uses 3 linear accelerometers to measure the acceleration and 3 rate gyros to measure rotational velocity. The axes of an inertial measurement unit can be seen in Figure 1-4. Three accelerometers are placed in X, Y and Z axes which are orthogonal each other [25]

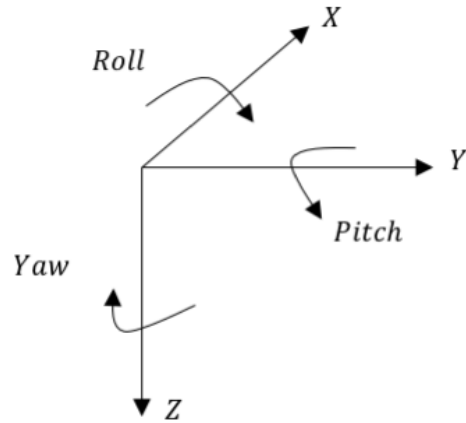


Figure 1-4 IMU Measurement Axes

Studies on inertial measurement units are the result of need of the autonomous navigation systems for military applications [26] [27]. Autonomous means all the necessary information is measured by the aircraft itself. Hence, the system is protected from the jam threat. The acceleration feedback is provided by the IMUs for the autopilot control algorithms of the tactical and ballistic missiles. In addition, the position information of the aircraft can be calculated by utilizing IMU acceleration and rate measurements. Although Global Positioning System may provide more accurate positioning, it is an external signal for the aircraft and might be jammed from the enemy, which is a crucial issue for the military applications. Therefore, in order to navigate a military aircraft, the aircraft accelerations and rotational rates should be measured accurately, and the noise should be filtered out [3] [26] [27]. To illustrate, during the operation, a missile body is exposed to mechanical vibrations due to propulsion, aerodynamic flow etc. Hence, vibration isolation is a critical issue in order to eliminate the negative effects of these vibrations. In other words, the motivation for vibration and shock isolation of an IMU is not only protection of the electronic parts from the failure but also increasing measurement accuracy of the device in terms of noise and bias at the sensor response.

Although vibration and shock isolation are critical for the measurement performance of IMU, it changes the dynamics of the IMU, i.e., it may cause

measurement errors as well. Zaiss studied on IMU measurement errors and defines the characteristics of these errors [4]. The errors due to mechanical filtering (vibration isolation) are as follows

- Misalignment
- Phase delay
- Altered magnitude response

Misalignment should be considered during the design of an IMU isolation system. If static and/or dynamic deflections become excessive, the positioning of the IMU in the aircraft may lead to misalignment. To reduce the resonance response of the system, damping is integrated to the system. However, this causes phase delay in the IMU response. This delay can result in “artificial” coning and sculling and can cause attitude and position drift [4]. Also based on environmental conditions such as temperature and frequency content of excitations, magnitude response changes due to physical nonlinearities of the isolators.

The motivation for the vibration isolation may vary based on the way that IMU uses to measure accelerations and rotational rates. Therefore, the effects of mechanical vibrations on inertial measurement unit performance should be identified.

1.4.3 Classification of the Inertial Measurement Units

Inertial measurement units are generally classified as their gyroscope mechanism, since the almost all inertial measurement units have MEMS based accelerometers. In addition, the vibration is the target input for the accelerometers and its dynamical behavior can be predicted unlike the gyroscopes [7]. Therefore, isolation of mechanical vibrations is more critical for gyroscope measurement accuracy.

According to IMU gyroscopes, they can be classified in two main group, which are unconventional and conventional. The diagram of the classification can be seen in Figure 1-5. According to type of the IMU, the motivation for the vibration and shock isolation might differ.

For the aerospace applications of the inertial measurement units, unconventional gyroscopes are commonly used due to the practical reasons such as weight and dimensions [25]. Therefore, in this thesis unconventional gyroscopes are discussed.

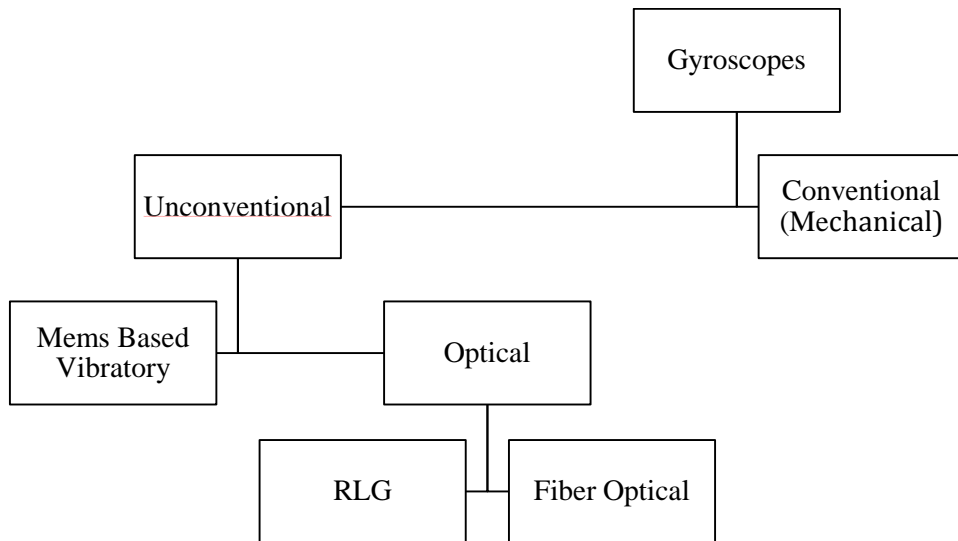


Figure 1-5 Classification of the Gyroscopes

1.4.3.1 Optical Gyroscopes

In the industry, two types of optical gyroscopes are available. One of these, Ring Laser Gyroscopes(RLG), consists of the optical parts (corner prisms, mirrors etc) and sensitive electronics (Figure 1-6). Therefore, these optical parts should be protected from the vibratory environment. RLG is based on creating a continuous light path using three or more mirrors. The working principle can be basically explained by the fact that the both laser beams oscillate at the same optical frequency, when the sensor is stationary. However, due to rotation in the perpendicular axis, optical frequency changes. By utilizing this change, the angular rotation rate is measured [25].

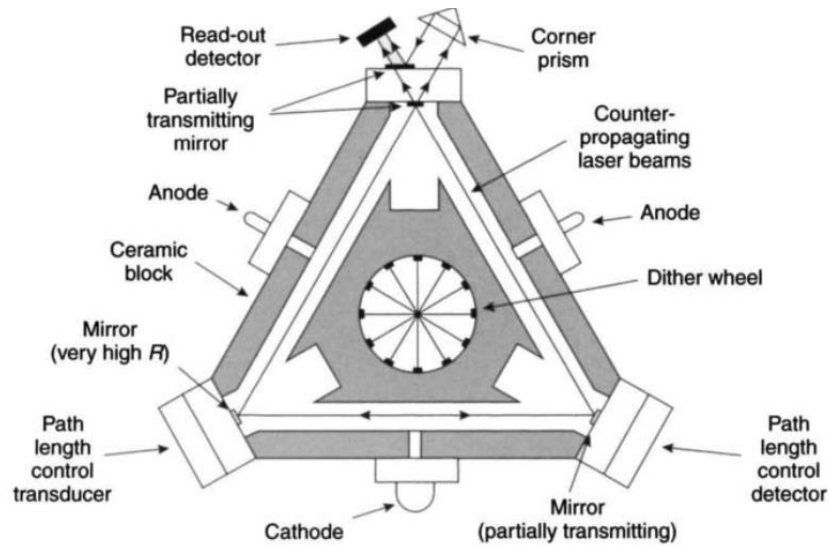


Figure 1-6 Ring Laser Gyroscopes [25]

The other common type of the optical gyroscopes is called as Fiber Optic Gyroscope. As can be seen in Figure 1-7 light beam is split into two beams that propagate in opposite directions. Then, these two beams are combined and observed by a detector. If there is no rotation, two light beams are identical and there is no phase angle. However, if the coil is rotated, then this rotation leads to a phase difference between the light beams. Using this phase difference, angular velocity is measured. Its main advantages on RLG gyroscopes can be shorten as compactness, having low bias and cost. However, vibration leads to distortion of the coil and this causes the measurement errors. In addition, similar to RLG gyroscopes, vibration and shock may harm the optical parts of the fiber optic gyroscopes and it should be isolated from mechanical vibrations and shock [25].

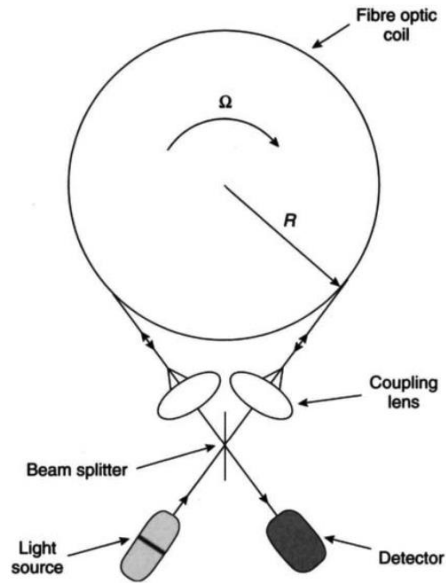


Figure 1-7 Fiber Optic Gyroscopes [25]

1.4.3.2 MEMS Based Gyroscopes

MEMS based gyroscopes are devices which measure the angular rate of a system using the Coriolis Forces. The measurement mechanism can be seen in Figure 1-8. Basically, drive mass is excited at its resonance frequency and Coriolis force is measured from the sense mass. By utilizing this force, angular rate is measured [7] [25].

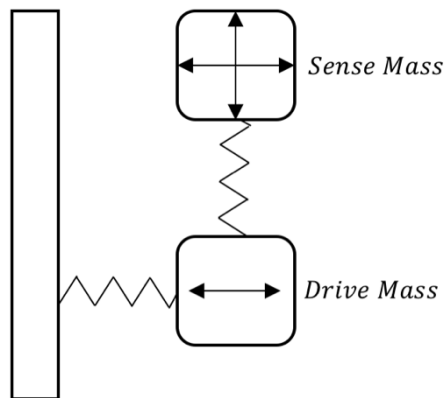


Figure 1-8 MEMS based Gyroscope

As can be seen from Figure 1-9, The main advantage of the MEMS based IMUs is their low cost. However, MEMS based IMUs cannot provide as high performance

as optical gyros. Although, up to a bias level of 0.01deg/hour, MEMS based IMUs are feasible, their performance is limited by this value with the current technology [26] [27].

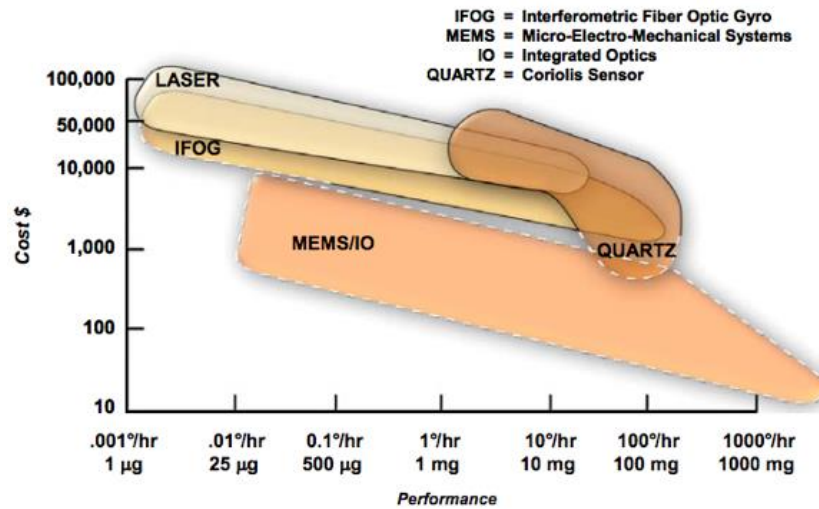


Figure 1-9 Cost/Performance Chart for IMUs [26]

Unlike the accelerometers, vibrations in the sense direction of MEMS gyros causes unpredictable errors in the output and cannot be compensated with the electronics. Although high Q factor is a desired characteristic for the sensitivity of the gyro, it also means amplification of the undesired mechanical vibration amplitudes and distortions in the signal output. Increasing resonant frequency so that the vibration input does not contain signal around resonant frequency may solve the problem but increasing resonant frequency results in decreasing the displacement amplitude in the sense direction [7]. Another problem may be fatigue for the MEMS gyroscopes. Vibration may cause micro cracks, bonding area cracks etc.

1.4.4 Isolator Models

For the passive vibration isolation purposes, viscoelastic materials are widely used in the industry [28] [29] [9] [30]. Damping characteristic of the viscoelastic materials is still an open research area and there is no complete mathematical model considering the whole characteristics of the viscoelastic material for the both time domain and frequency domain dynamic analysis. There exist linear models

describing the dynamic behavior of the viscoelastic materials. These models are based on the different combination of the linear spring and viscous damper [31] [32] [14]. One of them is Voigt Model which is shown in Figure 1-10 a. In this model spring and viscous damper is connected in parallel. Because of their analytical simplicity, it is used widely for modeling elastomeric isolators.

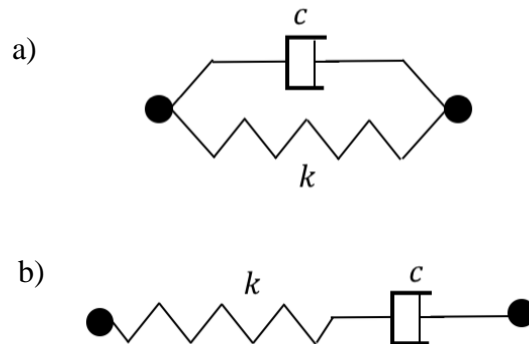


Figure 1-10 (a) Voigt Model (b) Maxwell Model

However, the dynamic test results of the elastomeric materials show that frequency dependency of the isolator cannot be represented in Voigt Model [31] [33]. Maxwell Model is an alternative approach for the linear isolator model Figure 1-10 b. This model consists of a serial combination of the spring and viscous damper. Although Maxwell Model is useful for the linear time domain analysis, for the frequency analysis, frequency depended complex stiffness model (structural damping model) is more effective. Furthermore, commercial isolator test results and their catalog values represented in structural damping model as given in Equation (1-1) [31] [18].

$$k^* = (1 + \eta i)E, \quad (1-1)$$

where k^* is the complex stiffness, η is the loss factor and E is the stiffness. These linear models do not consider the nonlinearity of the viscoelastic materials. However, it is well-known that isolator parameters are function of

- Temperature
- Frequency
- Dynamic strain [30].

The temperature dependency of elastomer which is a viscoelastic material is shown in Figure 1-11. As can be seen from Figure 1-11, stiffness decreases as the temperature increases for different types of viscoelastic materials such as EPDM (Ethylene Propylene Diene Monomers), IR (Isoprene Rubber), SBR (Styrene-Butadiene Rubber), NR (Natural Rubber).

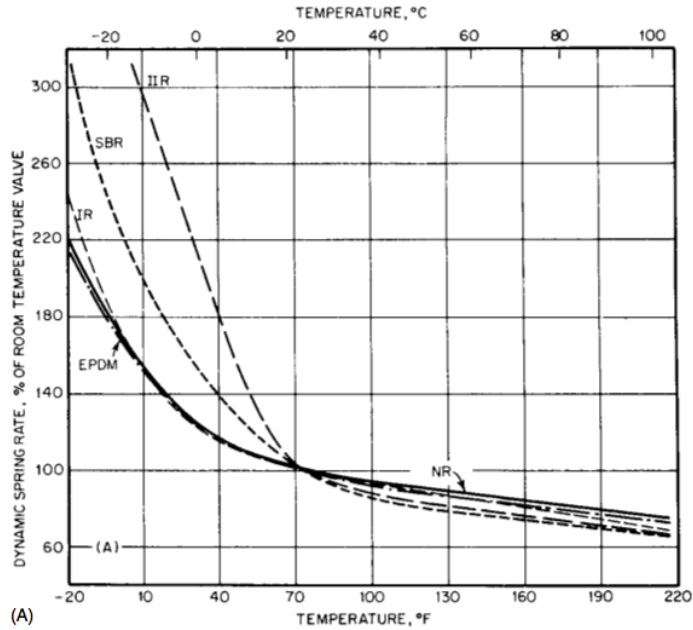


Figure 1-11 Temperature and frequency dependency [9]

In stress strain curve of the natural rubber is shown in Figure 1-12. As can be seen from the Figure 1-12, the stress-strain curve is also nonlinear for the viscoelastic materials [34]. In addition to analytical difficulties, implementation of these nonlinearities requires a lot of testing and of course knowledge of the dynamical behavior of the elastomer completely.

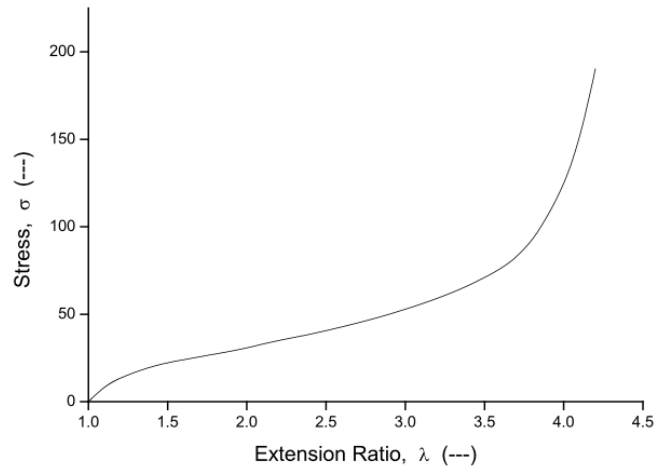


Figure 1-12 Stress Strain Curve of the Elastomer Tensile Specimen [34]

1.4.5 System Models and Design Criteria

In literature, six-degree-of-freedom mathematical model is widely used for the vibration isolation system design [18]. The global coordinate frame is attached to the center of the gravity of the rigid body. The isolators are modeled as 3 mutually orthogonal complex stiffnesses and loss factors. As can be seen in Figure 1-13, they can be attached to any position on the rigid body with any orientation. According the coordinates of the isolator, stiffness matrix is written.

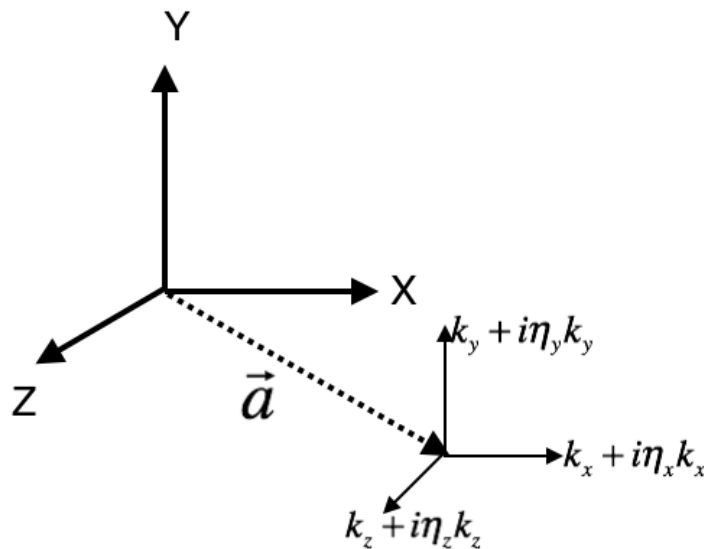


Figure 1-13 Mathematical Model

With the position vector of the isolators and their orthogonal complex stiffness properties, stiffness matrix can be written [28]. Since the global coordinate frame is placed on center of gravity of the rigid body, mass matrix is a six-by-six matrix containing mass and mass moment of inertias. By utilizing the stiffness and mass matrixes, equation of motion can be written for the six-degree-of-freedom model as follows: [17]

$$[M]\{\ddot{x}\} + [K + iH]\{x\} = \{f\}. \quad (1-2)$$

where $\{x\}$ is the displacement vector, $[M]$ is the mass matrix, $[K]$ is the stiffness, $[H]$ is the structural damping matrix. From six-degree-of-freedom model, below analysis can be performed.

- Modal Analysis-obtaining natural frequencies and mode shapes
- Harmonic Response Analysis
- Static Deflection Analysis
- Random Vibration Analysis

The system is designed according to objective function which is combination of the above analyses. In order to obtain accurate analysis results and optimum design, the system parameters and system inputs should be known accurately. If the test data exist for the system input and parameters, reliable results can be obtained using these test data. For example, Kaul uses the test data to obtain the road load profile while designing engine mount of a motorcycle [35]. However, in system design stage, the test data may not be available. In this case, standards might be helpful to derive the system excitation levels. MIL-STD-810 is outcome of a lot of test results performed in all over the world. It is possible to have the test method and vibration profile for a specific system such as military aircrafts (helicopters, jets) and operational conditions (Landing, gunfire, takeoffs etc.) [36]. An example profile can be seen in Figure 1-14. The W_0 value is determined according to operational conditions defined in the standard.

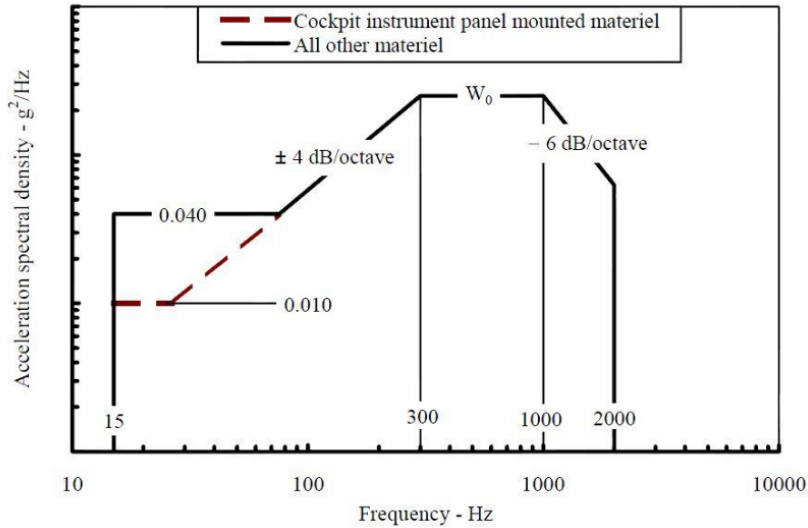


Figure 1-14 Jet Aircraft Vibration Exposure [36]

1.4.6 Nonlinear Isolators

As stated before, the passive isolation techniques are widely used due to its cost effectiveness and simplicity. Recently, nonlinear isolators have become a popular research area and there are variety of studies about the theory and application of the nonlinear isolators [37] [38]. These nonlinear isolators can be implemented to applications where the ultra-low frequency isolation is needed such as measurement devices, automotive industry (passenger comfort, vehicle seat isolation) and aerospace applications. Recent studies show that in addition to nonlinearity of the isolators which is discussed in Section 1.4.4, using geometrical nonlinearities which are integrated to the system intentionally, isolator performance can be improved [39]. These nonlinearities can be categorized by stiffness nonlinearities and damping nonlinearities or combination of them.

1.4.6.1 Stiffness Nonlinearities

A linear mass/spring/damper system has transmissibility is less than unity at excitation frequencies $\omega > \sqrt{2k/m}$, where k is the stiffness of the mount and m is the mass being supported [1]. While decreasing k increases the isolation region, it causes static deflection problems due to the dead weight of the system to be

isolated. Therefore, it is not possible to decrease the natural frequency of the structure that is isolated by using linear passive vibration isolation techniques, beyond some specific limits [40] [41]. Static deflection can be defined as deflection under deadweight of system that is supported by an elastic foundation. In addition to deadweight, continuous acceleration of moving base may also contribute to this deflection. Especially for the measurement devices used in military application might be exposed to approximately continuous 60g-100g based on the application such as missiles, gun fire etc. [26] [27]. Furthermore, isolation motivation for sensitive measurement devices not only the protection of the equipment but also the eliminating the negative effects of the mechanical vibrations on the measurement accuracy. For the inertial measurement units, increasing linear viscous damping and/or lowering natural frequency creates the phase delays at low frequencies which might be the working frequency range of the IMU. This trend can be seen in Figure 1-15. Although increasing linear damping reduce resonance amplitudes, phase response starts to bend at lower frequencies. In addition, isolation region performance is affected adversely. For the navigation algorithms, this delay may cause the instability problems for the system [4]. Therefore, isolation system parameter should be chosen carefully considering phase response.

From this point of view, thanks to nonlinear isolators having High-Static-Low-Dynamic-Stiffness (HSLDS) or quasi-zero-stiffness nonlinear isolators these disadvantages can be eliminated [42] [43]. Huang explained the HSLDS isolators as a non-linear vibration isolator that utilizes negative stiffness mechanisms to obtain ultra-low frequency isolation, while static deflections are considerably lower than the linear isolators [44].

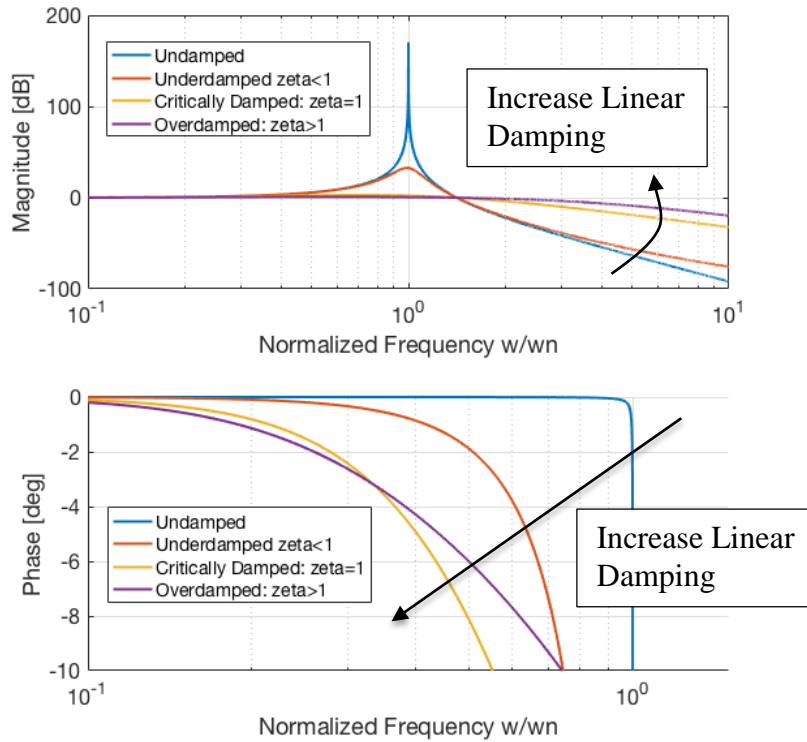


Figure 1-15 Effect of Viscous Damping on Frequency Response Function

If the parameters are designed carefully, even quasi-zero-stiffness around the equilibrium point can also be obtained [45] [46]. In the literature, the HSLDS or quasi-zero-stiffness characteristic is achieved by combining negative stiffness correctors with a positive stiffness which carries the deadweight. Many methods for obtaining negative stiffness were reviewed by the Ibrahim in his review of passive vibration isolation methods [39].

Few of these methods are placing the stiffness element horizontal to the excitation directions, using buckled beams (Euler Beams) [39], magnetic negative stiffness correctors [47] and combination of the buckled beams and the geometrical nonlinearities [48]. The negative stiffness mechanism is shown in the Figure 1-16. The model consists of a rigid mass m , vertical spring of stiffness k_v , preloaded horizontal spring stiffness k_o [40]. In this system, all the elements are physically linear. However due to the horizontal springs, system is geometrically nonlinear. For the small perturbations from the equilibrium position, horizontal springs act as a

negative stiffness spring and this stiffness is nonlinear due to kinematic relationship between the force and the displacement. Therefore, for an input range the dynamic stiffness is much smaller than the static stiffness which carries the deadweight of the system [49].

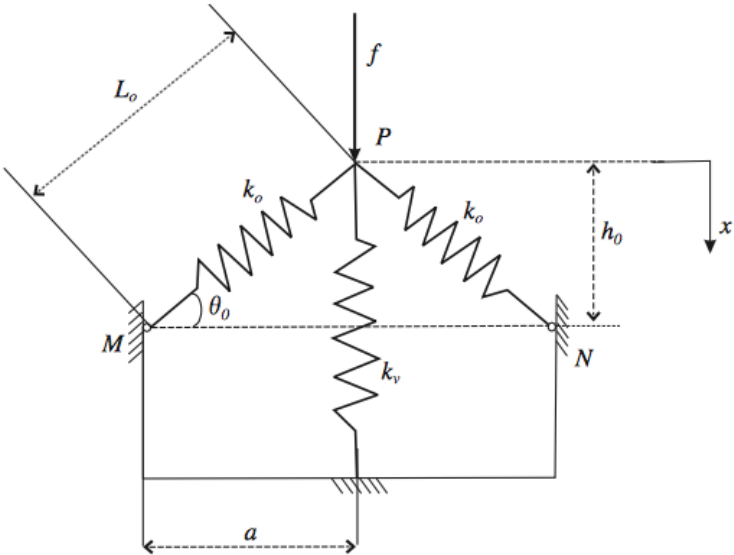


Figure 1-16 Nonlinear Isolator Model [40]

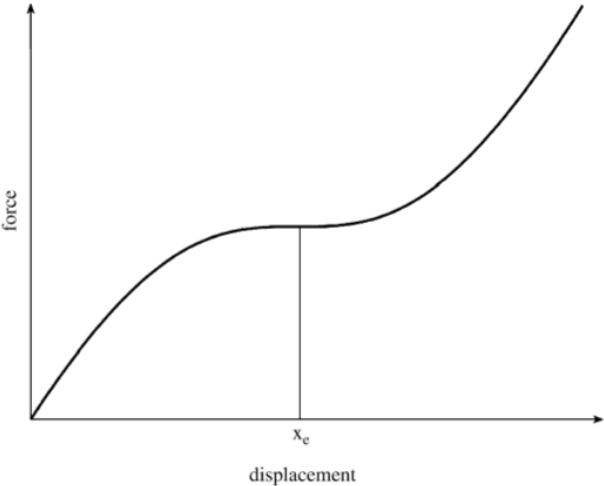


Figure 1-17 Force Displacement Curve [40]

The force and displacement curve of the mechanism shown in Figure 1-16 can be seen in Figure 1-17. As can be seen from Figure 1-17, the stiffness of the

geometrically nonlinear isolator is cubic like. If parameters are designed carefully, even quasi-zero-stiffness mechanism can be obtained. Le studied on the same mechanism and obtain a design for the low frequency vibration isolation of the vehicle seat [50].

In addition, Huang studied on the HSLDS nonlinear isolators built by Euler beams formed negative stiffness corrector. The stiffness model which is used in this study is represented in Figure 1-18. Four buckled Euler beams are placed obliquely to behave as the stiffness corrector. “V” shape grooves support the beams and constrain them. These beams are relaxed at initial state. Then, it buckles due to the vertical load. When it reaches the final position, the static load is carried out by the vertical linear spring [48].

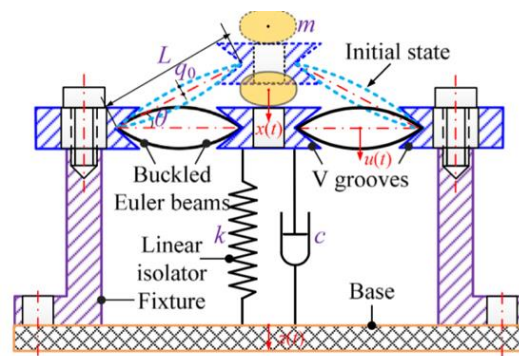


Figure 1-18 Euler beam formed negative stiffness corrector [48]

Zhou obtained the quasi zero stiffness isolator using the cam roller mechanism [51]. The disengagement of the cam roller mechanism is considered in a piecewise nonlinear dynamic model. In Zhou’s study, the effect of the system damping and the input forcing level is discussed. Huang presented a quasi-zero-stiffness using knife edge supported beam and obtain a compact design for a nonlinear isolator [52]. Shaw suggested a design methodology using the two simple parameters that are defined in his study. The effect of these two parameters is discussed [53].

Meng utilized the disk springs to obtain anti-restoring force and studied the effect of the overload and underload conditions [54]. Sun showed that the quasi-zero-stiffness mechanism can be obtained by the scissor-like structured platform. In this

design, all the components are linear. The geometrical nonlinearities come from the special geometry of the scissor like platform. Sun states that the scissor like nonlinear isolator have better isolation performance than the quasi-zero-stiffness isolators in terms of loading capacity and stability. In this type of structure, damping (joint friction, horizontal friction and air damping) is also implemented to the system nonlinearly. Thanks to damping, stability performance is improved, and it is shown that jumping phenomena can be avoided [55] [56]. This mechanism is studied for multi-direction vibration isolation problems and QSZ vibration isolation performance is obtained in three directions [57].

In the one stage QSZ vibration isolation systems, the rate of the isolation is limited to $-2\log(\omega)$ which is equal to 40dB/decade [17]. To improve the rate of the isolation region, two stage vibration isolation was studied by Lu. After implementation of the second stage, the system become two-degrees-of-freedom system and the rate of the isolation increases to 80dB/decades [58].

In these studies, using the Taylor series expansion, nonlinear equations due to geometry of the isolator are reduced to polynomials and using single harmonic balance method or averaging method the nonlinear problem is solved [44].

The other method for obtaining the QSZ stiffness is using magnetism. Carella suggested a compact quasi-zero-stiffness mechanism using two linear mechanical springs and magnets [59]. Instead of using linear horizontal pre-compressed springs, magnets in repulsion is added horizontally to the system as indicated in Xu's study. To overcome the mistuned mass problems, tunable QSZ isolator was presented by Zhou. By integrating electromagnets to the system, magnetic field and magnetic forces can be tuned [60]. Furthermore, magnetic levitation method also offers a QSZ stiffness mechanism around an equilibrium point [61]. The six-degrees-of-freedom characteristic was analyzed by Zhu [62]. Moreover, Wu studied on a magnetic spring with negative stiffness (MS- NS) [47]. Likely the Euler beam formed correctors, magnetic spring acts as a negative stiffness for small perturbations around the equilibrium position. The system model can be seen in Figure 1-19. Wu states that the natural frequency of the system can be reduced

while the system can carry the same dead weight by using the negative stiffness correctors (Figure 1-19 (a)). Another alternative is anti-spring systems [39]. The magnets are displaced one with respect to other in the vertical direction. The mechanism is shown in Figure 1-19 (b). Ibrahim placed this mechanism at the end of a cantilever beam and obtains anti restoring force which reduces the natural frequency of the cantilever beam.

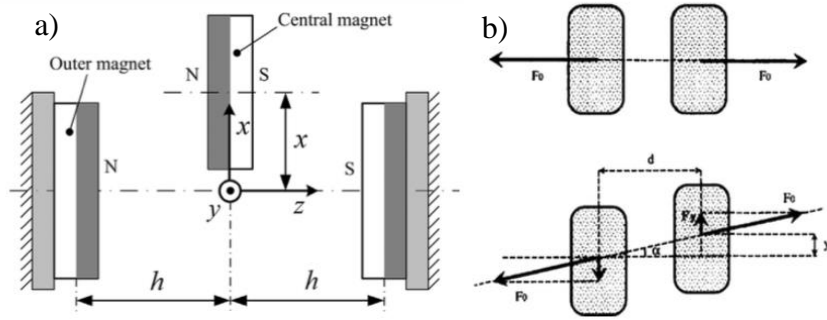


Figure 1-19 (a) Negative Magnetic Spring (b) Anti-spring system

The main disadvantage of these nonlinear isolators is dependency of the performance on the system inputs. If the system input levels are not determined precisely, the system response may be different than the design limits and jumping phenomena may be observed since the cubic stiffness exist in the equation of motion [44] [45]. Even, the system resonance response might be greater than the linear isolation system [63]. The other problem with the nonlinear passive isolators is mistuning of the isolated mass. For the overload an underload case, the bias term in the response affects isolation performance adversely [44, 52]. Meng discussed the effect of the mistuned mass and states that the resonance frequency increases when the system is overloaded or underloaded and FRFs become highly nonlinear. [54].

1.4.6.2 Damping Nonlinearities

To improve the isolation performance, another important nonlinearity is studied on the damping characteristic of vibration isolators. In the mechanical systems, damping is an important property for the vibration isolation purposes. It is a

vibration energy dissipation mechanism and therefore the resonance response depends on the damping characteristic of the mechanical system. Although increasing damping in a mechanical system decreases the vibration amplitude at the resonance, it leads to higher vibration transmissibility at isolation region. [64]. Also, it bends the phase diagram of the response at lower frequencies than the resonance frequency. If the system to be isolated is a measuring device, this lag may become important. Ideal damping behavior for this type of isolation problem would be decreasing resonance amplitude without bending phase diagram for the stiffness-controlled region. Studies show that desired damping characteristic can be achieved by cubic damping type nonlinear element. There are various studies on the vibration characteristic of the cubic damping mechanism. Jing studied on the frequency domain analysis and theoretical background of the cubic damping mechanism [65, 66]. Lv generalized the nonlinear damping force and studies on the effect of the order of the nonlinearity and the nonlinear damping ratios [67]. H. Laalej verified the effect of the cubic damping experimentally [68]. In his study, cubic damping characteristic is provided by active control force. In addition, Jazar suggests that similar characteristics can be achieved geometrically nonlinear damping. [64]. This system is physically more achievable than the cubic damping. In Figure 1-20, geometrically nonlinear damping is demonstrated. Mickens and Tang studied on the free vibrations of this system [69, 2]. Tang and Brennan explained the vibration transmission characteristic of this system and compare with the cubic damping [70].

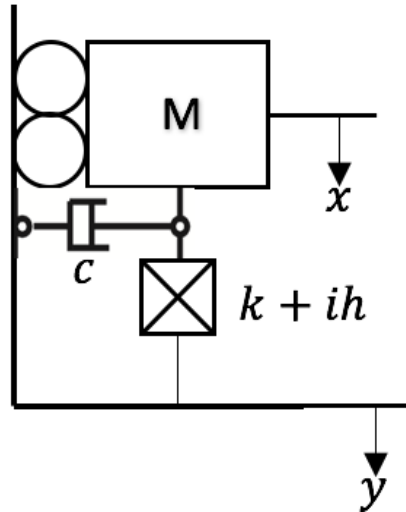


Figure 1-20 Cubic Damping Mechanism

Cheng, combined the QZS mechanism with the geometrically nonlinear damping [71]. With the combination of the nonlinear damping and QZS isolator, the stability performance is improved, and it is shown that unbounded response to base excitation can be eliminated. Also, highly nonlinear behavior of the QZS can be improved and jumping phenomena is avoided by utilizing geometrically nonlinear damping.

Dry friction is another nonlinear damping mechanism used in mechanical systems such as large space structures and turbomachinery [72, 73, 74, 75, 76]. Macro-slip model is widely used in the literature for dynamic analysis of dry friction due to its mathematical simplicity. Macro-slip model assumes the entire friction as either slipping or complete-stuck. Friction damper is generally modeled as a spring one end of which slip if the spring force exceeds certain value (Figure 1-21). Therefore, damping is only effective at resonance regions if slip force is chosen carefully. However, in the case where friction damper is in complete stuck mode, it introduces additional stiffness to the system.

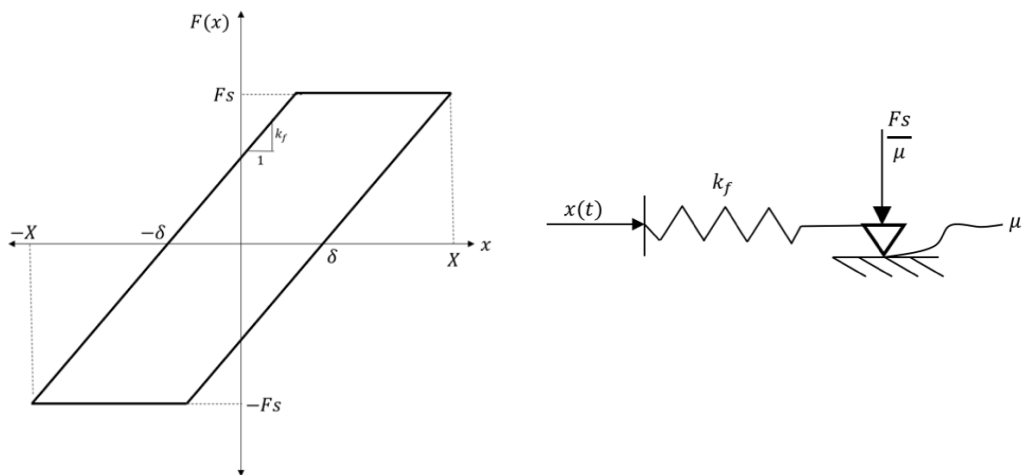


Figure 1-21 Dry Friction Model [77]

Another damping mechanism used for the isolation purposes is eddy current damper. From the basics of the electromagnetic theory, eddy currents are generated when a conductive plate is moved through a stationary magnetic field [78, 79]. Because of the electrical resistance of the conductive material, eddy currents generate heat on the conductive material. For a continuously moving conductive metal, electromotive force (emf) is generated which is proportional to the velocity of the conductive metal Figure 1-22.

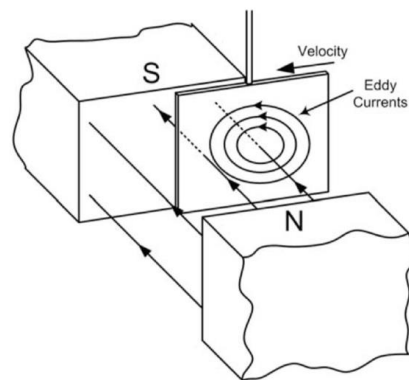


Figure 1-22 Eddy Current Damping Mechanism [80]

This results in dissipative forcing with proportional to velocity. Since eddy current damping mechanism is non-contacting damping forces, they are widely used in

motor brake systems, non-contact measurement devices. Recently, this mechanism is used for attenuation of the vibration amplitudes. Sodano uses eddy current damper for suppression of membrane vibrations [80, 81]. In his study, theoretical development for the eddy current damper with the beam model is performed and test results is discussed.

The methods used for obtaining High-Static-Low Dynamic stiffness isolator and nonlinear damping are summarized in Figure 1-23.

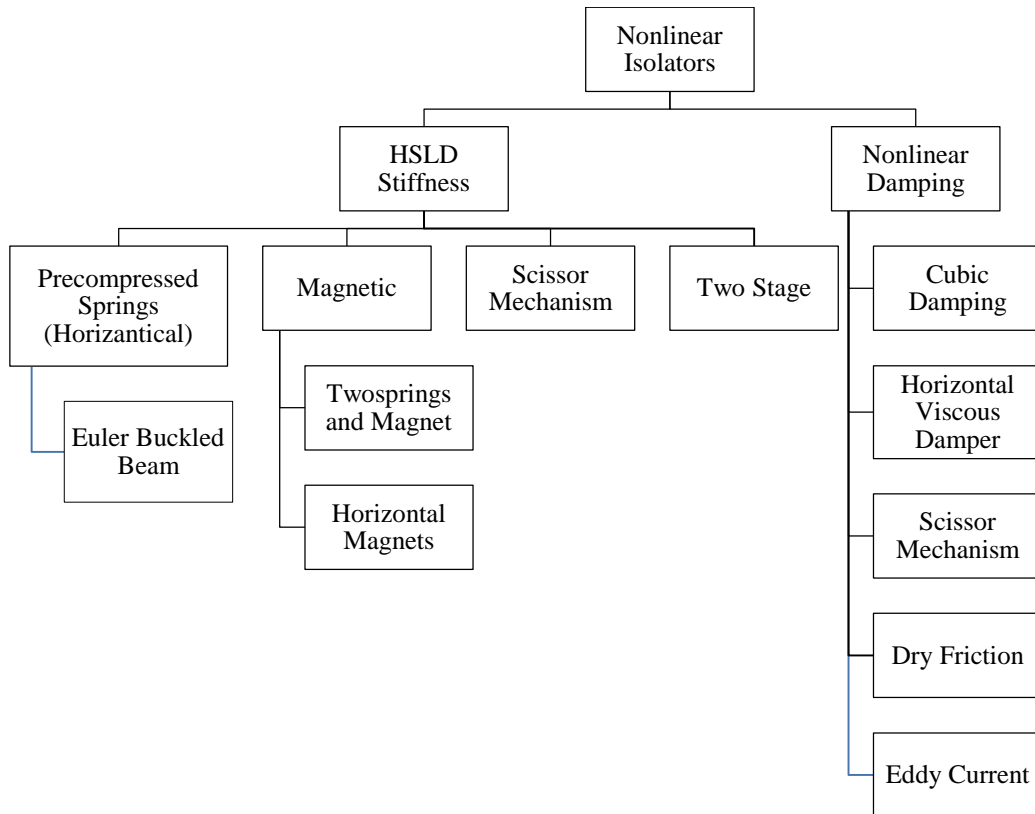


Figure 1-23 Nonlinear Isolators

CHAPTER 2

LINEAR ISOLATION SYSTEMS

2.1 Mathematical Model

2.1.1 Isolator Model

In this chapter, isolators are modeled as elastic elements containing linear stiffness and structural damping in its 3 orthogonal axes. As stated in Chapter 1, dynamic properties of elastomers are dependent on environmental conditions such as temperature, dynamic strain and frequency spectrum of excitation. In this chapter, these parameters are assumed to be constant.

Damping properties of industrial elastomeric isolators are generally given in hysterical damping model and damping characteristic is defined as loss factor. Therefore, stiffness and loss factor of an isolator in 3 mutual orthogonal axes must be defined in the mathematical model. Torsional stiffness, torsional damping and mass of the isolator are neglected.

Isolator can be added to 6 degrees of freedom model in any position and orientation (Figure 2-1). For ease of calculations, global reference frame is taken as center of gravity of the rigid body. Principal elastomer axes can be reduced to global reference frame by defining position vector and angles between principle axes and global reference frame. Global reference frame and isolator axes can be seen in Figure 2-2. Isolator properties are defined in Q, P, R axes. If the isolator is attached to the system with angle, isolator stiffness can be written for global frame axes using Equations (2-1) to (2-6).

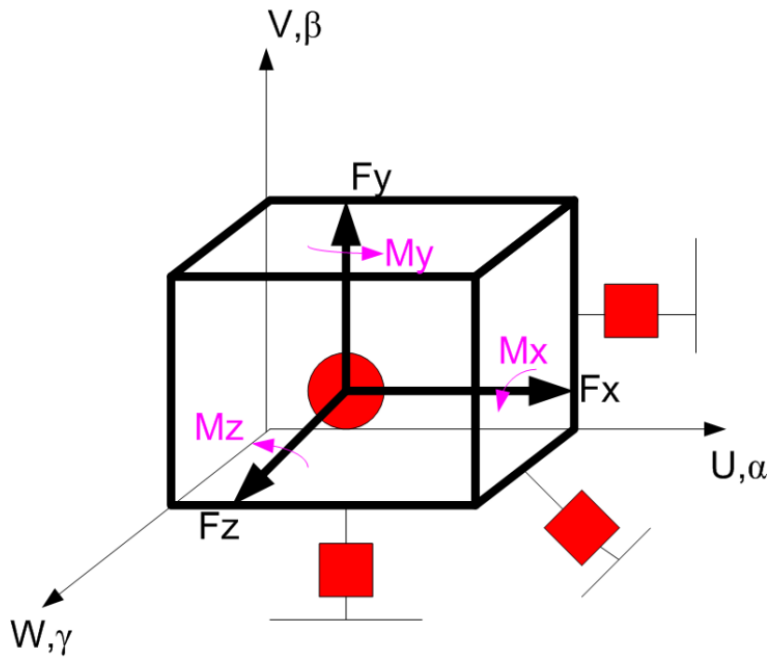


Figure 2-1 Isolator Model

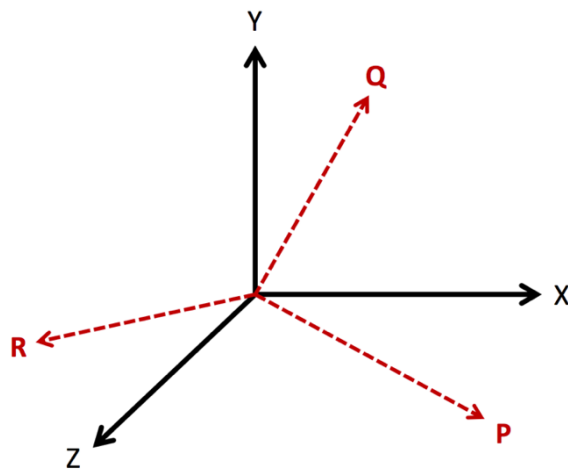


Figure 2-2 Global Reference Frame [19]

$$k_{xx} = k_p \alpha_{xp}^2 + k_q \alpha_{xq}^2 + k_r \alpha_{xr}^2, \quad (2-1)$$

$$k_{yy} = k_p \alpha_{yp}^2 + k_q \alpha_{yq}^2 + k_r \alpha_{yr}^2, \quad (2-2)$$

$$k_{zz} = k_p \alpha_{zp}^2 + k_q \alpha_{zq}^2 + k_r \alpha_{zr}^2, \quad (2-3)$$

$$k_{xy} = k_p \alpha_{xp} \alpha_{yp} + k_q \alpha_{xq} \alpha_{yq} + k_r \alpha_{xr} \alpha_{yr}, \quad (2-4)$$

$$k_{xz} = k_p \alpha_{xp} \alpha_{zp} + k_q \alpha_{xq} \alpha_{zq} + k_r \alpha_{xr} \alpha_{zr}, \quad (2-5)$$

$$k_{yz} = k_p \alpha_{yp} \alpha_{zp} + k_q \alpha_{yq} \alpha_{zq} + k_r \alpha_{yr} \alpha_{zr}, \quad (2-6)$$

where α represents the angles between global reference frame and principle axes, k_p, k_r, k_q are the principles stiffness values, $k_{xx}, k_{yy}, k_{zz}, k_{xy}, k_{xz}, k_{yz}$ are the reduced stiffness values.

2.1.2 Vibration Isolation System

As can be seen in Figure 2-1, rigid mass to be isolated has 3 linear and 3 rotational degrees of freedom. Therefore, system has six equations of motion which are given in Equations (2-7) to (2-12). These equations can be found in literature [28, 18]. In these equations, x, y, z are defined as displacement of rigid mass in X, Y, Z axes of global reference frame. α, β, γ are rotational displacements, a_x, a_y, a_z are position vector of isolator with respect to global reference frame. Since this mathematical model is used for isolation purposes, forcing is defined as base excitation in 3 linear axes of global reference frame. In other words, $F_{x,y,z}, M_{x,y,z}$ are taken as zero. System inputs are displacement of the base which are defined as $u, v, w, \alpha_{in}, \beta_{in}, \gamma_{in}$. $m, I_{xx}, I_{yy}, I_{zz}, I_{xy}, I_{yz}, I_{xz}$ are mass properties of the rigid body at center of gravity. Taking stiffness of the isolator as complex stiffness i.e. $k^* = (1 + i\eta)k$, damping characteristic of the isolator is represented in the model.

$$\begin{aligned} m\ddot{x} + \Sigma k_{xx}(x - u) + \Sigma k_{xy}(y - v) + \Sigma k_{xz}(z - w) + \Sigma(k_{xz}a_y \\ - k_{xy}a_z)(\alpha - \alpha_{in}) + \Sigma(k_{xx}a_z - k_{xz}a_x)(\beta - \beta_{in}) \\ + \Sigma(k_{xy}a_x - k_{xx}a_y)(\gamma - \gamma_{in}) = F_x, \end{aligned} \quad (2-7)$$

$$\begin{aligned} m\ddot{y} + \Sigma k_{xy}(x - u) + \Sigma k_{yy}(y - v) + \Sigma k_{yz}(z - w) + \Sigma(k_{yz}a_y \\ - k_{yy}a_z)(\alpha - \alpha_{in}) + \Sigma(k_{xy}a_z - k_{yz}a_x)(\beta - \beta_{in}) \\ + \Sigma(k_{yy}a_x - k_{xy}a_y)(\gamma - \gamma_{in}) = F_y, \end{aligned} \quad (2-8)$$

$$\begin{aligned} m\ddot{z} + \Sigma k_{xz}(x - u) + \Sigma k_{yz}(y - v) + \Sigma k_{zz}(z - w) + \Sigma(k_{zz}a_y \\ - k_{yz}a_z)(\alpha - \alpha_{in}) + \Sigma(k_{xz}a_z - k_{zz}a_x)(\beta - \beta_{in}) \\ + \Sigma(k_{yz}a_x - k_{xz}a_y)(\gamma - \gamma_{in}) = F_z, \end{aligned} \quad (2-9)$$

$$\begin{aligned}
I_{xx}\ddot{\alpha} - I_{xy}\ddot{\beta} - I_{xz}\ddot{\gamma} + \Sigma(k_{xz}a_y - k_{xy}a_z)(x - u) + \Sigma(k_{yz}a_y \\
- k_{yy}a_z)(y - v) + \Sigma(k_{zz}a_y - k_{yz}a_z)(z - w) + \Sigma(k_{yy}a_z^2 \\
+ k_{zz}a_y^2 - 2k_{yz}a_ya_z)(\alpha - \alpha_{in}) + \Sigma(k_{xz}a_ya_z + k_{yz}a_xa_z \\
- k_{zz}a_xa_y - k_{xy}a_z^2)(\beta - \beta_{in}) + \Sigma(k_{xy}a_ya_z + k_{yz}a_xa_y \\
- k_{yy}a_xa_z - k_{xz}a_y^2)(\gamma - \gamma_{in}) = M_x,
\end{aligned} \tag{2-10}$$

$$\begin{aligned}
I_{yy}\ddot{\beta} - I_{xy}\ddot{\alpha} - I_{yz}\ddot{\gamma} + \Sigma(k_{xx}a_z - k_{xz}a_x)(x - u) + \Sigma(k_{xy}a_z \\
- k_{yz}a_x)(y - v) + \Sigma(k_{xz}a_z - k_{zz}a_x)(z - w) \\
+ \Sigma(k_{xz}a_ya_z + k_{yz}a_xa_z - k_{zz}a_xa_y - k_{xy}a_z^2)(\alpha - \alpha_{in}) \\
+ \Sigma(k_{xx}a_z^2 + k_{zz}a_x^2 - 2k_{xz}a_xa_z)(\beta - \beta_{in}) + \Sigma(k_{xy}a_xa_z \\
+ k_{xz}a_xa_y - k_{xx}a_ya_z - k_{yz}a_x^2)(\gamma - \gamma_{in}) = M_y,
\end{aligned} \tag{2-11}$$

$$\begin{aligned}
I_{zz}\ddot{\gamma} - I_{xz}\ddot{\alpha} - I_{yz}\ddot{\beta} + \Sigma(k_{xz}a_x - k_{xx}a_y)(x - u) + \Sigma(k_{yy}a_x \\
- k_{xy}a_y)(y - v) + \Sigma(k_{yz}a_x - k_{xz}a_y)(z - w) \\
+ \Sigma(k_{xy}a_ya_z + k_{yz}a_xa_y - k_{yy}a_xa_z - k_{xz}a_y^2)(\alpha - \alpha_{in}) \\
+ \Sigma(k_{xy}a_xa_y + k_{xz}a_xa_y - k_{xx}a_ya_z - k_{yz}a_x^2)(\beta - \beta_{in}) \\
+ \Sigma(k_{xx}a_y^2 + k_{yy}a_x^2 - 2k_{xz}a_xa_y)(\gamma - \gamma_{in}) = M_z,
\end{aligned} \tag{2-12}$$

where Σ represents the sum of reduced stiffness of each isolator. Equations of motions can be written in matrix form following as

$$[M]\{\ddot{\mathbf{x}}\} + ([K] + i[H])\{\mathbf{x}\} = \{\mathbf{F}\}. \tag{2-13}$$

Mass and stiffness matrices represented in Equation (2-13) are given by

$$[M] = \begin{bmatrix} m & 0 & 0 & 0 & 0 & 0 \\ 0 & m & 0 & 0 & 0 & 0 \\ 0 & 0 & m & 0 & 0 & 0 \\ 0 & 0 & 0 & I_{xx} & -I_{xy} & -I_{xz} \\ 0 & 0 & 0 & -I_{xy} & I_{yy} & -I_{yz} \\ 0 & 0 & 0 & -I_{xz} & -I_{yz} & I_{zz} \end{bmatrix}, \tag{2-14}$$

$$[K] = \begin{bmatrix} K_{11} & K_{12} & K_{13} & K_{14} & K_{15} & K_{16} \\ K_{21} & K_{22} & K_{23} & K_{24} & K_{25} & K_{26} \\ K_{31} & K_{32} & K_{33} & K_{34} & K_{35} & K_{36} \\ K_{41} & K_{42} & K_{43} & K_{44} & K_{45} & K_{46} \\ K_{51} & K_{52} & K_{53} & K_{54} & K_{55} & K_{56} \\ K_{61} & K_{62} & K_{63} & K_{64} & K_{65} & K_{66} \end{bmatrix}. \tag{2-15}$$

Coefficients of stiffness matrix are given by Equation (2-16) and (2-36)

$$K_{11} = \Sigma k_{xx}, \quad (2-16)$$

$$K_{12} = K_{21} = \Sigma k_{xy}, \quad (2-17)$$

$$K_{13} = K_{31} = \Sigma k_{xz}, \quad (2-18)$$

$$K_{14} = K_{41} = \Sigma(k_{xz}a_y - k_{xy}a_z), \quad (2-19)$$

$$K_{15} = K_{51} = \Sigma(k_{xx}a_z - k_{xz}a_x), \quad (2-20)$$

$$K_{16} = K_{61} = \Sigma(k_{xy}a_x - k_{xx}a_y), \quad (2-21)$$

$$K_{22} = \Sigma k_{yy}, \quad (2-22)$$

$$K_{23} = K_{32} = \Sigma k_{yz}, \quad (2-23)$$

$$K_{24} = K_{42} = \Sigma(k_{yz}a_y - k_{yy}a_z), \quad (2-24)$$

$$K_{25} = K_{52} = \Sigma(k_{xy}a_z - k_{yz}a_x), \quad (2-25)$$

$$K_{26} = K_{62} = \Sigma(k_{yy}a_x - k_{xy}a_y), \quad (2-26)$$

$$K_{33} = \Sigma k_{zz}, \quad (2-27)$$

$$K_{34} = K_{43} = \Sigma(k_{zz}a_y - k_{yz}a_z), \quad (2-28)$$

$$K_{35} = K_{53} = \Sigma(k_{xz}a_z - k_{zz}a_x), \quad (2-29)$$

$$K_{36} = K_{63} = \Sigma(k_{yz}a_x - k_{xz}a_y), \quad (2-30)$$

$$K_{44} = \Sigma(k_{yy}a_z^2 + k_{zz}a_y^2 - 2k_{yz}a_ya_z), \quad (2-31)$$

$$K_{45} = K_{54} = \Sigma(k_{xz}a_ya_z + k_{yz}a_xa_z - k_{yy}a_xa_y - k_{xy}a_z^2), \quad (2-32)$$

$$K_{46} = K_{64} = \Sigma(k_{xy}a_ya_z + k_{yz}a_xa_y - k_{yy}a_xa_z - k_{xz}a_y^2), \quad (2-33)$$

$$K_{55} = \Sigma(k_{xx}a_z^2 + k_{zz}a_x^2 - 2k_{xz}a_xa_z), \quad (2-34)$$

$$K_{56} = K_{65} = \Sigma(k_{xy}a_xa_z + k_{xz}a_xa_y - k_{xx}a_ya_z - k_{yz}a_x^2), \quad (2-35)$$

$$K_{66} = \Sigma(k_{xx}a_y^2 + k_{yy}a_x^2 - 2k_{xy}a_xa_y), \quad (2-36)$$

Structural damping matrix H can be found by multiplying stiffness matrix by loss factor assuming all loss factor of isolators are same.

$$[H] = \eta[K]. \quad (2-37)$$

If isolators with different loss factors are used, structural damping can be found by using the same equations with stiffness matrix coefficients. k terms in the equations must be replaced by h which can be found by multiplying k with related loss factor.

$$\sum_{i=1}^n h_i = \sum_{i=1}^n \eta_i k_i. \quad (2-38)$$

where n is the number of the isolators. As stated before, input vector is defined as base excitation and F can be calculated as Equation (2-39) to (2-45) .

$$\{\mathbf{F}\} = \begin{Bmatrix} F_1 \\ F_2 \\ F_3 \\ F_4 \\ F_5 \\ F_6 \end{Bmatrix}, \quad (2-39)$$

$$F_1 = \sum_{i=1}^n (k_{xxi} + i\eta_i k_{xxi})u + \sum_{i=1}^n (k_{xyi} + i\eta_i k_{xyi})v + \sum_{i=1}^n (k_{xzi} + i\eta_i k_{xzi})w, \quad (2-40)$$

$$F_2 = \sum_{i=1}^n (k_{xyi} + i\eta_i k_{xyi})u + \sum_{i=1}^n (k_{yyi} + i\eta_i k_{yyi})v + \sum_{i=1}^n (k_{yzi} + i\eta_i k_{yzi})w, \quad (2-41)$$

$$F_3 = \sum_{i=1}^n (k_{xzi} + i\eta_i k_{xzi})u + \sum_{i=1}^n (k_{yzi} + i\eta_i k_{yzi})v + \sum_{i=1}^n (k_{zzi} + i\eta_i k_{zzi})w, \quad (2-42)$$

$$\begin{aligned} F_4 = \sum_{i=1}^n & \left(- (k_{yyi}a_{zi} + i\eta_i k_{yyi}a_{zi})v + (k_{zzi}a_{yi} + i\eta_i k_{zzi}a_{yi})w \right. \\ & + (k_{xzi}a_{yi} + i\eta_i k_{xzi}a_{yi})u - (k_{xyi}a_{zi} + i\eta_i k_{xyi}a_{zi})u \\ & \left. + (k_{yzi}a_{yi} + i\eta_i k_{yzi}a_{yi})v - (k_{xzi}a_{zi} + i\eta_i k_{xzi}a_{zi})w \right), \end{aligned} \quad (2-43)$$

$$\begin{aligned}
F_5 = \sum_{i=1}^n & \left((k_{xx_i} a_{z_i} + i\eta_i k_{xx_i} a_{z_i}) u - (k_{zz_i} a_{x_i} + i\eta_i k_{zz_i} a_{x_i}) w \right. \\
& - (k_{xz_i} a_{x_i} + i\eta_i k_{xz_i} a_{x_i}) u + (k_{xy_i} a_{z_i} + i\eta_i k_{xy_i} a_{z_i}) v \\
& \left. - (k_{yz_i} a_{x_i} + i\eta_i k_{yz_i} a_{x_i}) v + (k_{xz_i} a_{z_i} + i\eta_i k_{xz_i} a_{z_i}) w \right), \quad (2-44)
\end{aligned}$$

$$\begin{aligned}
F_6 = \sum_{i=1}^n & \left(- (k_{xx_i} a_{y_i} + i\eta_i k_{xx_i} a_{y_i}) u + (k_{yy_i} a_{x_i} + i\eta_i k_{yy_i} a_{x_i}) v \right. \\
& - (k_{xy_i} a_{x_i} + i\eta_i k_{xy_i} a_{x_i}) u - (k_{xy_i} a_{y_i} + i\eta_i k_{xy_i} a_{y_i}) v \\
& \left. + (k_{yz_i} a_{x_i} + i\eta_i k_{yz_i} a_{x_i}) w - (k_{xz_i} a_{y_i} + i\eta_i k_{xz_i} a_{y_i}) w \right), \quad (2-45)
\end{aligned}$$

Excitation vector can be also represented in terms of system matrices as given in Equation (2-46).

$$[M]\{\ddot{\mathbf{x}}\} + ([K] + i[H])\{\mathbf{x}\} = ([K] + i[H])\{\mathbf{x}_{in}\}, \quad (2-46)$$

where \mathbf{x}_{in} is the excitation vector.

2.1.3 Dynamics Analyses

Dynamic analyses by utilizing the mathematical model are given by

- Modal Analysis
- Static Deflection Analysis
- Harmonic Analysis
- Random Vibration Analysis
- Shock Analysis

2.1.3.1 Eigenvalue Problem-Modal Analysis

In this analysis, eigenvalue problem is solved, and undamped natural frequencies and mode shapes are obtained. Mode shapes and natural frequencies are critical parameters to obtain the harmonic responses and to evaluate the isolation performance. Undamped equation of motion is given by

$$([K] - \omega^2[M])\{\mathbf{U}\} = 0. \quad (2-47)$$

where \mathbf{U} is 6x1 displacement vector in 6 degrees of freedom. Equation (2-47) has solution only if determinant of $[K] - \omega^2[M]$ equals to zero.

$$|[K] - \omega^2[M]| = 0. \quad (2-48)$$

Since stiffness and mass matrices are 6x6 matrices, there are six ω values make determinant zero and these are defined as undamped natural frequencies of the system. Related mode shape can be found following as

$$([K] - \omega_i^2[M])\{U_i\} = 0..i = 1..6. \quad (2-49)$$

2.1.3.2 Static Displacement Analysis

Since stiffness matrix is obtained, displacement can be calculated for given static loading vector $\{F\}$.

$$\{F\} = [K]\{x_{static}\}. \quad (2-50)$$

By multiplying by inverse of stiffness matrix, static displacements are given by

$$\{x_{static}\} = [K]^{-1}\{F\}. \quad (2-51)$$

This response is critical for evaluating isolator displacement limit under maximum accelerations.

2.1.3.3 Harmonic Analysis

Since size of the system is six degrees of freedom, matrix inversion can be performed easily utilizing package programs such as MATLAB, MathCAD etc. Therefore, receptance matrix method is used in harmonic response analysis. Since steady state solutions are harmonic for harmonic excitations, response can be represented by complex numbers. Detailed information about the assumed solution method can be found in [17, 8]. If equation of motion is rewritten in complex form,

$$[M]\{\ddot{x}\} + ([K] + i[H])\{x\} = ([K] + i[H])\{x_{in}\}. \quad (2-52)$$

If stiffness is defined as function of frequency, equation of motion is given by

$$[M]\{\ddot{x}\} + ([K(\omega)] + i[H(\omega)])\{x\} = ([K(\omega)] + i[H(\omega)])\{x_{in}\}. \quad (2-53)$$

In Equation (2-53) $\{x\}$ is replaced by $\{X^* e^{i\omega t}\}$. Since frequency of steady state solution is same with the input frequency,

$$\begin{aligned} (-\omega^2[M] + [K(\omega)] + i[H(\omega)])\{\mathbf{X}^*\} \\ = ([K(\omega)] + i[H(\omega)])\{\mathbf{X}_{in}\}, \end{aligned} \quad (2-54)$$

$$\{\mathbf{X}^*\} = (-\omega^2[M] + [K(\omega)] + i[H(\omega)])^{-1}([K(\omega)] + i[H(\omega)])\{\mathbf{X}_{in}\}. \quad (2-55)$$

Receptance matrix is given by

$$\alpha = (-\omega^2[M] + [K(\omega)] + i[H(\omega)])^{-1}. \quad (2-56)$$

The response at center of gravity of the rigid mass can be transformed to response of any given point by utilizing transformation matrix that is given as Equation (2-57)

$$\{\mathbf{X}_p^*\} = [R] \begin{Bmatrix} x_p \\ y_p \\ z_p \end{Bmatrix} - \begin{Bmatrix} x_p \\ y_p \\ z_p \end{Bmatrix} + \{\mathbf{X}^*\}_{trans}. \quad (2-57)$$

where $\{\mathbf{X}_p^*\}$ is the response at given position P whose position vector is defined as $\begin{Bmatrix} x_p \\ y_p \\ z_p \end{Bmatrix}$

with respect to global reference frame and $[R]$ is the rotation matrix [18].

$$\begin{aligned} [R] \\ = \begin{bmatrix} 1 & 0 & 0 \\ 0 & \cos(\alpha) & -\sin(\alpha) \\ 0 & \sin(\alpha) & \cos(\alpha) \end{bmatrix} \begin{bmatrix} \cos(\beta) & 0 & \sin(\beta) \\ 0 & 1 & 0 \\ \sin(\beta) & 0 & \cos(\beta) \end{bmatrix} \begin{bmatrix} \cos(\gamma) & -\sin(\gamma) & 0 \\ \sin(\gamma) & \cos(\gamma) & 0 \\ 0 & 0 & 1 \end{bmatrix}. \end{aligned} \quad (2-58)$$

2.1.3.4 Random Vibration Analysis

In engineering applications, vibrations inputs are not finite. Therefore, Fourier transform cannot be applied, and input function cannot be represented by harmonics. In this case, statistical methods are utilized [8, 18]. Especially, for military applications vibration inputs are generally defined as Power Spectral Density (PSD). Thus, observing response of isolation system under random excitations is critical. For six degrees of freedom system input spectral density matrix is given by

$$[S_{in}] = \begin{bmatrix} S_{xx} & 0 & 0 & 0 & 0 & 0 \\ 0 & S_{yy} & 0 & 0 & 0 & 0 \\ 0 & 0 & S_{zz} & 0 & 0 & 0 \\ 0 & 0 & 0 & 0 & 0 & 0 \\ 0 & 0 & 0 & 0 & 0 & 0 \\ 0 & 0 & 0 & 0 & 0 & 0 \end{bmatrix}. \quad (2-59)$$

$[S_{in}]$ which is given as acceleration power density, can be converted into displacement spectrum density.

$$S_{in_{disp}}(i, i) = \frac{S_{in}(i, i)}{\omega^4}. \quad (2-60)$$

In modal domain, displacement spectral density is given by

$$[S_{\eta_{in}}] = [\phi]^{-1} [S_{in_{disp}}] [\phi^{T*}]^{-1}. \quad (2-61)$$

Frequency response function is given by

$$[S_{\eta_{out}}] = [\bar{T}] [S_{\eta_{in}}] [\bar{T}]^{T*}, \quad (2-62)$$

where

$$[\bar{T}] = \begin{bmatrix} \omega_1 & \dots & 0 \\ \vdots & \ddots & \vdots \\ 0 & \dots & \omega_n \end{bmatrix} (1 + i\eta)[\bar{\alpha}] \quad (2-63)$$

$$[\bar{\alpha}] = \left(\begin{bmatrix} \omega_1 + \eta\omega_1 i - \omega^2 & \dots & 0 \\ \vdots & \ddots & \vdots \\ 0 & \dots & \omega_n + \eta\omega_n i - \omega^2 \end{bmatrix} \right) \quad (2-64)$$

The details of the random vibration analysis can be found in [18].

2.1.3.5 Shock Analysis

This analysis is performed in time domain by using 4th order Runge-Kutta solver of MATLAB Simulink. Since there is no solution for hysteric damping in time domain, H matrix should be converted into viscous damping matrix C using Equation (2-65).

$$[C] = [\phi]^T \begin{bmatrix} \ddots & \dots & 0 \\ \vdots & 2\omega_n \zeta_n & \vdots \\ 0 & \dots & \ddots \end{bmatrix} [\phi]. \quad (2-65)$$

where ζ_n is the modal damping ratio, $[\phi]$ is the normalized modal matrix. Relationship between modal damping coefficient and loss factor can be approximated as Equation (2-66) assuming loss factor of all isolator is same.

$$\zeta_{eq} \approx \frac{\eta}{2}. \quad (2-66)$$

Block diagram of the time simulation is given in Figure 2-3. $\{x\}$ is defined as 6x1 position vector.

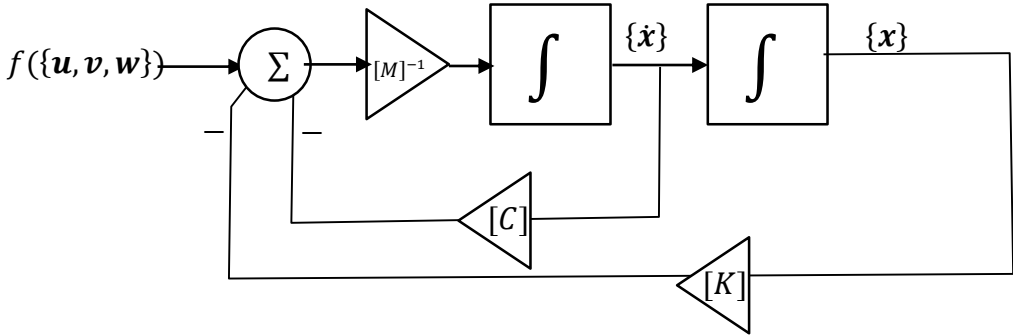


Figure 2-3 Simulink Model for Time Simulation

2.2 Developed Vibration Isolation Analysis Software-VIASoft

To analyze different vibration isolation design alternatives and evaluate their response, a graphical user interface (GUI) shown in Figure 2-4 is developed. GUI consists of 3 subgroups

- Create Model
- Analysis
- Results and Reporting

As can be seen in Figure 2-4 switching pages is performed by ribbon menu. In addition, software warns user about performed software activities via information box. User can see the current configuration at left bottom of the program.

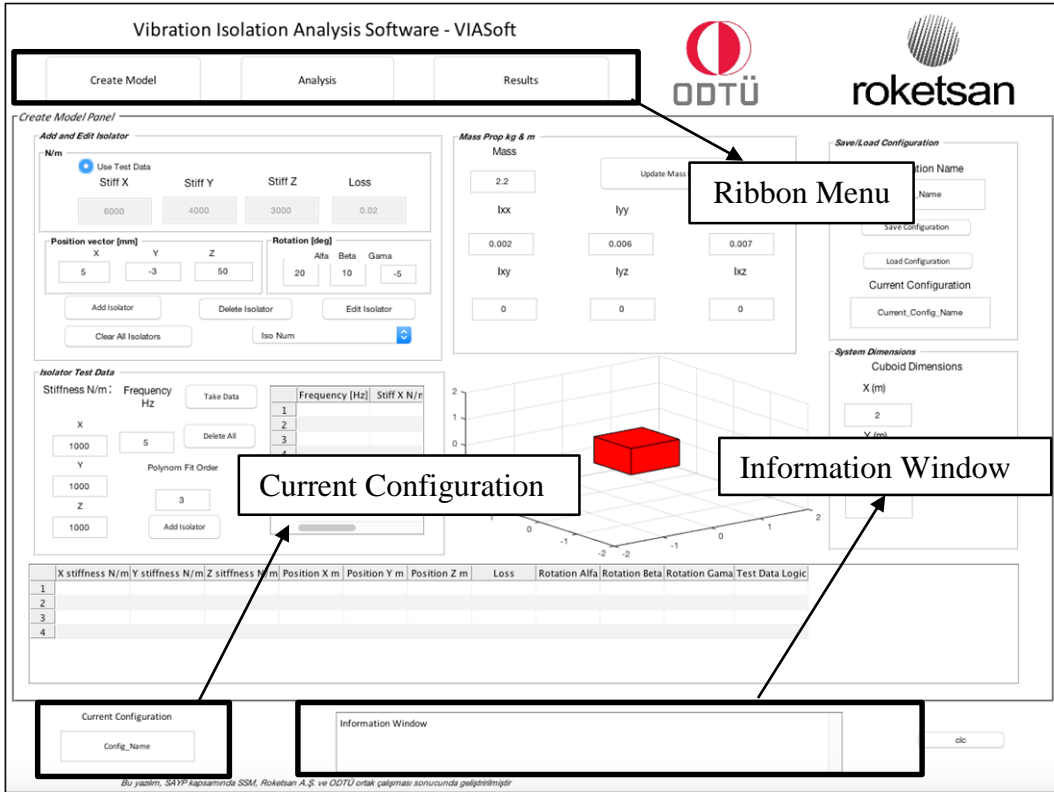


Figure 2-4 Vibration Isolation Analysis Program VIASoft

2.2.1 Creating Model

In this section, user creates isolation model by entering mass and isolator properties which are stiffness values, position vectors, loss factors and inertia values. If dynamic test data is available for isolator, it can be entered to program by using the “Isolator Test Data” panel. Configuration can be saved, and it can be called for further analyses. “Save/Load Configuration” options can be seen in Figure 2-5.

Required properties to define one isolator are following as

- Loss factors and stiffness values in 3 principal axes
- Position vector of isolator with respect to center of mass (X,Y,Z)
- Rotation angles

After entering these values, isolator is added to the software and added isolators can be seen in table which is shown in Figure 2-5. In addition, isolator positions are shown graphically. Isolator properties which added to system can be updated by

“Edit Isolator” button. Likely, mass properties are updated by “Update Mass Prop” button.

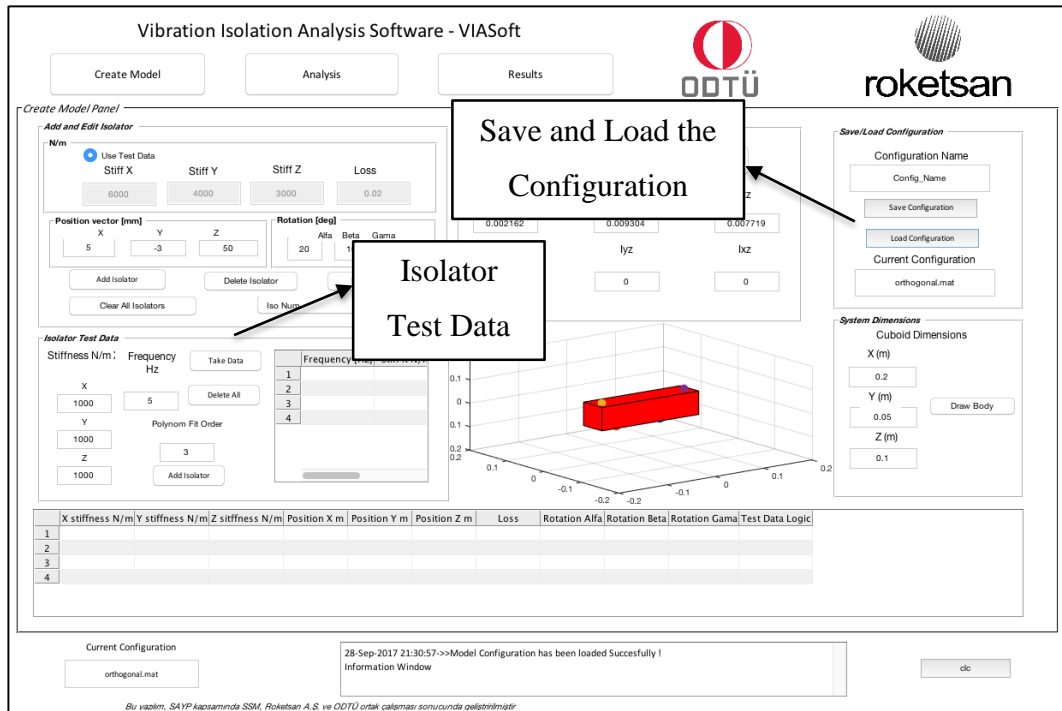


Figure 2-5 Create Model

2.2.2 Analysis

In this section, required system inputs for analyses are entered. For different configurations, analyses can be saved with different names to see and compare different configurations easily. Available analyses are given by

- Modal Analysis
- Harmonic Analysis
- Static Deflection Analysis
- Random Vibration Analysis
- Shock Analysis in Time Domain

2.2.2.1 Modal Analysis

Since this analysis is performed by using only system matrices (mass and stiffness), it is not needed to define any system input. 6 natural frequencies of the system are shown on the screen and results are saved in entered analysis name (Figure 2-6).

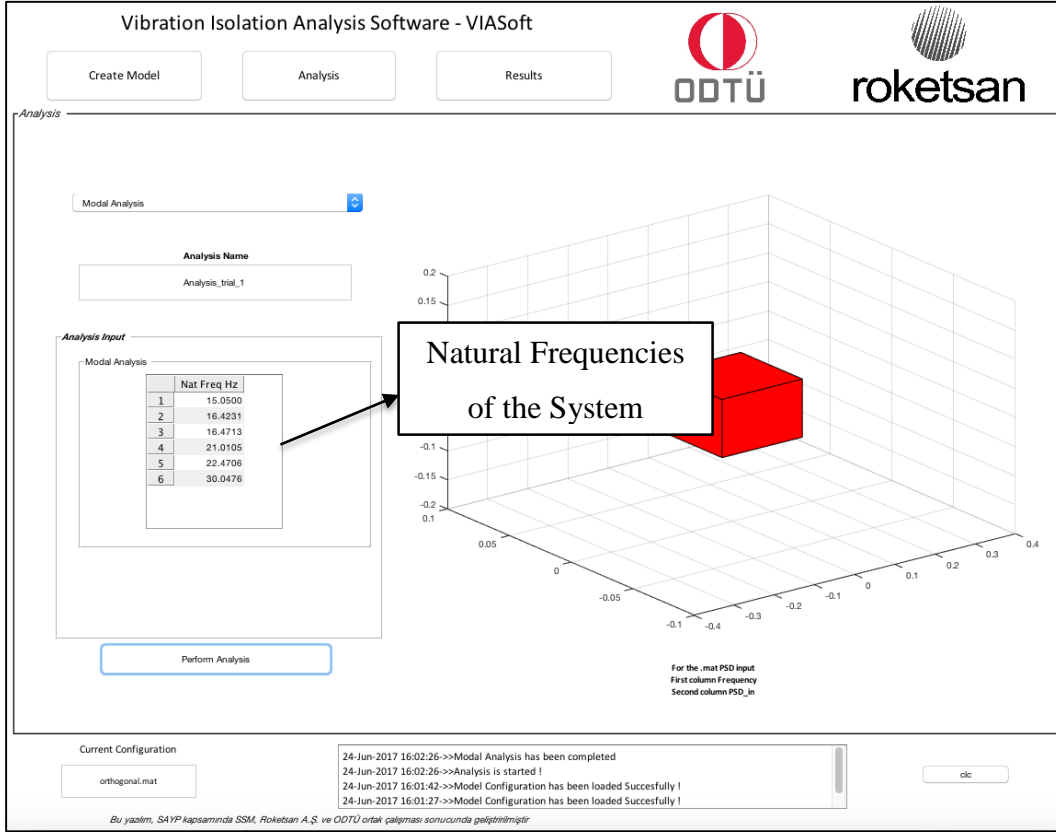


Figure 2-6 Modal Analysis

2.2.2.2 Harmonic Analysis

In this section, user enters the frequency range and the excitation levels. Then pressing “Perform Analysis” button system results are saved in entered analysis name. Frequency Response Functions can be obtained by simply entering “1” for excitation levels (Figure 2-7).

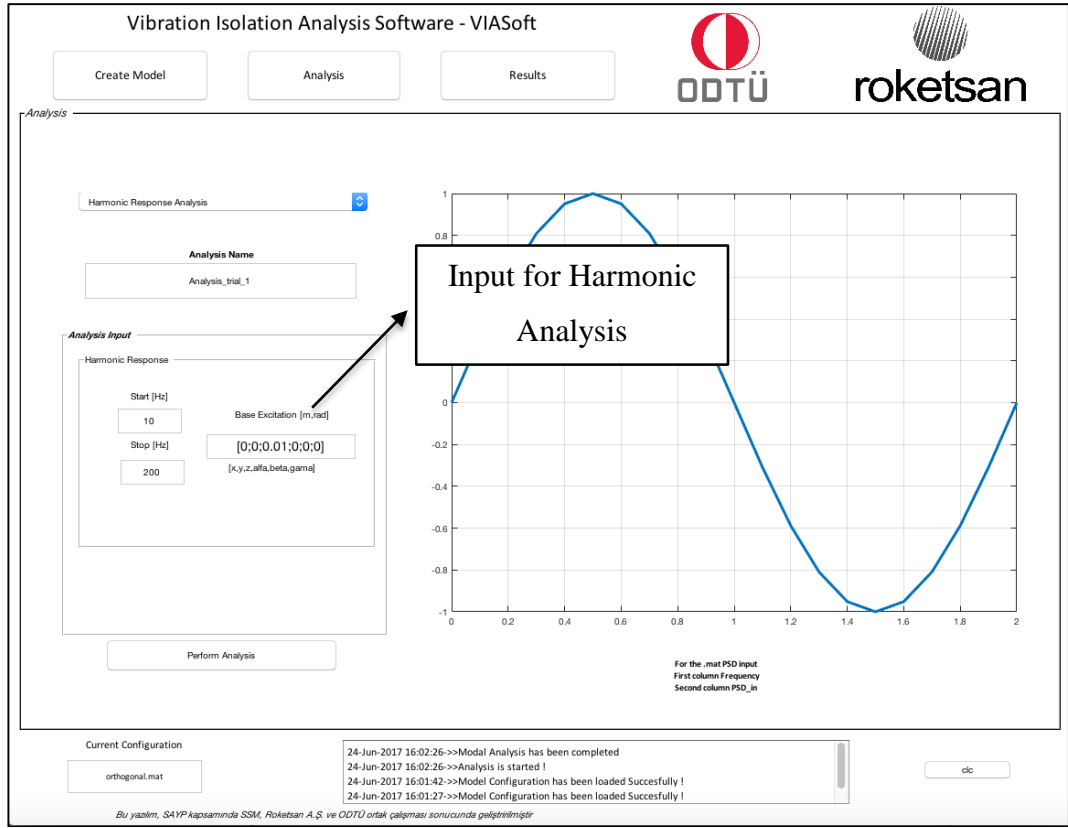


Figure 2-7 Harmonic Analysis

2.2.2.3 Static Displacement Analysis

In this section user defines the constant acceleration level of the base. Then forcing is calculated by simply multiplying acceleration values in [g] by mass for each axis. Especially, for the military application, maximum isolator displacements i.e. strain levels should be known under maximum acceleration. As can be seen in Figure 2-8, static deflections of isolator and rigid mass are calculated by software under 1 g gravity i.e. weight of the rigid body in Y direction. Static deflection of any desired position can be obtained “Results” section.

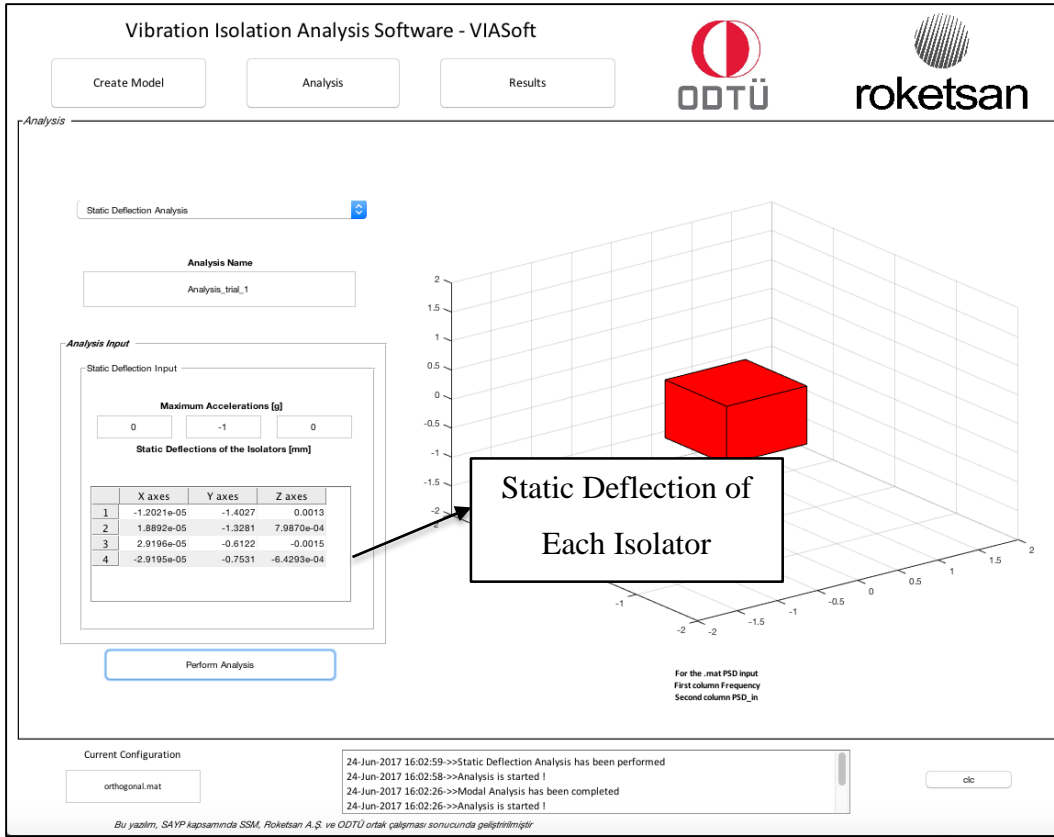


Figure 2-8 Static Displacement Analysis

2.2.2.4 Random Vibration Analysis

In this section, user defines the random vibration profile in 3 linear axes of global reference frame. Interface is written so that users enter profiles that is given in table easily as the way defined in MIL-STD-810 G. User first choose the axes and then, enter table values point by point. In addition, PSD can be defined to software in “.mat” format. Screenshot of the interface can be seen in Figure 2-9.

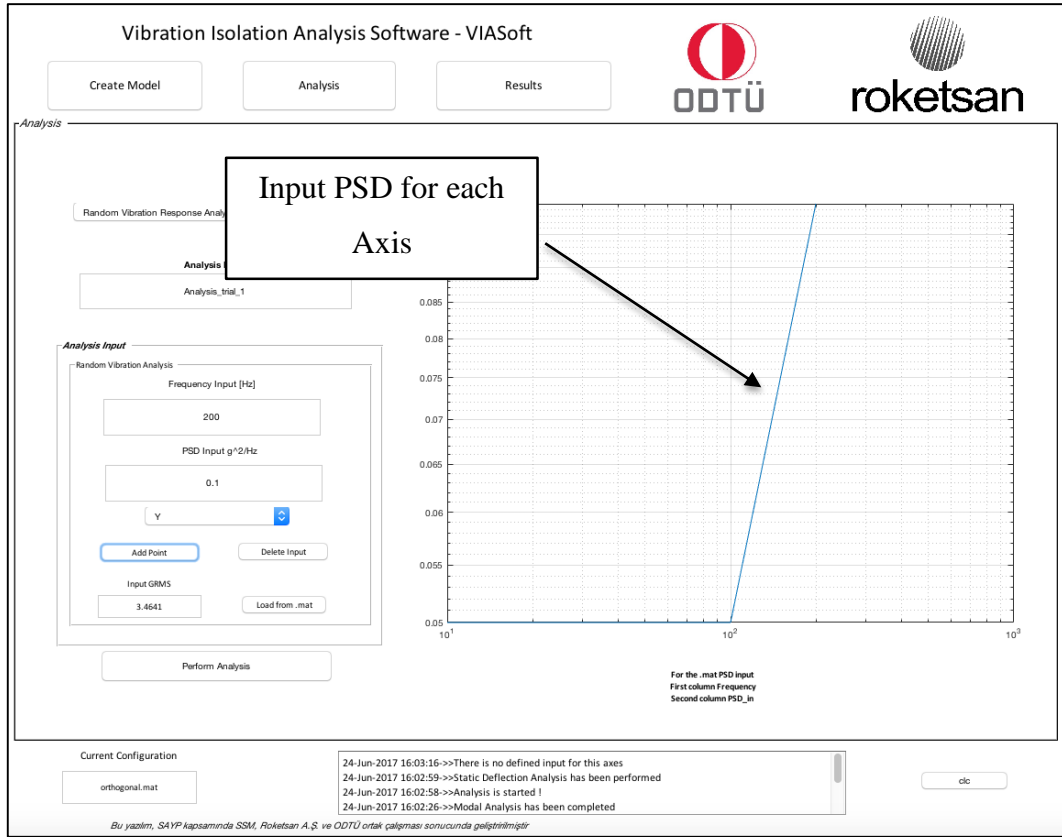


Figure 2-9 Random Vibration Analysis

2.2.2.5 Shock Analysis in Time Domain

In this section, user defines the half sine shock profile for 3 linear axes of global reference frame (Figure 2-10). Amplitude and the duration of half sine and time simulation duration are entered to software. By pressing “Perform Analysis” button, time simulation is started.

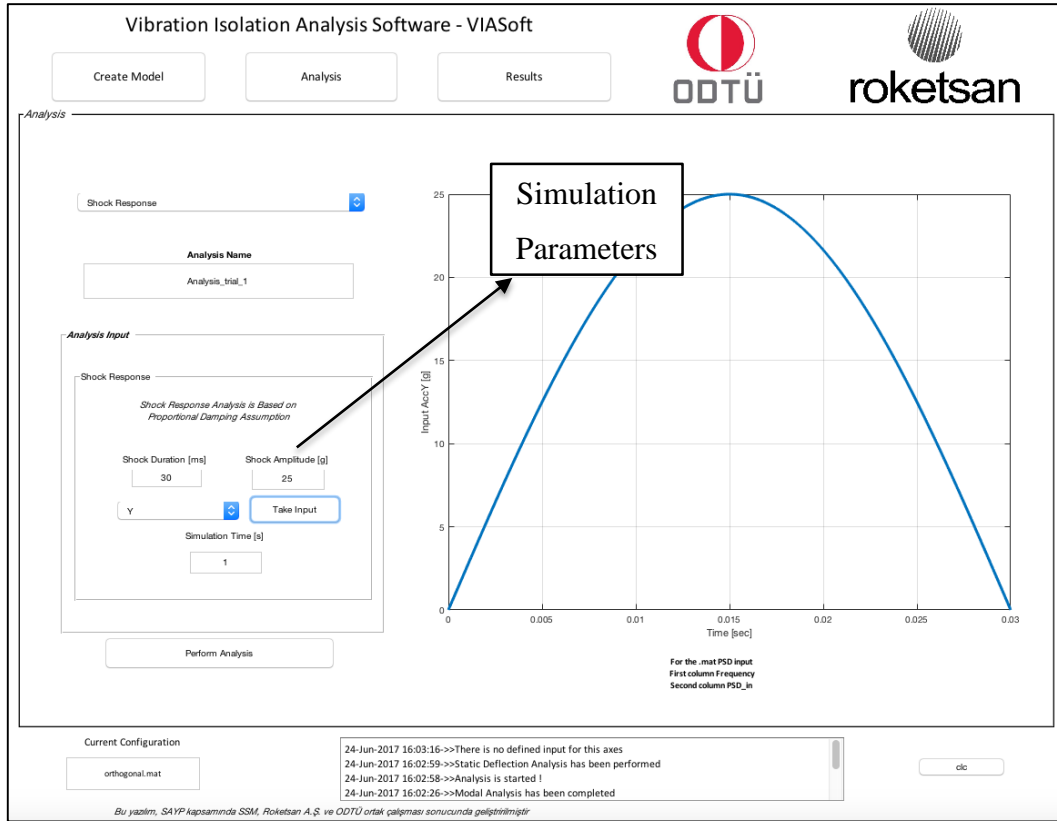


Figure 2-10 Shock Analysis

2.2.3 Results and Reporting

In this section, user postprocesses and compares different analyses results obtained in “Analysis” Section. Firstly, user chooses analysis on which user wants to work by “Choose Analysis” section that is shown in Figure 2-11 and Figure 2-12. Then software lists the available analyses. As can be seen in Figure 2-11, modal analysis results are shown by animation. In addition, time domain shock analysis is animated by representing rigid body as cuboid.

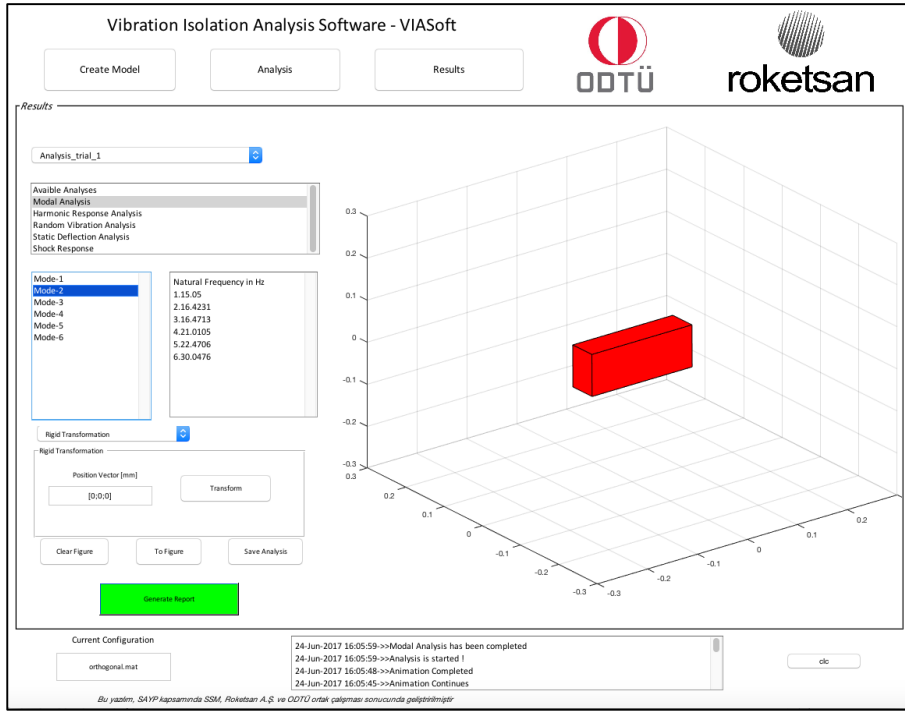


Figure 2-11 Results and Reports -1

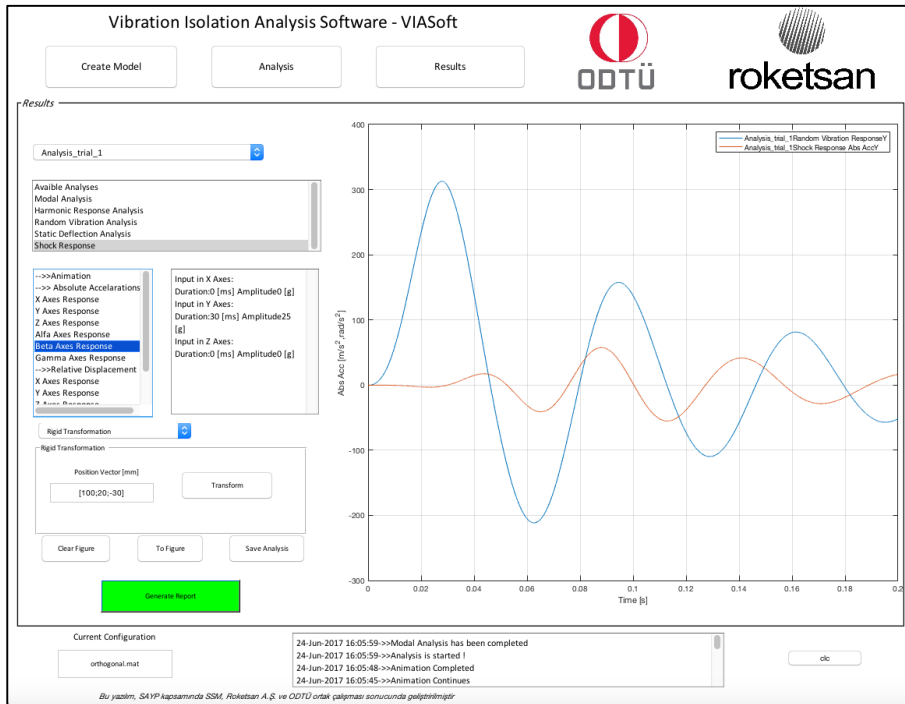


Figure 2-12 Results and Reports-2

“Generate Report” button creates analysis report using all required model information and analysis results. In addition, results and data set can be saved in a proper structure by using “Save Analysis” button. Example of analysis report is shown in Figure 2-13.

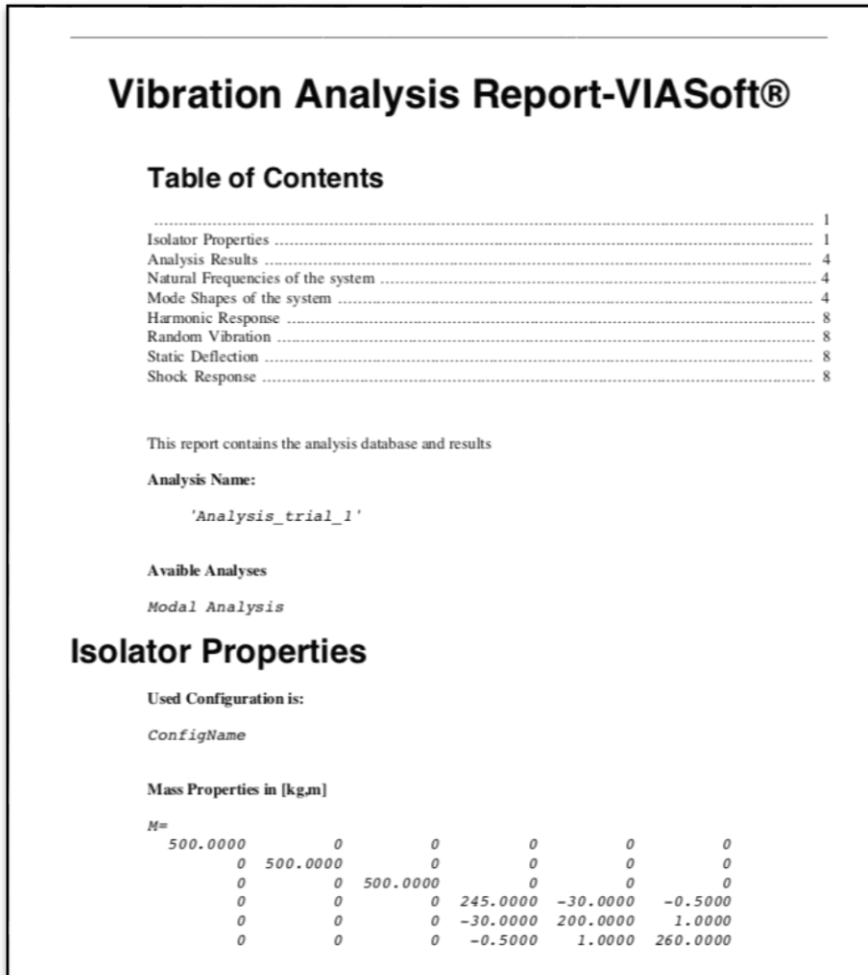


Figure 2-13 Analysis Report Cover Page

2.3 Verification of Developed Analysis Software

In the literature, the verification of the similar six degrees-of-freedom vibration isolation mathematical model was conducted by commercial Finite Element Analysis (FEA) software [18]. In this study, the vibration analysis software is verified by both experiments and finite element analyses. Firstly, modal analysis is performed by using a commercial finite element software to ensure that system

matrices are obtained properly by developed vibration analysis software. Harmonic response and random response analyses are verified by shaker table experiments.

2.3.1 Finite Element Method

In order to verify the modal analysis software developed in MATLAB, a rigid mass having six degrees of freedom is modeled in ANSYS. Results obtained from developed software VIASoft and ANSYS are compared. The rigid body, which is suspended by four isolators, is shown in Figure 2-14

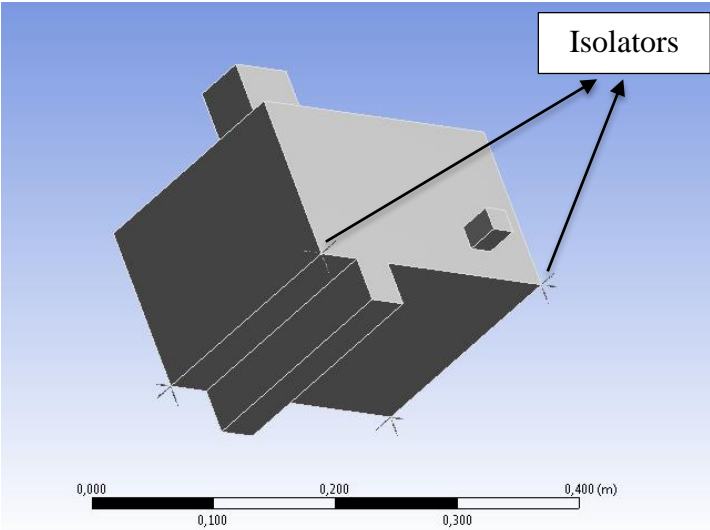


Figure 2-14 Rigid Body with Isolators

The inertial properties of the rigid mass are given by Table 2-1. These values are obtained by Computer Aided Drawings (CAD) programs.

Table 2-1 Inertial Properties

M [kg]	62.1886
I_{xx} [kgm²]	0.3483
I_{yy} [kgm²]	0.4644
I_{zz} [kgm²]	0.5319
I_{xy} [kgm²]	-0.0041
I_{yz} [kgm²]	0.0054
I_{xz} [kgm²]	0.0043

As can be seen from Figure 2-14, rigid body is suspended by four isolators. The stiffness and loss factor values of the isolators is given by Table 2-2. Isolator position vectors with respect to C.G. of the rigid mass is given by Table 2-3.

Table 2-2 Isolator Stiffness and Loss Factors

Isolator	Stiffness-X [N/m]	Stiffness-Y [N/m]	Stiffness-Z [N/m]	Loss Factor
1	120000	120000	120000	0.1
2	120000	120000	120000	0.1
3	120000	120000	120000	0.1
4	120000	120000	120000	0.1

Table 2-3 Isolator Positions

Isolator	Position-X [mm]	Position-Y [mm]	Position-Z [mm]
1	-128.7	101.1	73.2
2	121.3	101.1	73.2
3	-128.7	-98.9	73.2
4	121.3	-98.9	73.2

Then, modal analysis is performed, and the undamped natural frequencies are compared in Table 2-4. As can be seen from Table 2-4, the results are agreed well, and maximum error does not exceed %0.12. Therefore, it can be concluded that for a given mass and isolator properties system matrices are obtained properly by developed software.

Table 2-4 Undamped Natural Frequencies

Mode Number	FEA	VIASoft	Error [%]
1	10.472 Hz	10.474 Hz	0.0191
2	11.400 Hz	11.401 Hz	0.0088
3	13.983 Hz	13.982 Hz	0.0072
4	24.049 Hz	24.078 Hz	0.1206
5	24.773 Hz	24.799 Hz	0.1050
6	25.052 Hz	25.080 Hz	0.1118

2.3.2 Experimental Studies

Harmonic response and random response analyses of the vibration isolation analysis software are verified by conducting shaker table experiments on an isolation system. The results obtained from the experiments and analysis program are compared. Sine sweep and random vibration experiments are performed, and accelerations are measured during the experiments. Experiments are performed for an inertial measurement unit which is suspended by four LORD- SMB003-0500-9, FLEX-BOLT® SMALL SANDWICH mounts (Figure 2-15). The system is modeled in the vibration analysis software as well. After creating the model, software visualizes the isolators positions and the IMU as shown in Figure 2-16.

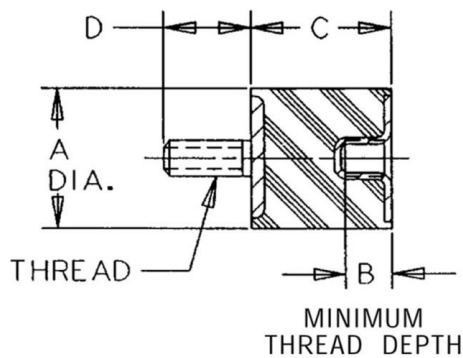


Figure 2-15 LORD Rubber Sandwich Isolator

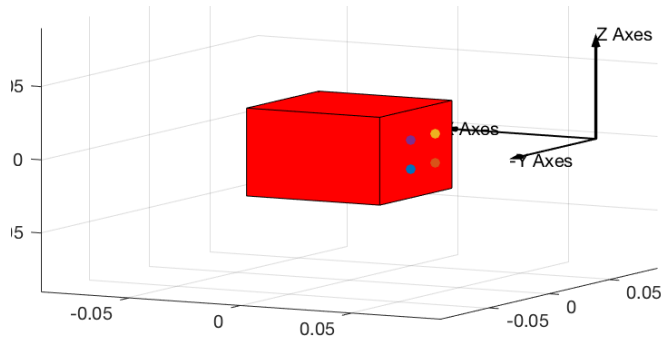


Figure 2-16 Representation of Isolator Position in the Software

The experiment schematic can be seen in Figure 2-17. Three accelerometers are mounted on the IMU and acceleration data is recorded via data acquisition card (DAQ). In order to measure the excitations, one triaxial accelerometer is placed on the shaker table.

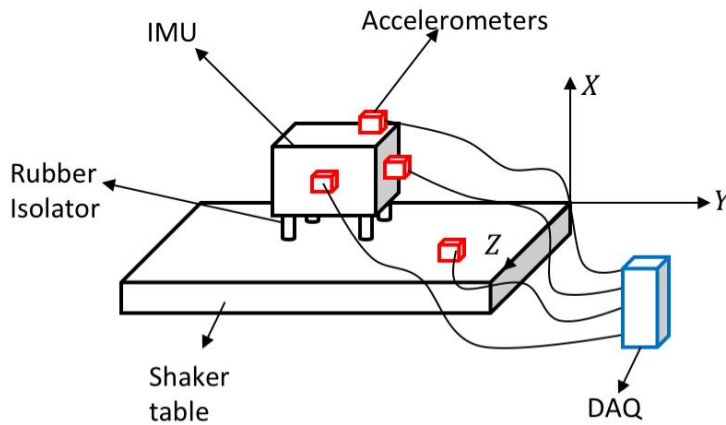


Figure 2-17 Experiment Schematic

During the experiments, the equipment that is listed in Table 2-5 is used. SIRIUS 8 ICP channel cards are used for data acquisition. Sensitivities of the accelerometers are selected according to expected acceleration levels.

The experiment matrix is shown in Table 2-6. For each 3 axes, sine sweep and random vibration are performed. Sine sweep and random vibration tests are repeated for different excitation levels to observe the effect of dynamic strain on stiffness.

Table 2-5 Experiment Equipment

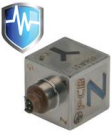


Accelerometer Model	Description	Figure	Quantity
PCB® Model 356A32	Triaxial, mini (5 gm) high sensitivity, ICP® accel., 100 mV/g		3
PCB® Model 356A16	Triaxial, high sensitivity, ceramic shear ICP® accel., 100 mV/g		1
DEWESOFT SIRIUS®-8xACC	16 ICP Channel Data Acquisition Card		2

Table 2-6 Experiment Matrix

Test Number	Excitation Direction	Excitation Type	Excitation Parameters
1	X Axis	Sine Sweep	20-200 Hz Constant Acceleration-1g
2	X Axis	Sine Sweep	20-200 Hz Constant Acceleration-2g
3	X Axis	Sine Sweep	20-200 Hz Constant Acceleration-4g
4	X Axis	Random	20-2000 Hz 2 grms White Noise
5	Y Axis	Sine Sweep	20-200 Hz Constant Acceleration-1g
6	Y Axis	Sine Sweep	20-200 Hz Constant Acceleration-2g
7	Y Axis	Sine Sweep	20-200 Hz Constant Acceleration-4g
8	Y Axis	Random	20-2000 Hz 2 grms White Noise
9	Z Axis	Sine Sweep	20-200 Hz Constant Acceleration-1g
10	Z Axis	Sine Sweep	20-200 Hz Constant Acceleration-2g
11	Z Axis	Sine Sweep	20-200 Hz Constant Acceleration-4g
12	Z Axis	Random	20-2000 Hz 2 grms White Noise

2.3.3 Harmonic Response Analysis Verification

In order to verify the harmonic response analysis of the software, sine sweep experiment is conducted in 3 orthogonal axes of the isolation prototype. The time signal that is shown in Figure 2-18 is converted in to frequency domain by utilizing Fast Fourier Transform (FFT) algorithm of MATLAB. Transmissibility is calculated by Equation (2-67).

$$Transmissibility(\omega) = \frac{FFT(\ddot{x})}{FFT(\ddot{u})}. \quad (2-67)$$

where \ddot{x} is the response accelerations and \ddot{u} is the excitation acceleration. The isolation prototype inertia properties are obtained from the Computer Aided Design (CAD) software. The isolator positions and stiffness properties are entered to the software and excitation in translational axes are applied. The response accelerations are obtained for C.G. of the rigid mass and then transformed to response at acceleration mounting positions.

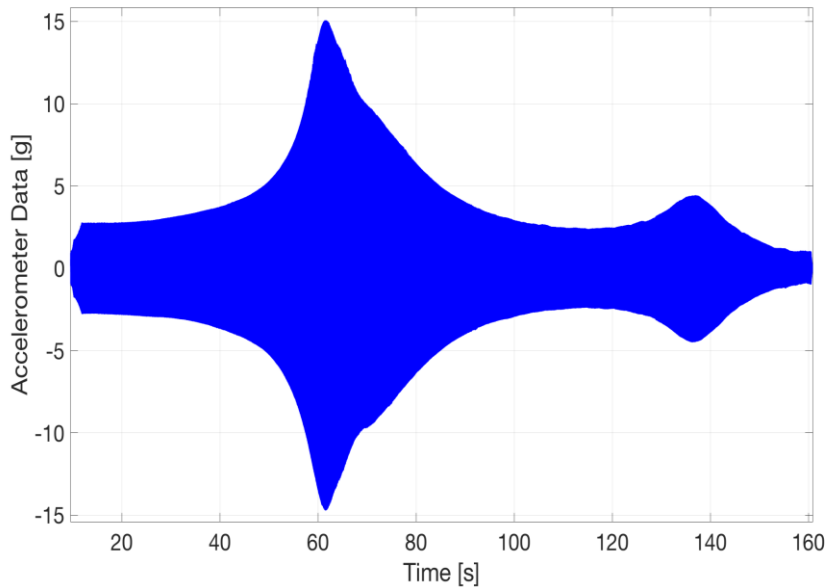


Figure 2-18 Acceleration Time Signal

Experiment results and software analysis results are compared in Figure 2-19 to Figure 2-27. As stated in Section 1.4.4, the isolator stiffness and damping properties are depended on the excitation frequency, dynamic strain and temperature. As can

be seen from Figure 2-19 to Figure 2-27, as dynamic strain increases, stiffness of the isolators decreases, and resonance frequencies thus decrease as well. The deviation of analysis software result from experiments can be explained by the assumptions made in the analyses, the approximations used for calculating system parameters and measurement errors. These assumptions and approximations can be listed as follows

- There is no torsional stiffness of isolators
- Loss factor and stiffness are constant
- Mass matrix of IMU is approximated by a CAD software
- Accelerometer positions w.r.t. global reference frame is approximated by a CAD software
- Isolator positions w.r.t. global reference frame is approximated by a CAD software

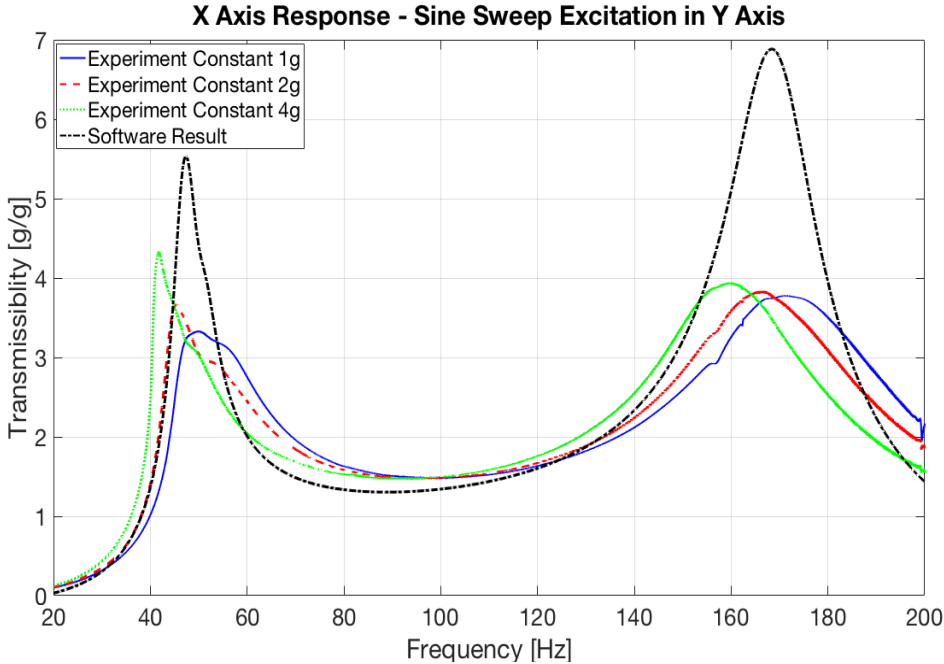


Figure 2-19 X Axis Response – Excitation in Y Axis

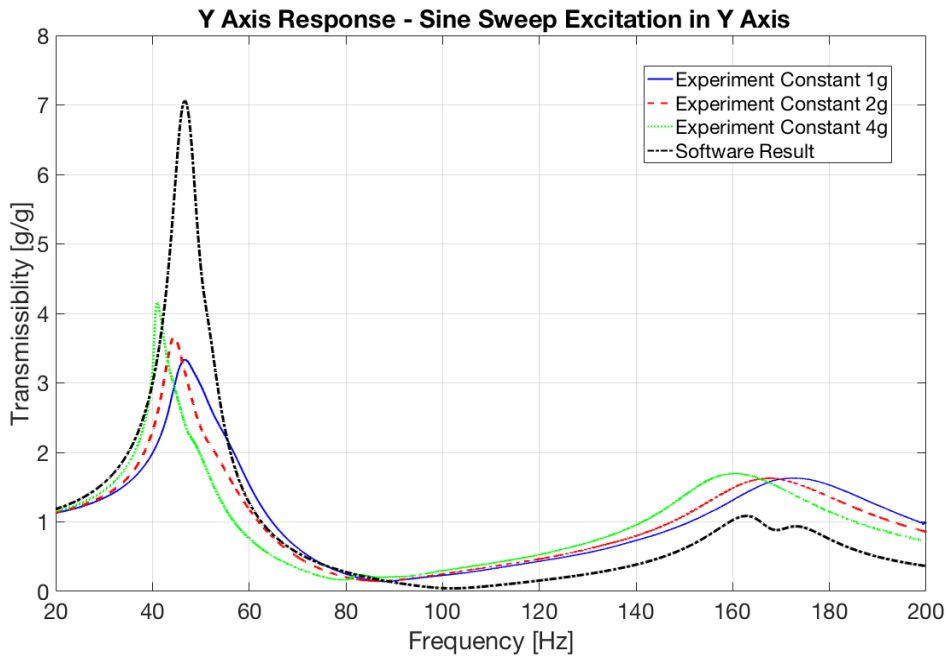


Figure 2-20 Y Axis Response – Excitation in Y Axis

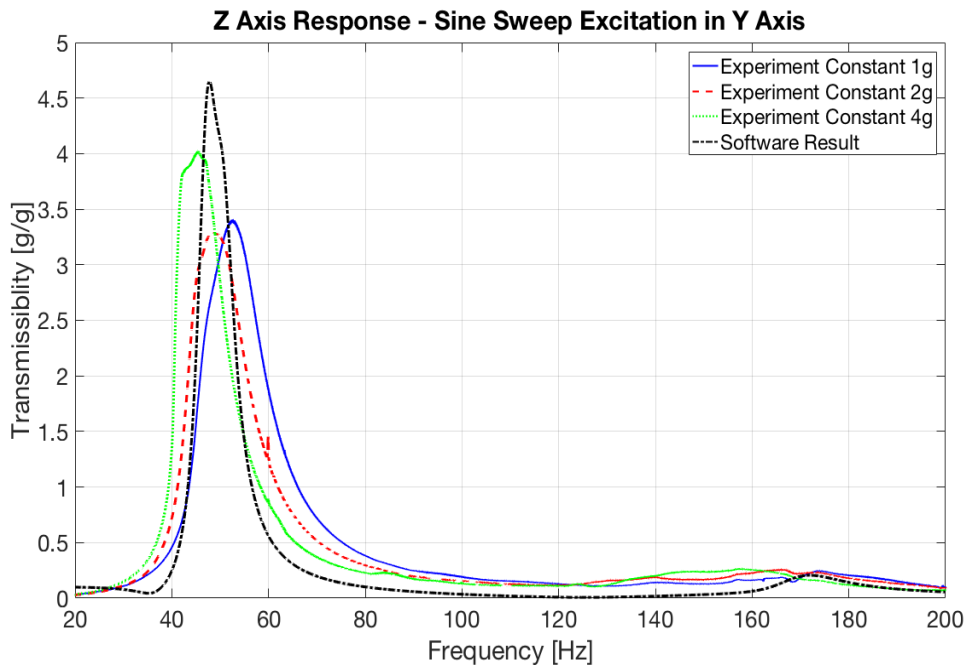


Figure 2-21 Z Axis Response – Excitation in Y Axis

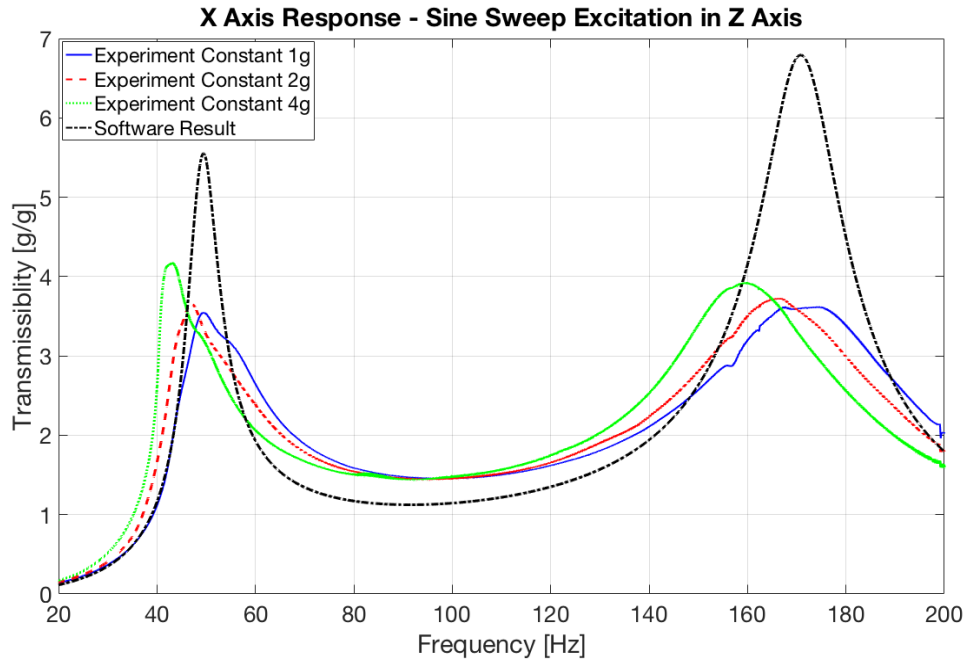


Figure 2-22 X Axis Response – Excitation in Z Axis

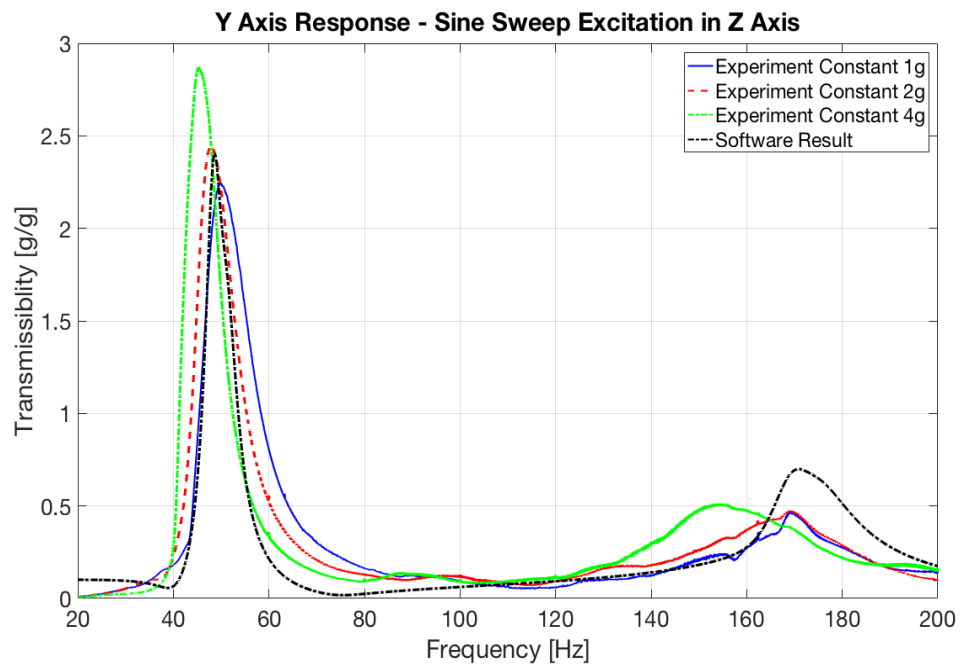


Figure 2-23 Y Axis Response – Excitation in Z Axis

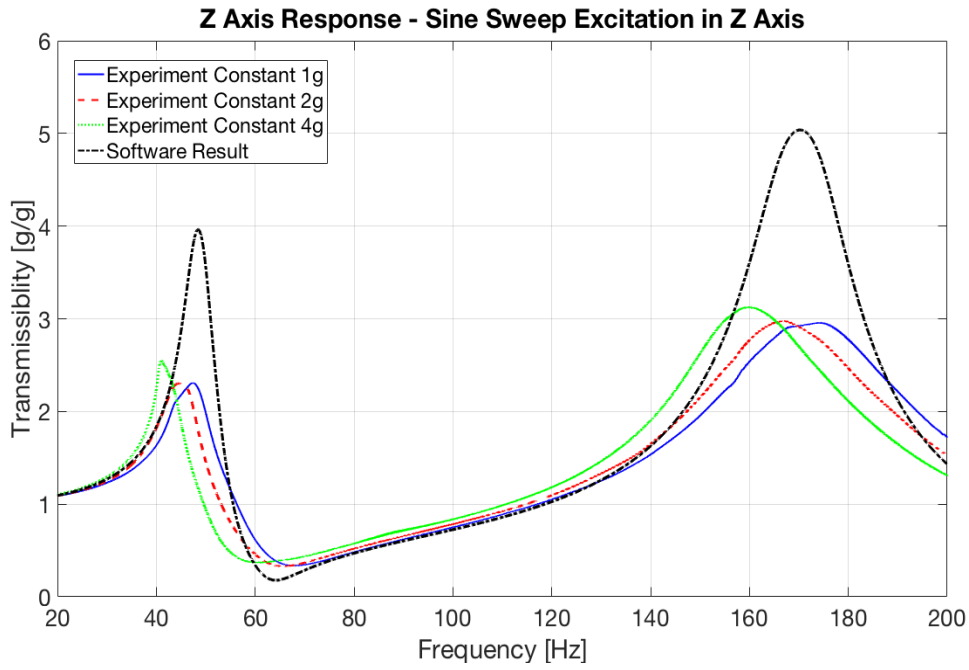


Figure 2-24 Z Axis Response – Excitation in Z Axis

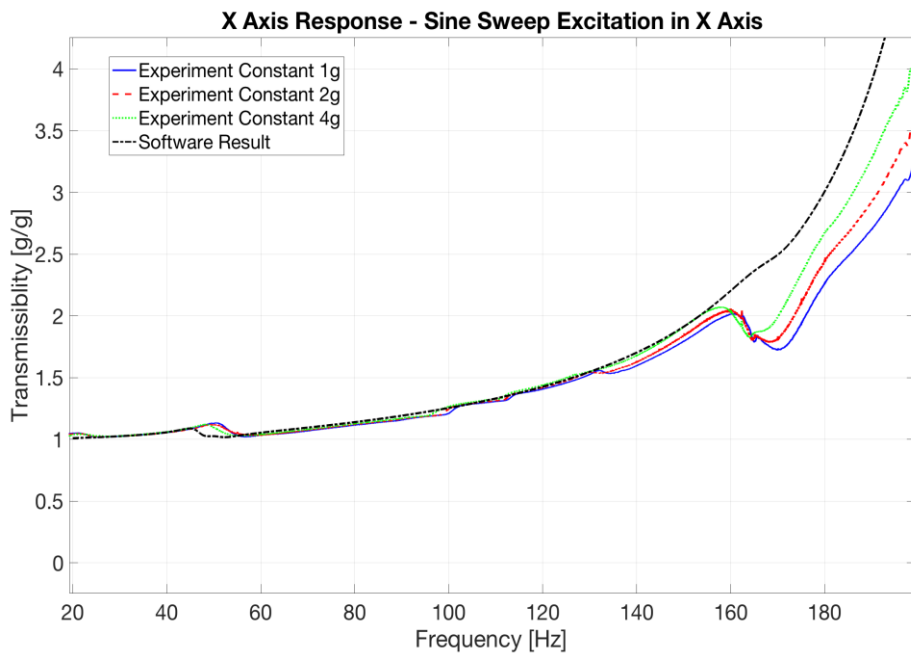


Figure 2-25 X Axis Response – Excitation in X Axis

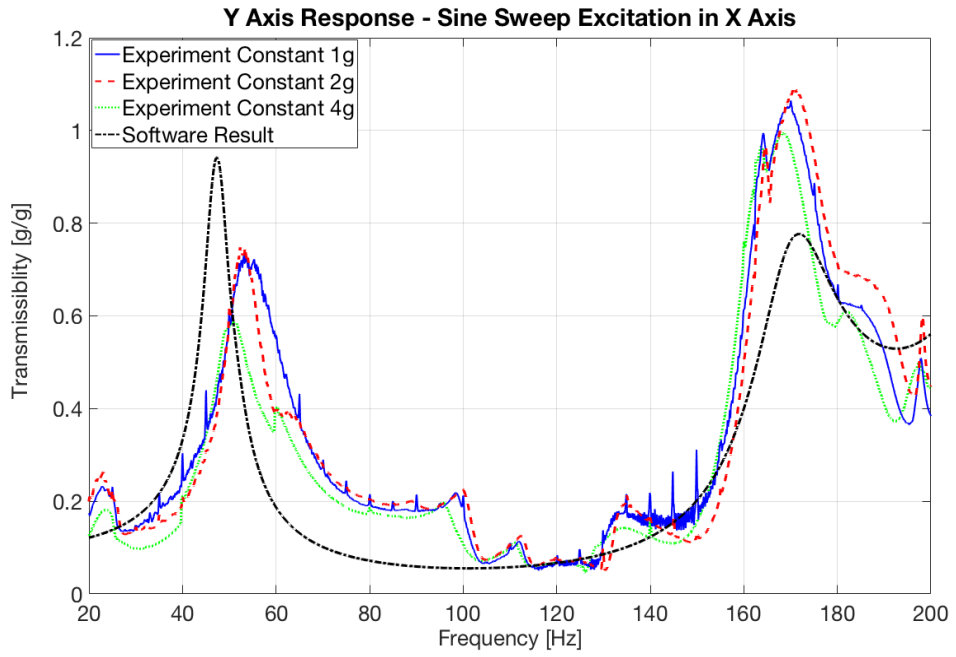


Figure 2-26 Y Axis Response – Excitation in X Axis

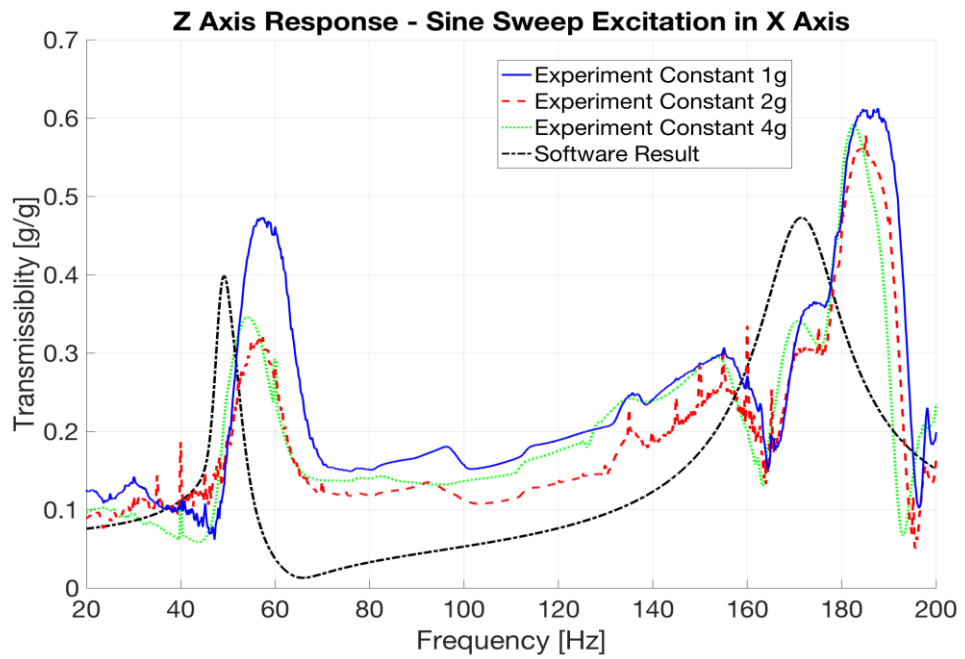


Figure 2-27 Z Axis Response – Excitation in X Axis

2.3.4 Random Vibration Analysis Verification

In order to verify the random vibration analysis, pink noise between the frequency range 20-2000 Hz is applied in 3 translational axes of the isolation prototype. The PSD acceleration excitations for software analyses are taken from the accelerometer data that is mounted on the shaker table. PSD accelerations of the C.G. are calculated then they are transformed to accelerometer mounting points. Software analysis results and experiment results are plotted Figure 2-28 to Figure 2-36. As can be seen from the figures, analysis and experiments agree well for the cases where the excitation and the measurement axes are the same. For the other cases, deviations can be explained by the assumptions and approximations that are listed in Section 2.3.3. Furthermore, at higher frequencies, internal resonances of the rubber isolator or the IMU can be seen from the response curves.

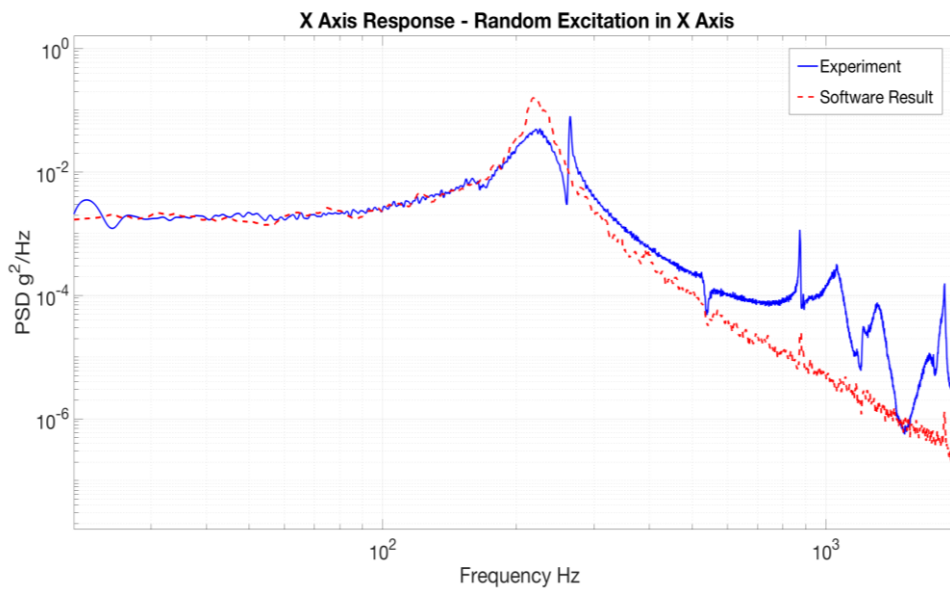


Figure 2-28 PSD Acceleration X Axis - Excitation in X Axis

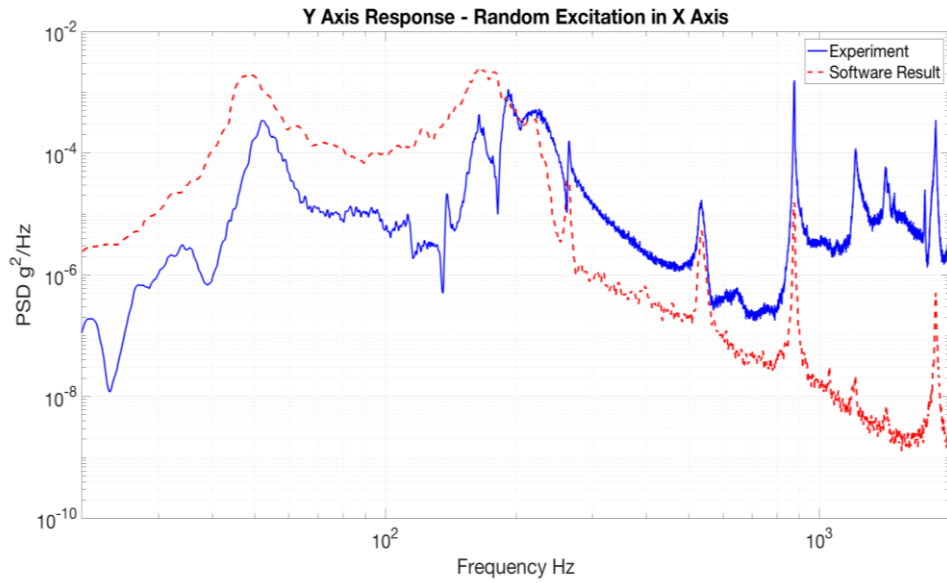


Figure 2-29 PSD Acceleration Y Axis - Excitation in X Axis

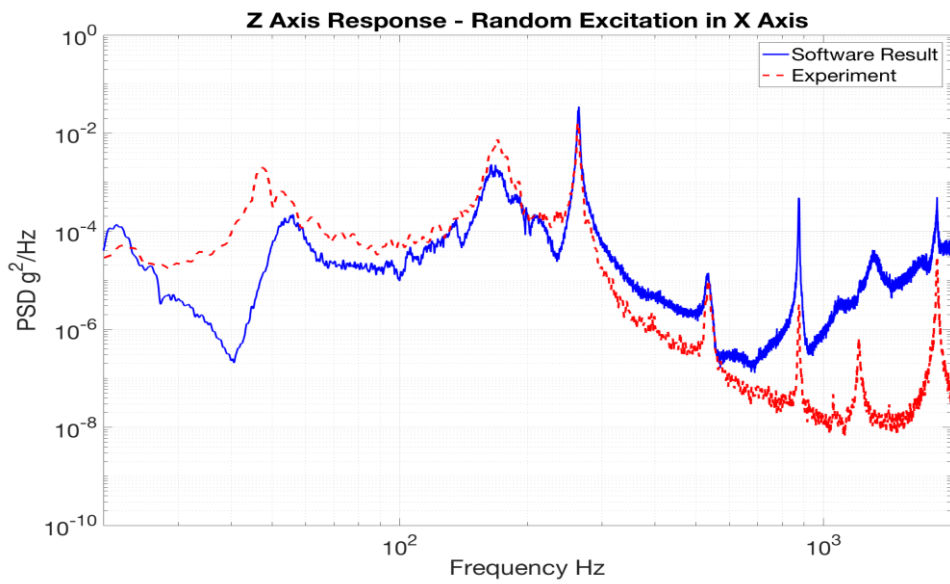


Figure 2-30 PSD Acceleration Z Axis - Excitation in X Axis

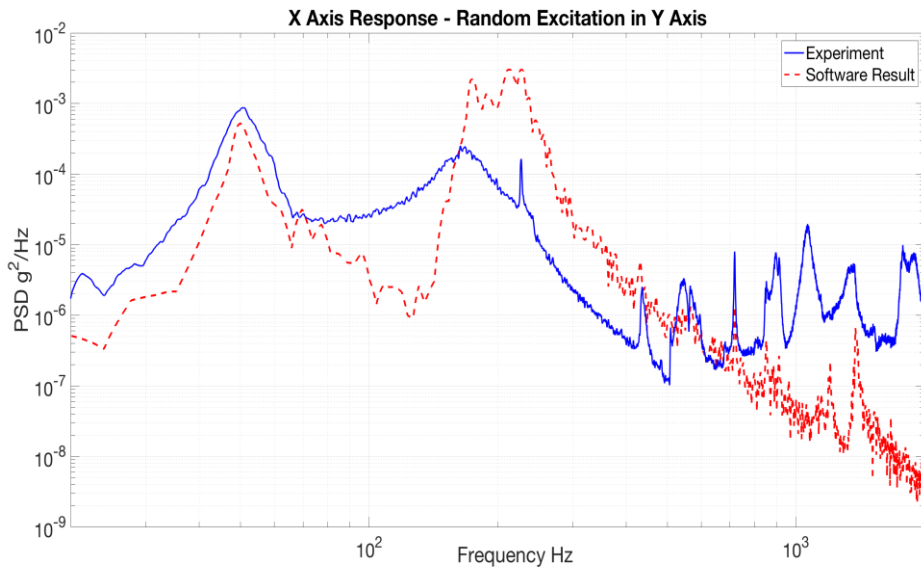


Figure 2-31 PSD Acceleration X Axis - Excitation in Y Axis

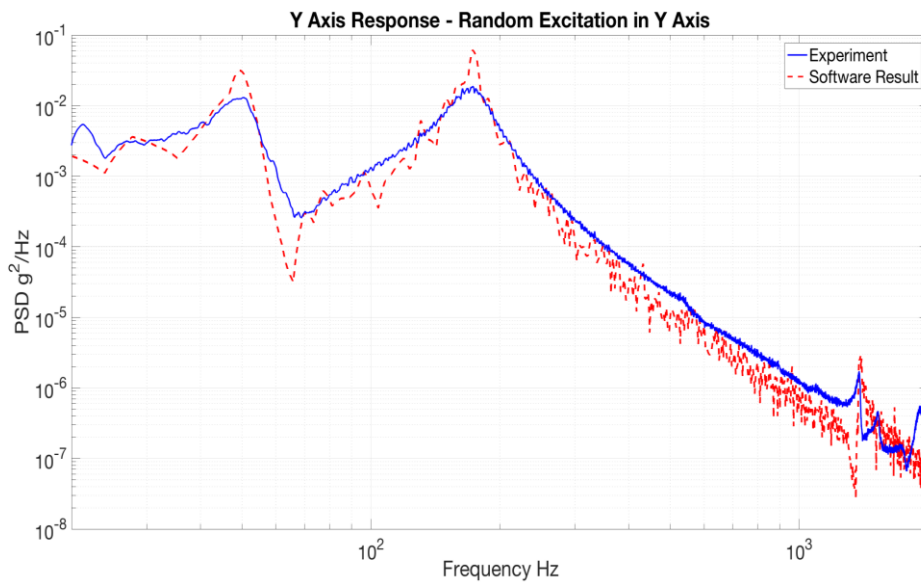


Figure 2-32 PSD Acceleration Y Axis - Excitation in Y Axis

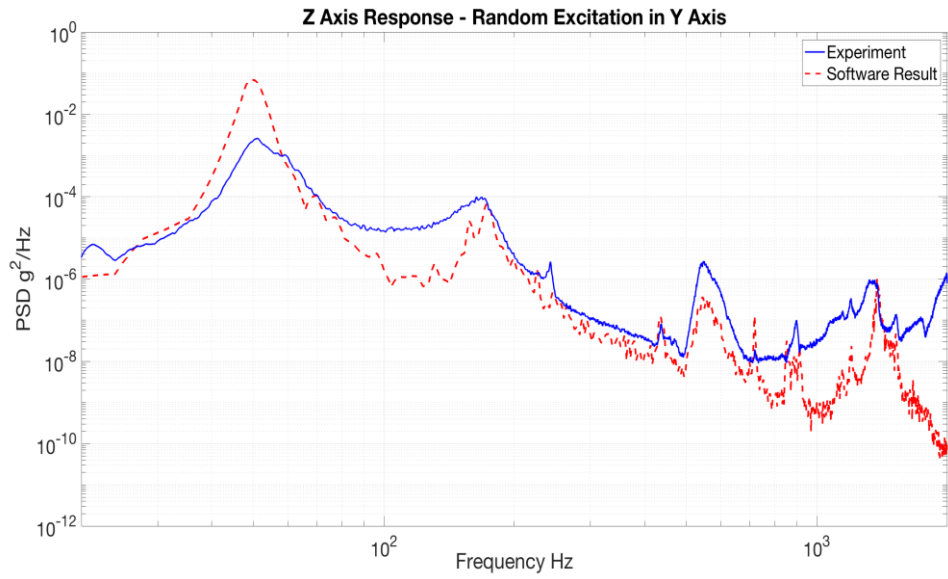


Figure 2-33 PSD Acceleration Z Axis - Excitation in Y Axis

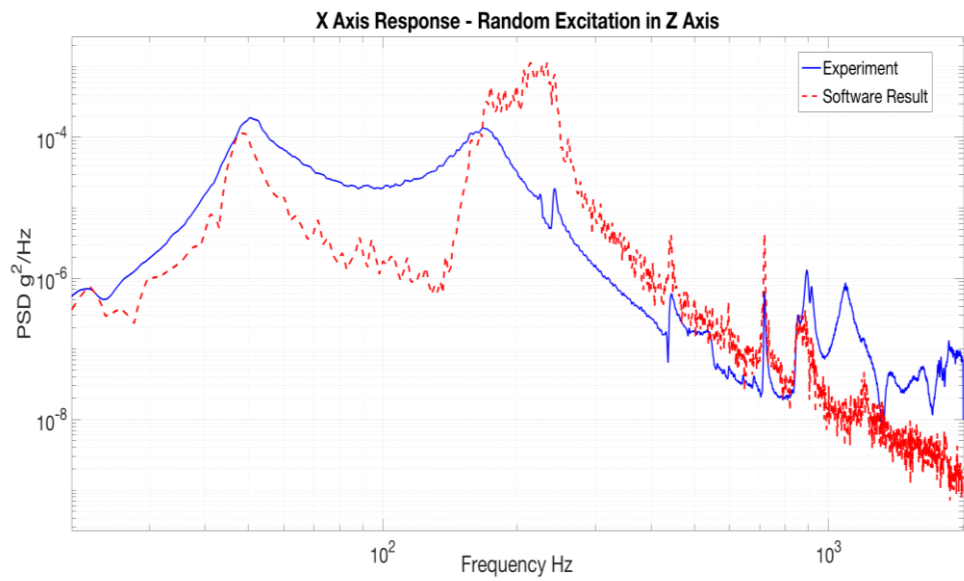


Figure 2-34 PSD Acceleration X Axis - Excitation in Z Axis

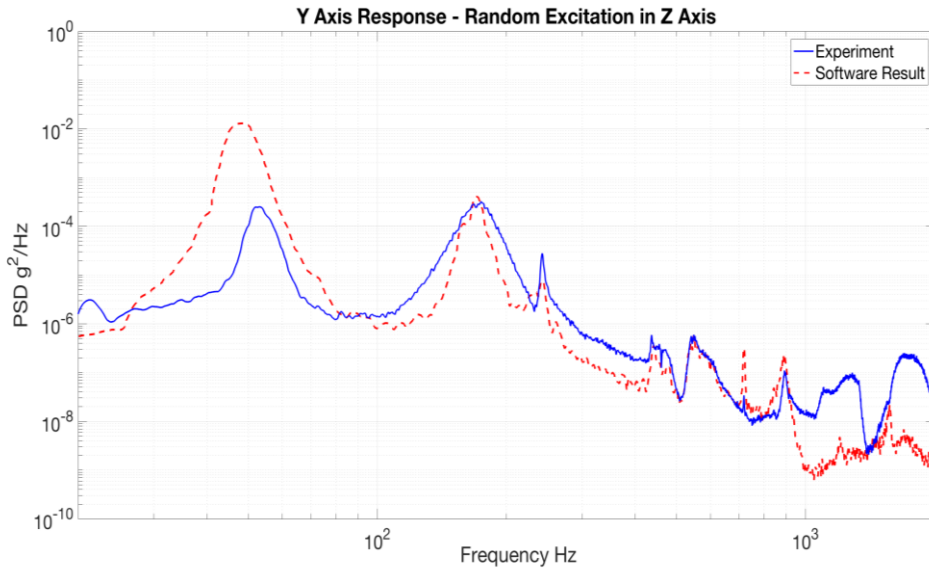


Figure 2-35 PSD Acceleration Y Axis - Excitation in Z Axis

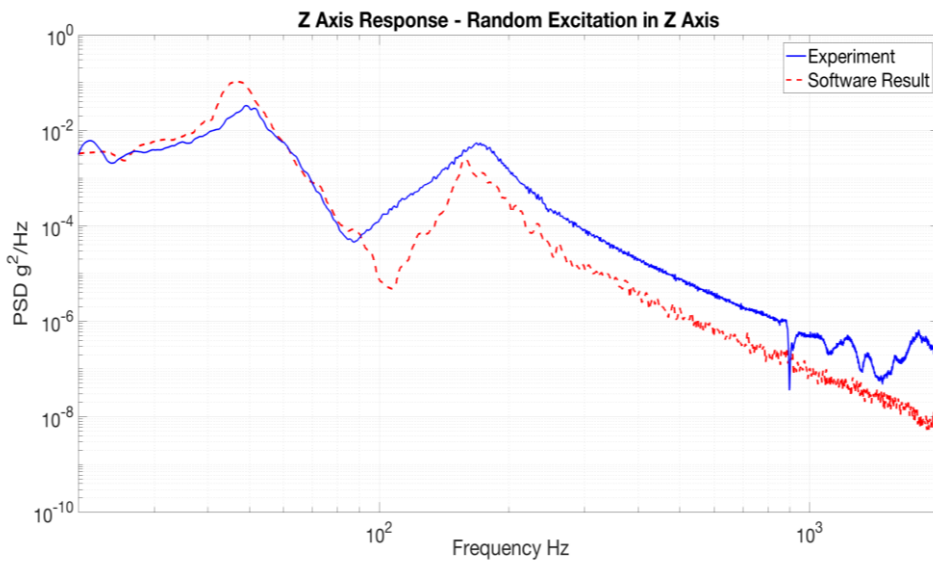


Figure 2-36 PSD Acceleration Z Axis - Excitation in Z Axis

CHAPTER 3

NONLINEAR ISOLATION SYSTEMS

The limitations of the linear isolation systems are explained in Chapter 1. In this chapter, the nonlinear elements such as “High-Static-Low-Dynamic-Stiffness”, “Nonlinear Damping” and “Dry Friction Damper” are utilized in order to improve the isolation performance.

3.1 High Static Low Dynamic Stiffness Isolators

Static deflections due to static loadings limit the isolation performance of linear vibration isolation systems. Studies on nonlinear vibration isolators show that using geometrical nonlinearities which are integrated to the system intentionally, isolator characteristic can be improved [42, 44]. Quasi-zero stiffness (QZS) mechanisms, i.e. nonlinear isolators with high static and low dynamic stiffness characteristic, are used to decrease the natural frequency of the isolation structure and improve the isolation performance of the system while having the same loading capacity [45]. However, the resulting system is highly nonlinear and unstable solutions may occur as well. Therefore, isolation performance is highly dependent on system inputs and parameters. If system input levels are not determined precisely, system response may deviate from the design limits and jump-phenomena may be observed due to the cubic stiffness nonlinearity existing in the equation of motion [59]. Another disadvantage of the quasi-zero-stiffness isolators is mistuning of the weight of the isolated system. If the weight of the isolated system deviates from its rated value, equilibrium point shifts and bias term is thus observed in the response [44]. Since the mechanism does not operate around the equilibrium point where the stiffness is very low, resonance frequency increases.

In this section, a single degree of freedom system with a nonlinear isolator having QZS mechanism is considered. The nonlinear differential equations of motion of the

isolation system are converted into a set of nonlinear algebraic equations by using harmonic balance method, which are solved by using Newton’s method with arc-length continuation.

In addition to exact nonlinear forcing expression, validation of Taylor Series expansion of forcing, which is a method widely used by many researchers, is discussed [42]. Several case studies are performed and the effect of stiffness and loading deviations on the isolation performance is studied.

3.1.1 Stiffness Model of HSLDS isolator

The stiffness properties of the HSLDS mechanism is studied in detail by Carrella [45]. The corresponding mechanism is shown in Figure 3-1. Two pre-compressed spring which are hinged at both ends are placed horizontally. These springs are defined as the “negative stiffness” since they provide force in the direction of the motion. Although all of the components are linear, the forcing is nonlinear because of the kinematic relation between the force and displacement.

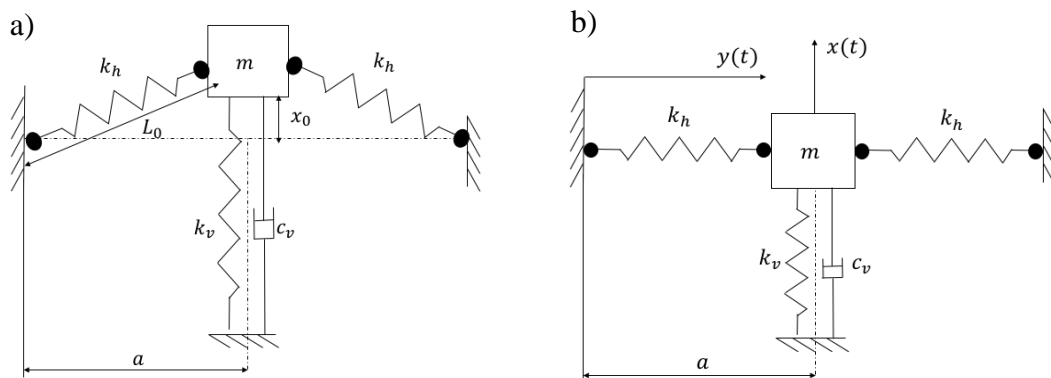


Figure 3-1 Nonlinear isolator with negative stiffness mechanism (a) initial unloaded state (b) equilibrium point

When the system at the equilibrium position, the vertical component of the compressed springs is zero Figure 3-1b. k_h is the parameter of the “horizontal springs and k_v, c_v are the parameters of the vertical spring and damper. The distance between the two ends of the horizontal elements is $y(t)$; the free length of

the horizontal spring is L_0 ; length of the horizontal spring at equilibrium point is a . The free body diagram of the mass for the static loadings can be seen in Figure 3-2.

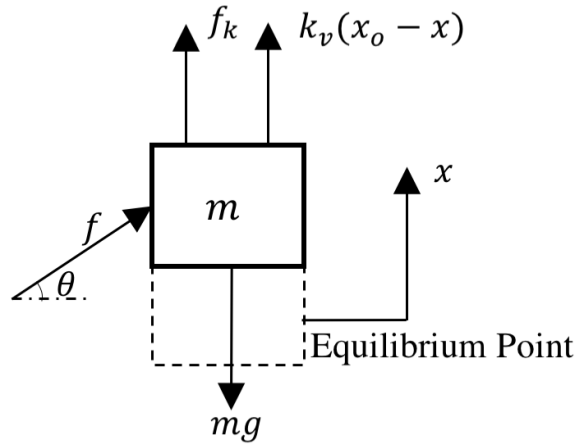


Figure 3-2 Free Body Diagram of the Mass

When loading f_k is applied to the mass, it will deflect from its equilibrium point. The amount of deflection is defined as x . The vertical force component of the horizontal springs can be found as follows [40, 82].

$$f_v = f \sin \theta = 2k_h(L_0 - y) \frac{x}{\sqrt{x^2 + a^2}}. \quad (3-1)$$

The relationship between the vertical displacement of the mass and the distance between two ends of the horizontal dashpots is given as

$$y(t) = \sqrt{x^2 + a^2}. \quad (3-2)$$

Considering the vertical spring and payload, the total vertical force created by the spring elements can be obtained as

$$mg = f_k + 2k_h \left(\frac{L_0}{\sqrt{x^2 + a^2}} - 1 \right) x + k_v (x_0 - x), \quad (3-3)$$

where $x_0 = \sqrt{L_0^2 + a^2}$. Assuming $mg = k_v x_0$, the non-dimensional form can be obtained as

$$\frac{f_k}{k_v a} = \left(\gamma \left(1 - \frac{\delta}{\sqrt{\hat{x}^2 + 1}} \right) + 1 \right) \hat{x}, \quad (3-4)$$

where $\delta = L_0/a$, $\gamma = 2k_h/k_v$, $\hat{x} = x/a$.

The effect of non-dimensional parameters can be seen in Figure 3-3 and Figure 3-4. From Figure 3-3, it can be concluded that increase of L_0/a ratio may result in even overall negative stiffness around the equilibrium point. Likely, if stiffer horizontal springs relative to vertical ones are placed, effect of negative stiffness becomes more dominant and overall negative stiffness may be obtained (Figure 3-4). The quasi zero stiffness characteristic can be obtained by proper selection of δ and γ . The stiffness can be obtained by differentiating the non-dimensional force displacement equation with respect to $\hat{x} = x/a$ as follows

$$k(\hat{x}) = \gamma \left(1 - \frac{\delta}{\sqrt{\hat{x}^2 + 1}} \right) + 1. \quad (3-5)$$

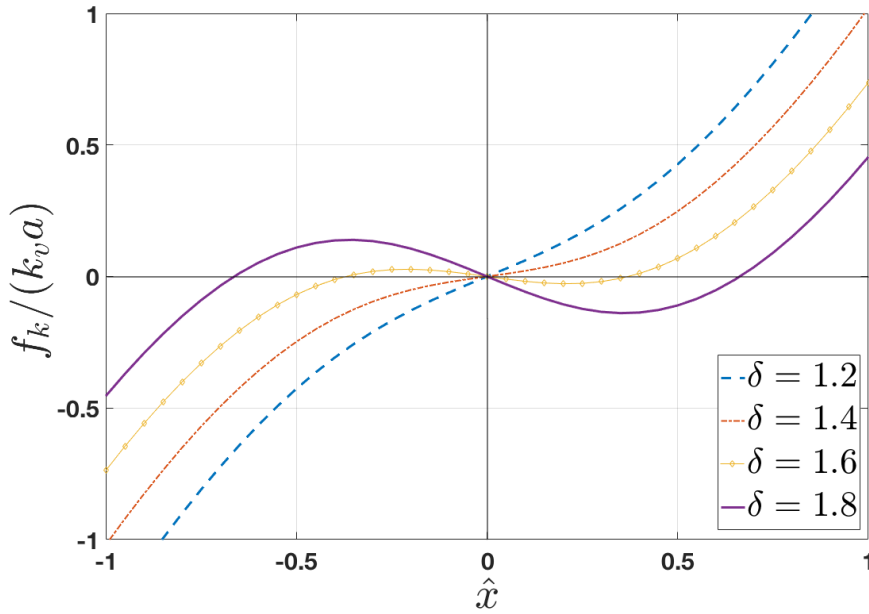


Figure 3-3 Effect of δ on nonlinear stiffness

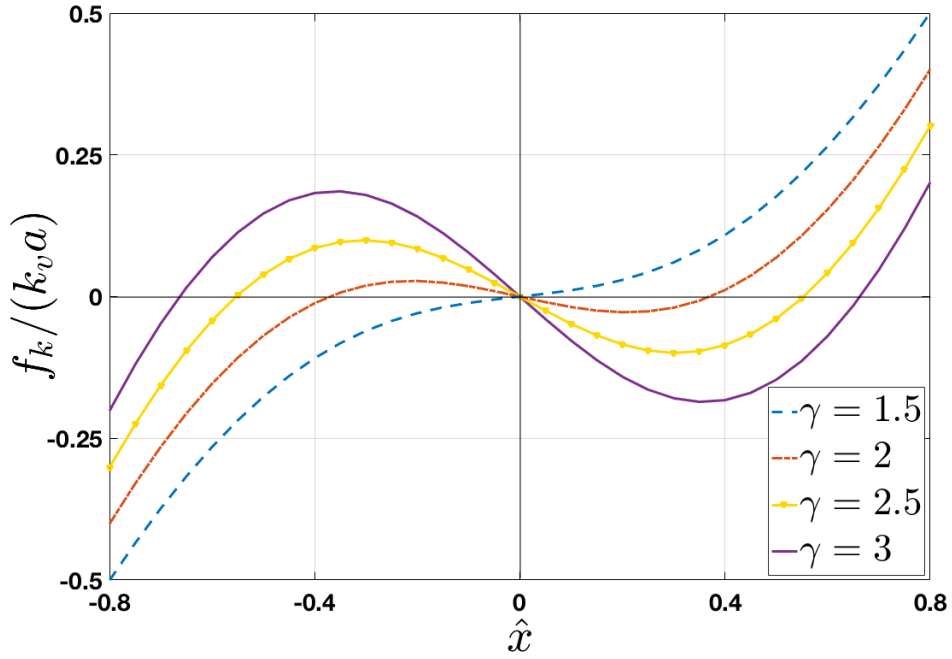


Figure 3-4 Effect of γ on nonlinear stiffness

Equation (3-1) can be expanded by using Taylor series around equilibrium point [40].

$$f_k(x) = 2k_h \left(1 - \frac{L_o}{\sqrt{x^2 + a^2}}\right) x + k_v(x), \quad (3-6)$$

$$f_k^{app}(x) = \sum_{n=0}^{\infty} \frac{f^n(0)}{n!} x^n, \quad (3-7)$$

$$f_k^{app}(x) = \left(k_v + 2k_h \left(1 - \frac{L_o}{a}\right)\right) x + \frac{1}{2} \frac{2k_h L_o}{a^3} x^3 - \frac{3}{8} \frac{2k_h L_o}{a^5} x^5 + \frac{5}{16} \frac{2k_h L_o}{a^7} x^7 + O(x^9), \quad (3-8)$$

where f_k^{app} is the Taylor Series Expansion of the loading f_k . In the non-dimensional form,

$$\frac{f_k^{app}(x)}{k_v a} = (1 + \gamma(1 - \delta))\hat{x} + \frac{1}{2}\gamma\delta\hat{x}^3 - \frac{3}{8}\gamma\delta\hat{x}^5 + \frac{5}{16}\gamma\delta\hat{x}^7 + O(\hat{x}^9). \quad (3-9)$$

The exact nonlinear spring force and the Taylor Series expansion comparison can be seen in Figure 3-5.

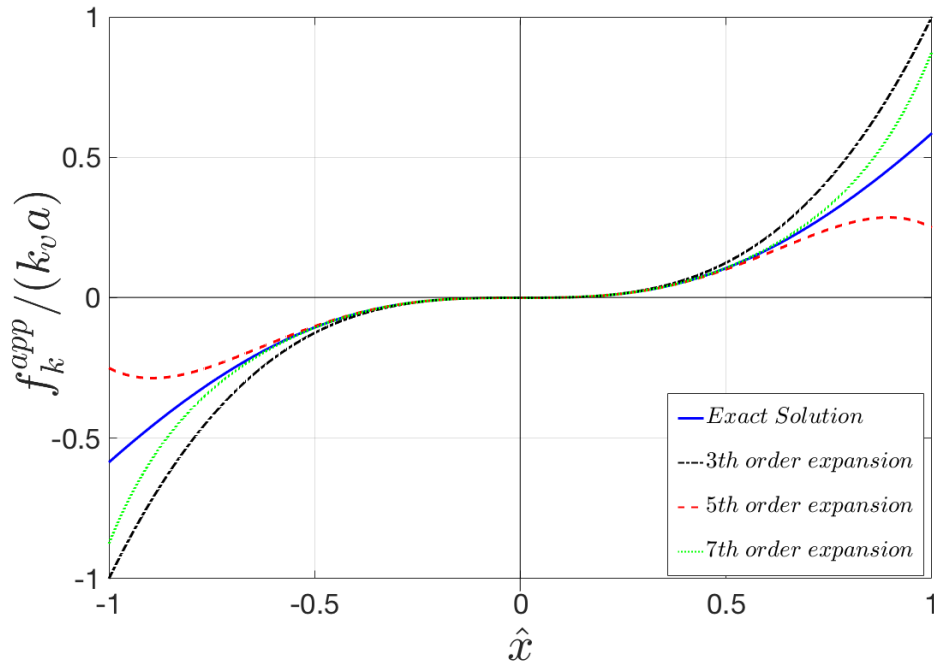


Figure 3-5 Taylor Series Expansion of QZS Isolator

If the QZS condition is satisfied, non-dimensional stiffness $\hat{k}(\hat{x})$ is equal to zero. Then,

$$\gamma(1 - \delta) + 1 = 0. \quad (3-10)$$

Taylor Series Expansion can be reduced to following form,

$$\frac{f(x)}{k_v a} = \gamma\delta\hat{x}^3 - \frac{3}{8}\gamma\delta\hat{x}^5 + \frac{5}{16}\gamma\delta\hat{x}^7 + O(\hat{x}^9). \quad (3-11)$$

3.1.2 Response to Base Excitation

For a single mass, isolated by a nonlinear isolator the equation of motion can be obtained as

$$m\ddot{x} + c\dot{x} + k_v(x - x_0) + 2k_h \left(1 - \frac{L_0}{\sqrt{u^2 + a^2}}\right)u = c\dot{z}(t) + k_v z(t) - mg, \quad (3-12)$$

where $u(t)$ is the relative displacement defined as $u(t) = x(t) - z(t)$. The isolator model for the base excitation is shown in Figure 3-6.

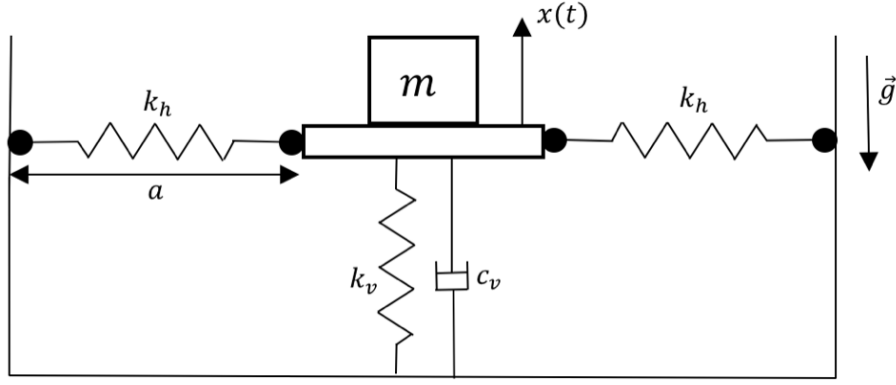


Figure 3-6 Base Excitation Model

For a single harmonic base input as $z(t) = Z \sin(\omega t)$, the response of the mass can as well be assumed harmonic in the following form $x(t) = X_0 + X_s \sin(\omega t) + X_c \cos(\omega t)$ by utilizing a single harmonic representation. If the expression, $k_v x_0 = mg$, is satisfied, then there is no bias term ($X_0 = 0$) at the response. In the following sections, the effect of stiffness and loading deviations, which makes the nonlinearity asymmetric, is investigated. Thus, the response is written in general form containing bias term. Similarly, the relative motion can be written in the following form

$$u(t) = U_0 + U \sin(\omega t + \phi) = U_0 + U \sin(\psi). \quad (3-13)$$

where, U_0 is the bias term in the relative displacement response, U is the amplitude of relative displacement response. For ease of calculation, $\omega t + \phi$ is represented as ψ . By using a single harmonic Fourier Series representation, the nonlinear forcing can be written as follows

$$f_n = f_{n0} + f_{ns} \sin(\omega t + \phi) + f_{nc} \cos(\omega t + \phi), \quad (3-14)$$

$$f_n = f_{n0} + (f_{ns} \cos \phi + f_{nc} \sin \phi) \sin(\omega t) + (f_{nc} \cos \phi + f_{ns} \sin \phi) \cos(\omega t). \quad (3-15)$$

where f_n is the single harmonic representation of the nonlinear forcing, f_{n0} is the bias terms, f_{ns} and f_{nc} are the sine and cosine Fourier Coefficients respectively. In order to validate Taylor Series Expansion, Fourier coefficients of both exact nonlinear forcing and Taylor Series representation of forcing are calculated. By

using the exact nonlinear forcing expression, Fourier coefficients can be calculated as

$$f_{n0} = \frac{1}{2\pi} \int_0^{2\pi} (F_{nl_s}) d\psi, \quad (3-16)$$

$$f_{nc} = \frac{1}{\pi} \int_0^{2\pi} (F_{nl_s}) \cos(\psi) d\psi, \quad (3-17)$$

$$f_{ns} = \frac{1}{\pi} \int_0^{2\pi} (F_{nl_s}) \sin(\psi) d\psi. \quad (3-18)$$

where F_{nl_s} is total vertical stiffness force and the exact forcing is given by

$$F_{nl_s} = 2k_h \left(1 - \frac{L_o}{\sqrt{(U_0 + U \sin(\psi))^2 + a^2}} \right) (U_0 + U \sin(\psi)). \quad (3-19)$$

By using Taylor Series Expansion defined in (3-9), nonlinear forcing can be approximated as follows

$$F_{nl_s}^{app} = a_3(U \sin(\psi))^3 + a_5(U \sin(\psi))^5 + a_7(U \sin(\psi))^7, \quad (3-20)$$

where $a_3 = \frac{k_h L_o}{a^3}$, $a_5 = -\frac{3}{4} \frac{k_h L_o}{a^5}$, $a_7 = \frac{5}{8} \frac{k_h L_o}{a^7}$. Analytical solutions can be obtained using Taylor Series expansion for no bias ($X_0 = 0$) and QZS ($\gamma(1 - \delta) + 1 = 0$) conditions. For the case in which nonlinear exact forcing formulation is used, Fourier Coefficients are calculated by numerical integration. Analytical solutions of approximate Fourier Coefficients are given by

$$f_{nc} = \frac{2}{\pi} \int_0^{\pi} (a_3(U \sin(\psi))^3 + a_5(U \sin(\psi))^5 + a_7(U \sin(\psi))^7) \cos(\psi) d\psi, \quad (3-21)$$

$$f_{ns} = \frac{2}{\pi} \left(\int_0^{\pi} (a_3(U \sin(\psi))^3 + a_5(U \sin(\psi))^5 + a_7(U \sin(\psi))^7) \sin(\psi) d\psi \right). \quad (3-22)$$

Integrals can be evaluated as

$$f_{nc} = 0, \quad (3-23)$$

$$f_{ns} = \frac{3}{4} a_3 U^3 + \frac{5}{16} a_5 U^5 + \frac{35}{64} a_7 U^7. \quad (3-24)$$

Then, nonlinear differential equation of motion, Equation (3-12) can be converted in to set of nonlinear algebraic equations by using Harmonic Balance Method (HBM) [83] and the resulting nonlinear algebraic equations of motion can be obtained as follows

$$R(x, \omega) = \begin{bmatrix} k_v & 0 & 0 \\ 0 & k_v - \omega^2 m & -c_v \omega \\ 0 & c_v \omega & k_v - \omega^2 m \end{bmatrix} \begin{Bmatrix} X_o \\ X_s \\ X_c \end{Bmatrix} + \begin{Bmatrix} f_{no} \\ f_{ns} \\ f_{nc} \end{Bmatrix} - \begin{Bmatrix} k_v x_0 - mg \\ k_v Z \\ c_v \omega Z \end{Bmatrix} = 0, \quad (3-25)$$

where $R(x, \omega)$ is the nonlinear vector function, x is the vector of unknowns and $x_0 = \sqrt{L_0^2 - a^2}$. As stated before, Equation (3-25) is written in general form containing bias term. However, if the condition, $k_v x_0 = mg$ is satisfied, then X_o, f_{no} are equal to zero.

The solution of the resulting set of nonlinear algebraic equations is obtained by utilizing Newton's method with arc-length continuation in order to follow the solution path even it reverses its direction. The additional arc-length equation is defined as follows which represents as an n-dimensional sphere in which the solution is sought

$$h(q_k) = \Delta q_k^T \Delta q_k - s^2 = 0. \quad (3-26)$$

Here $q_k = \{x_k \quad \omega_k\}^T$, $\Delta q_k = q_k - q_{k-1}$, k corresponds to the k^{th} solution point and s is the radius of the hypothetical sphere. A single step of Newton's iteration with arc-length continuation can be given as

$$q_k^{i+1} = q_k^i - \begin{bmatrix} \frac{\partial R(q_k^i)}{\partial x} & \frac{\partial R(q_k^i)}{\partial \omega} \\ \frac{\partial h(q_k^i)}{\partial x} & \frac{\partial h(q_k^i)}{\partial \omega} \end{bmatrix}^{-1} \begin{Bmatrix} R(q_k^i) \\ h(q_k^i) \end{Bmatrix}. \quad (3-27)$$

where i is the number of iterations. Details of the solution method can be found in [84, 85]

3.1.3 Stability of steady state solutions

Since it is a vibration isolation problem, stability of the solution is important parameter for the isolation performance. Especially, if the system to be isolated is a measurement device, the instability of the solution may result in chaotic measurements. Periodic solutions can be found by HBM. However, it doesn't provide any information about stability of the solution. Stability of the solution can be found by Hill's Method which is based on the Floquet Theory. Below eigenvalue problem can be used to obtain Floquet exponentials which contains information about stability of the solution [86, 87, 88]

$$\left(\frac{\partial R}{\partial x} + \lambda \Delta_1 + \lambda^2 \Delta_2\right) \phi = 0, \quad (3-28)$$

where ϕ is the complex Eigenvector, $\frac{\partial R}{\partial x}$ is the Jacobian Matrix. Δ_1 and Δ_2 are defined following as

$$\Delta_1 = \text{diag} \left(\begin{bmatrix} 2\omega m & c \\ c & -2\omega m \end{bmatrix}, \dots, \begin{bmatrix} 2H\omega m & c \\ c & -2H\omega m \end{bmatrix} \right), \quad (3-29)$$

$$\Delta_2 = I_{2H} \otimes m. \quad (3-30)$$

H is number harmonics and \otimes is Kronecker tensor product. Since Jacobian $\frac{\partial R}{\partial x}$ is already available, one can obtain complex eigenvalues λ_i . Assume that for single harmonic solution, Jacobian is given by

$$\frac{\partial R}{\partial x} = \begin{bmatrix} a_{11} & a_{12} \\ a_{21} & a_{22} \end{bmatrix}. \quad (3-31)$$

Then determinant is given by

$$\begin{aligned} &\lambda^4 m^2 + \lambda^2 (a_{11} m - 4m^2 \omega^2 m a_{22} - c^2) \\ &\quad + \lambda (-2a_{11} \omega m + 2\omega m a_{22} - a_{12} c - c a_{21}) \\ &\quad + a_{11} a_{22} - a_{12} a_{21} = 0. \end{aligned} \quad (3-32)$$

As stated in the [88], only two complex eigenvalues λ which have smallest imaginary parts are corresponds to Floquet exponents. The limit point should satisfy the below conditions,

$$\det\left(\frac{\partial R}{\partial x}\right) = 0 \text{ and } \left(\frac{\partial R}{\partial x}\right)^T \boldsymbol{\phi} \neq 0. \quad (3-33)$$

Stability of the solution can be determined by checking whether real part of the λ_i is positive or not. Therefore, condition for the stability follows that

$$Re(\lambda_i) < 0 \quad i = 1, 2. \quad (3-34)$$

3.1.4 Validation of Taylor Series Expansion

As stated in Section 3.1.1, assuming relatively small oscillations, Taylor Series representation can be used to evaluate integrals analytically. In literature, there are variety of studies which approximates the QZS nonlinear forcing as 3th order polynomial [71]. Shaw considered 5th order polynomial in his study for representation of QZS system [53]. In this section frequency response functions obtained by 3th, 5th and 7th order polynomials and numerical integration method are compared to obtain valid parameter range for the Taylor Series Expansion. The parameter set that is given by Table 2-5 is used for the validation of the solution. 3th order polynomial solution is obtained by setting $a_5 = 0, a_7 = 0$. Likely, 5th order polynomial solution is obtained by setting $a_7 = 0$.

Table 3-1 Parameter Set Used in Analyses

$m = 1 \text{ kg}$	$k_v = 20\,000 \text{ N/m}$
$k_h = 10\,000 \text{ N/m}$	$a = 0.08 \text{ m}$
$L_o = 0.016 \text{ m}$	$\xi_v = 0.015$

where $\xi_v = \frac{c}{2\sqrt{k_v m}}$, $\omega_o = \sqrt{\frac{k_v}{m}}$, $\Omega = \frac{\omega}{\omega_o}$ and ω is excitation frequency.

Frequency response functions can be seen in Figure 3-7, Figure 3-8 and Figure 3-9. As can be seen in Figure 3-7, 3th order polynomial approximation starts to deviate as base excitation increases. 3th order expansion starts to deviate $\hat{Z} = 0.035$ while 5th and 7th order expansions give accurate result up to $\hat{Z} = 0.045$.

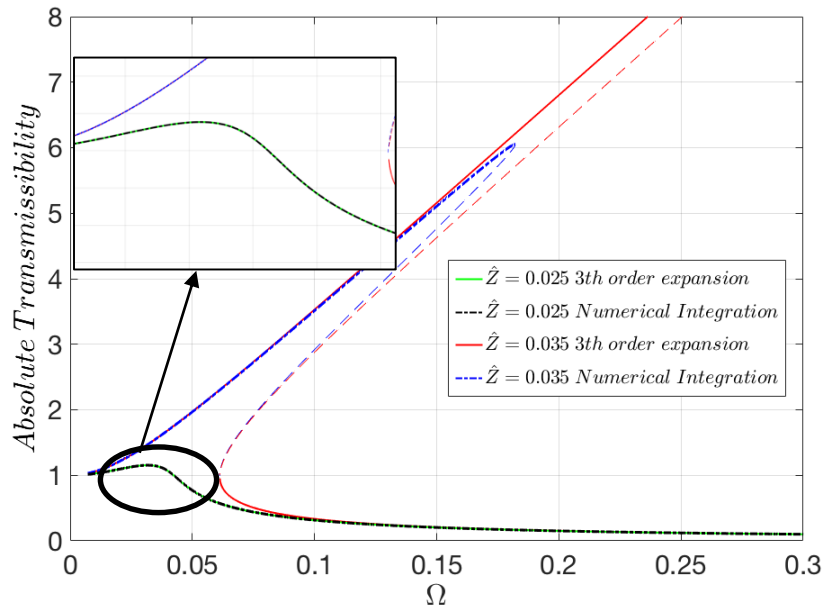


Figure 3-7 Comparison of Taylor Series Expansion and numerical integration ‘ - - ‘:unstable solutions ‘ -.- ‘ Taylor Series ‘ - ‘ Numerical Integration, 3th order approximation

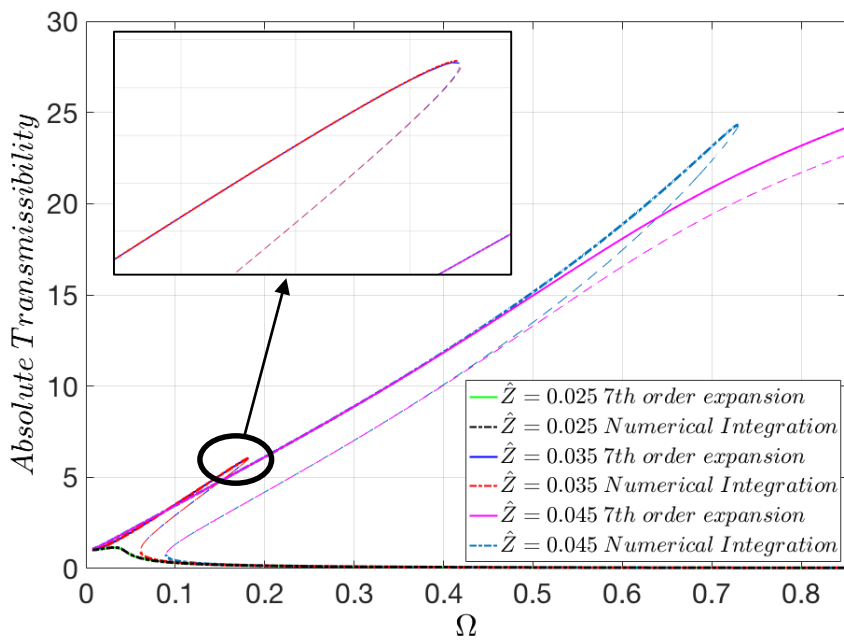


Figure 3-8 Comparison of Taylor Series Expansion and numerical integration ‘ - - ‘:unstable solutions ‘ -.- ‘ Taylor Series ‘ - ‘ Numerical Integration, 5th order approximation

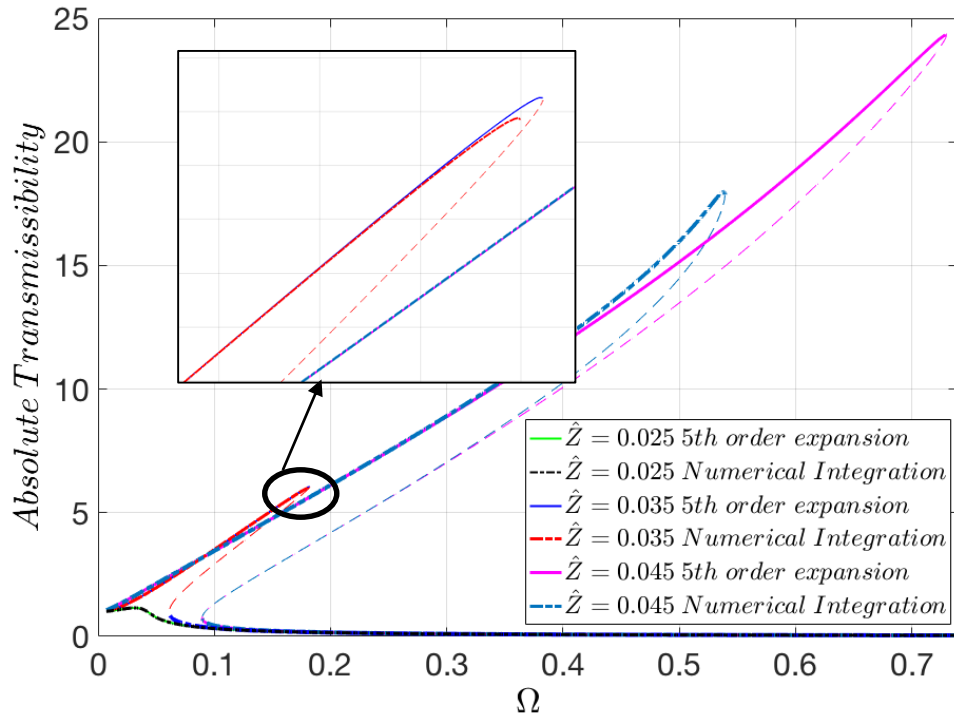


Figure 3-9 Comparison of Taylor Series Expansion and numerical integration ‘- - ‘:unstable solutions ‘-.-‘ Taylor Series ‘-‘ Numerical Integration, 7th order approximation

Accuracy of the frequency response functions of the Taylor Series expansion depends not only base excitation but also vertical damping. To map the effect of base excitation and vertical damping coefficient, error is defined as

$$E[\%] = \frac{\max(|FRF_{Taylor\ Series}|)}{\max(|FRF_{Numeric\ Integration}|)} \quad (3-35)$$

The results are tabulated at Table 3-2-3. It can be concluded that 5th order representation provides more accurate results for greater damping coefficient and base excitation range.

Table 3-2 Error Values of 3th Order Taylor Series Expansion

Error [%]	$\xi_v = 0.015$	$\xi_v = 0.017$	$\xi_v = 0.02$	$\xi_v = 0.022$
$\hat{Z} = 0.030$	0.0569	0.036	~0	~0
$\hat{Z} = 0.034$	5.548	0.071	0.001	~0
$\hat{Z} = 0.036$	> 100	0.287	0.009	~0
$\hat{Z} = 0.040$	> 100	> 100	0.1	~0.014

Table 3-3 Error Values of 5th Order Taylor Series Expansion

Error [%]	$\xi_v = 0.015$	$\xi_v = 0.017$	$\xi_v = 0.02$	$\xi_v = 0.022$
$\hat{Z} = 0.030$	~0	~0	~0	~0
$\hat{Z} = 0.035$	1.27	~0	~0	~0
$\hat{Z} = 0.040$	15.37	2.18	~0	~0
$\hat{Z} = 0.060$	46.69	38.59	26.07	17.51
$\hat{Z} = 0.080$	61.15	55.41	46.57	40.52

Table 3-4 Error Values of 7th Order Taylor Series Expansion

Error [%]	$\xi_v = 0.015$	$\xi_v = 0.017$	$\xi_v = 0.02$	$\xi_v = 0.022$
$\hat{Z} = 0.030$	~0	~0	~0	~0
$\hat{Z} = 0.035$	0.0484	~0	~0	~0
$\hat{Z} = 0.043$	> 100	4.87	~0	~0
$\hat{Z} = 0.045$	> 100	> 100	0.0084	~0
$\hat{Z} = 0.055$	> 100	> 100	> 100	3.25

3.1.5 Effect of QZS Isolation System

In order to satisfy the QZS condition, stiffness at the equilibrium point must be equal to zero as can be seen from the Equation (3-5). The non-dimensional parameters, which are defined in Equation (3-4), are taken as $\delta = 2, \gamma = 1, \xi_v = 0.015$. Different base excitations with different amplitudes are applied to the

nonlinear isolator which satisfies the quasi-zero-stiffness condition. The frequency response function (FRF) is given in Figure 3-10. As the base excitation amplitude increases, FRF bends towards higher frequencies due to the cubic stiffness effect of the QZS mechanism. The adverse effect of the QZS mechanism can be eliminated by increasing damping in the system. However, increasing the linear damping affects the isolation region adversely [2].

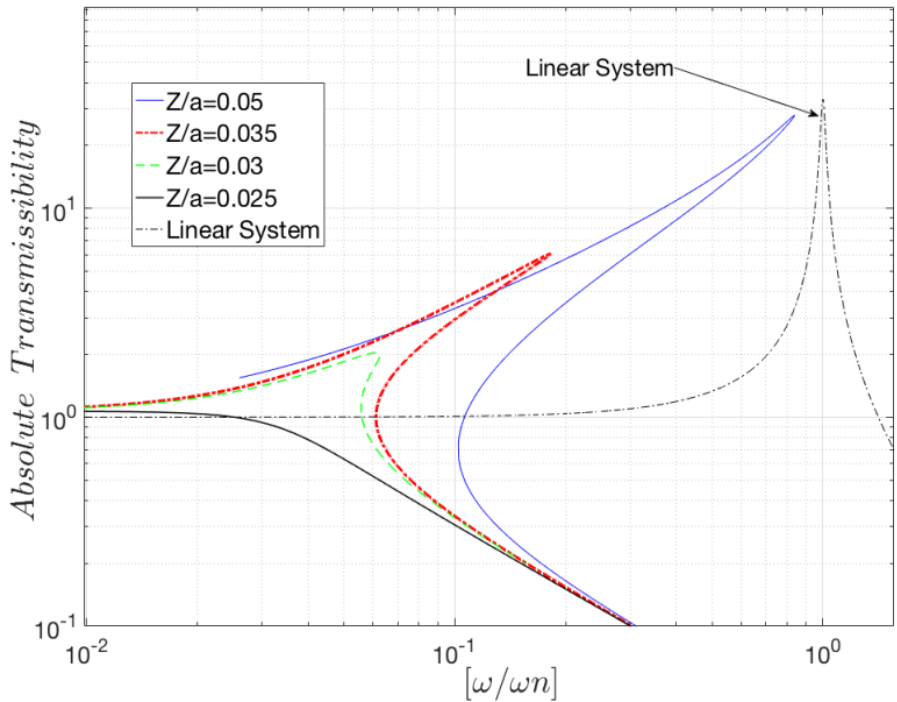


Figure 3-10 Effect of QZS Mechanism and nonlinear damping $\delta = 2$, $\gamma = 1$, $\xi_v = 0.015$

3.1.6 Load and Stiffness Deviation

Load and stiffness of the isolation system can be deviated from the design values. These can be due to parameter uncertainties and/or due to the constant acceleration of the base which can be observed in aircraft platforms. Therefore, the load on the isolation system deviates and equilibrium points shifts from the point where $x = 0$. This results in bias term in the Equation (3-13) and affects the isolation performance adversely. The absolute transmissibility curve for different normalized

deadweights is shown in Figure 3-11, where \hat{w} is the ratio of actual weight to design weight. It is observed that even slight deviations in weight result in an increase of the resonance amplitudes. The bias term of the response also increases due to deviation of the isolation weight which is shown in Figure 3-12.

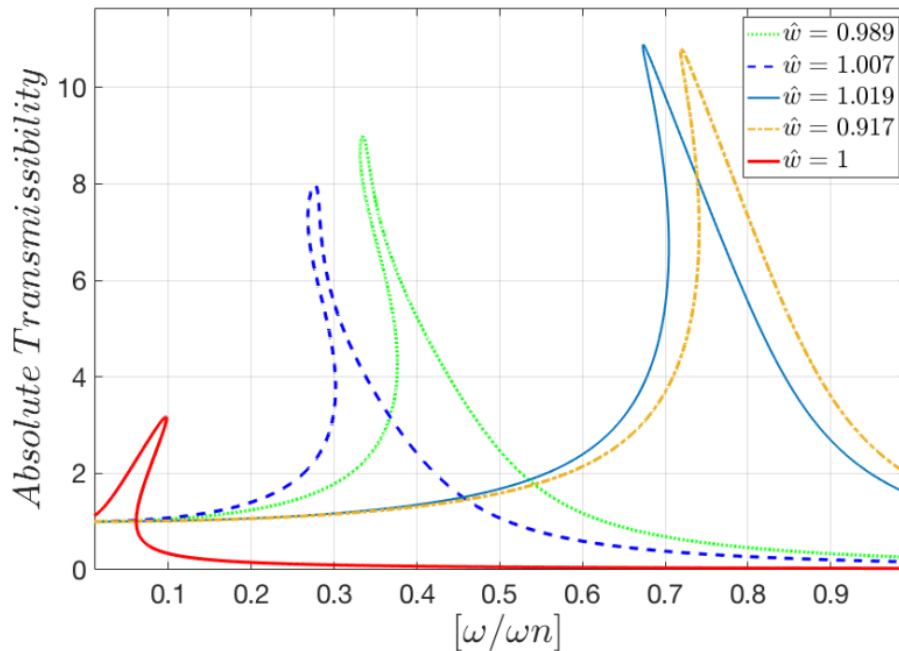


Figure 3-11 Effect of Load Deviations- Absolute Transmissibility $\delta = 2$, $\gamma = 1$,
 $\xi_v = 0.015, Z/a = 0.035$

The horizontal stiffness of the system may vary from its design value due to manufacturing errors and environmental conditions as a result of which the isolation performance may change as well. Absolute transmissibility function curves for different $\gamma = 2k_h/k_v$ values are shown in Figure 3-13. As the ratio of horizontal spring stiffness to vertical spring stiffness decreases, the resonance frequency increases.

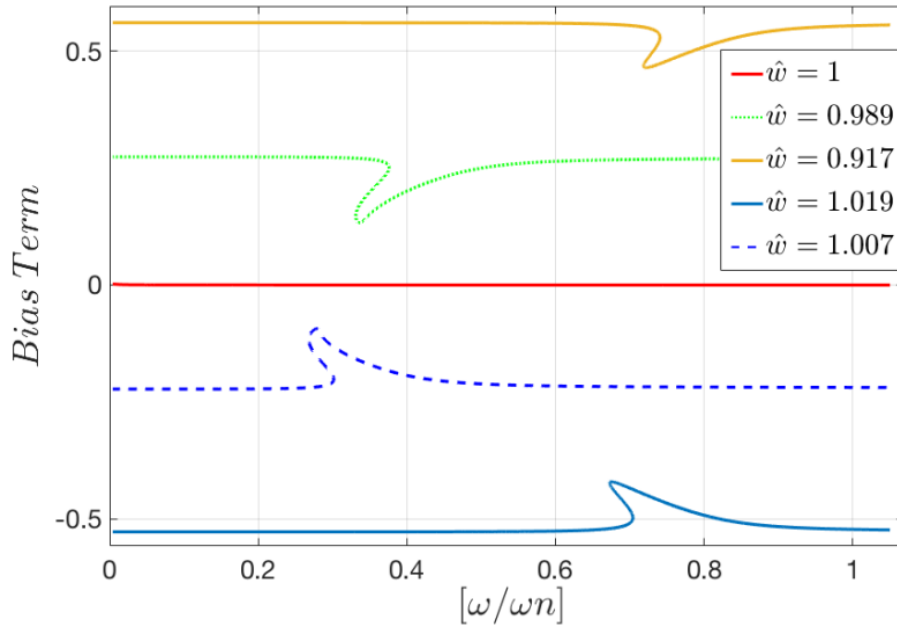


Figure 3-12 Effect of Load Deviations Bias Term in the response $\delta = 2, \gamma = 1,$
 $\xi_v = 0.015, Z/a = 0.030$

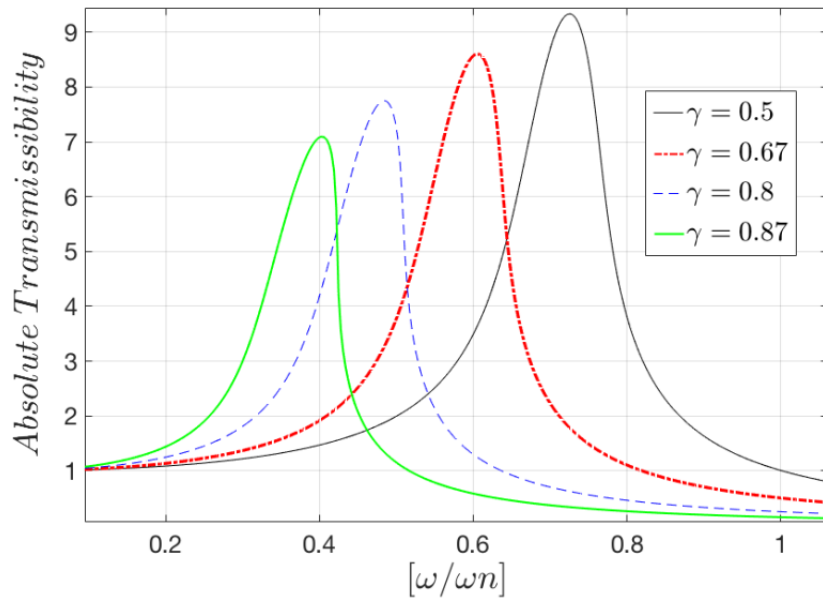


Figure 3-13 Effect of stiffness deviations $\delta = 2, \xi_v = 0.02, Z/a = 0.035$

3.2 Geometrically Nonlinear Viscous Damping

In mechanical systems, damping is an important property for the vibration isolation purposes. It is a vibration energy dissipation mechanism; hence, the resonance response depends on the damping characteristic of the mechanical system.

Although increasing damping in a mechanical system decreases the vibration amplitude at the resonance, it has an adverse effect in the isolation region [64] [2]. Higher damping ratios results in higher vibration transmissibility at the isolation region where transmissibility is lower than unity. Moreover, as linear viscous damping ratios increase, phase delay at lower frequencies increases, which might be a disadvantage for vibration isolation of measurement devices. Therefore, ideally, a damping mechanism would decrease resonance amplitudes, provide less phase delay at lower frequencies and low transmissibility at higher frequencies. Studies show that this damping characteristic can be achieved by use of cubic damping type nonlinear element [65, 66]. A more physically obtainable version of the cubic damping mechanism, i.e. geometrically damping mechanism, is studied by the Tang [70]. This mechanism is obtained by attaching a viscous damper horizontally to the system which behaves as cubic damping. With the combination of the nonlinear damping and QZS isolator, the stability performance of the isolation system is improved and unbounded response to base excitation can be eliminated [71].

3.2.1 Geometrically Nonlinear Damping Model

In this section, two viscous dampers are added to the system horizontally (Figure 3-14). When the system at the equilibrium position, the vertical component of the compressed springs is zero Figure 3-1b. c_h is the parameter of the “horizontal viscous damper” and k_v , c_v are the parameters of the vertical spring and damper. The distance between the two ends of the horizontal elements is $y(t)$; the free length of the horizontal spring is L_o .

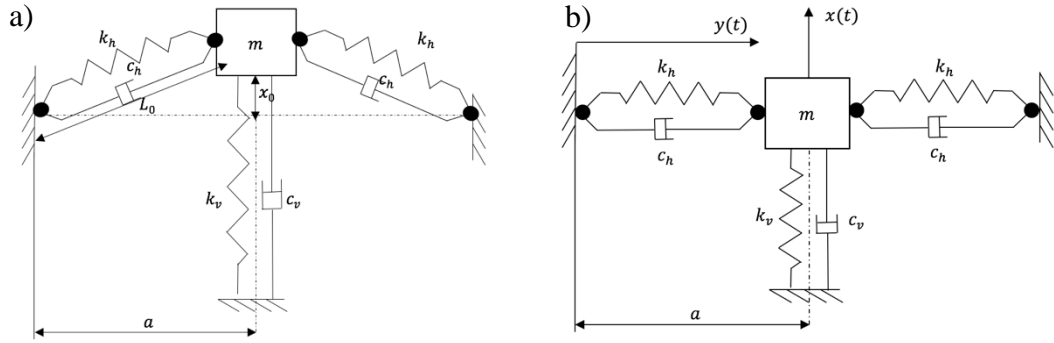


Figure 3-14 Nonlinear isolator with negative stiffness mechanism and geometrically nonlinear damping (a) initial unloaded state (b) equilibrium point

The vertical component of the damping force can be obtained as

$$f_d = \frac{2c_h x^2}{(a^2 + x^2)} \dot{x}, \quad (3-36)$$

And the non-dimensional form of it can be written as,

$$\frac{f_d}{2c_h \dot{\hat{x}}} = \frac{\hat{x}^2}{(1 + \hat{x}^2)}, \quad (3-37)$$

where \hat{x} is the non-dimensional displacement which is defined as $\hat{x} = x/a$.

For sinusoidal displacement input at different excitation levels, non-dimensional damping force is obtained, and it is given as a function of non-dimensional velocity and non-dimensional displacement in Figure 3-15 and Figure 3-16. For linear damping force this non-dimensional damping force is equal to 1 and it is independent of displacement. However, from Equation (3-37), it can be said that around the equilibrium point non-dimensional damping parameter is equal to zero since the angle between the damping force vector and vertical axes is equal to 90 degrees (Figure 3-15). Furthermore, the effective region of the nonlinear damping expands with increase of the amount of the displacement (Figure 3-16).

It should be noted that damping force is not only function of velocity, but it is also function of the displacement. Therefore, the adverse effect of the damping on the

isolation region can be eliminated since the nonlinear damping coefficient decreases as the displacement amplitude decreases.

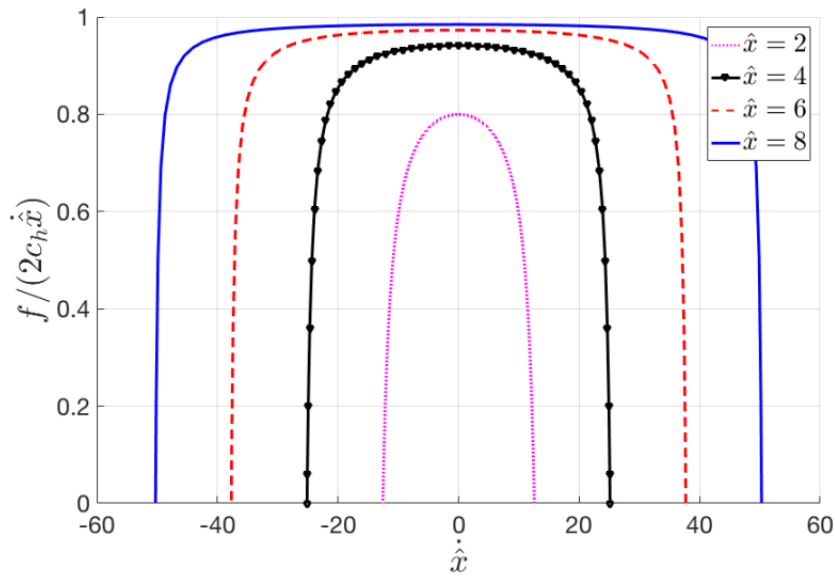


Figure 3-15 Non-dimensional damping force vs velocity for different sinusoidal excitation levels

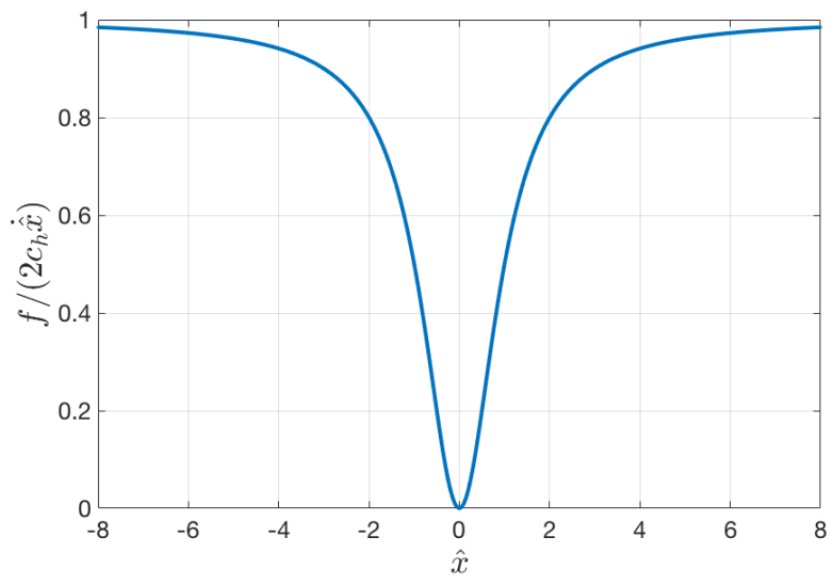


Figure 3-16 Non-dimensional damping force vs position for sinusoidal excitation

3.2.2 Response to Base Excitation

Geometrically nonlinear damping forcing is given by Equation(3-38).

$$F_{nlc} = \frac{2c_h(U_0 + U \sin(\psi))^2}{(a^2 + (U_0 + U \sin(\psi))^2)} (\omega U \cos(\psi)). \quad (3-38)$$

where U_0 is the bias term in the relative displacement response, U is the amplitude of relative displacement response. Then nonlinear differential equation of motion of single degree of freedom vibratory system becomes

$$\begin{aligned} m\ddot{x} + c\dot{x} + k_v(x - x_0) + 2k_h \left(1 - \frac{L_o}{\sqrt{u^2 + a^2}}\right) u + \frac{2c_h u^2}{(a^2 + u)} \dot{u} \\ = c\dot{z}(t) + k_v z(t) - mg \end{aligned} \quad (3-39)$$

To solve the nonlinear differential equation (3-39), the procedure explained in Section 3.1.2 is used.

The adverse effect of the QZS mechanism can be eliminated by increasing damping in the system. However, increasing the linear damping affects the isolation region adversely. This can be overcome by including nonlinear damping into the isolation system without affecting the isolation performance.

The effect of the increased nonlinear damping is studied for normalized base excitation amplitude of $Z/a = 0.035$ and the results obtained are given in Figure 3-17. It can be clearly seen that as nonlinear damping increases the resonance amplitudes decreases and resonance frequency shifts towards lower frequencies while the isolation performance of the system is not affected.

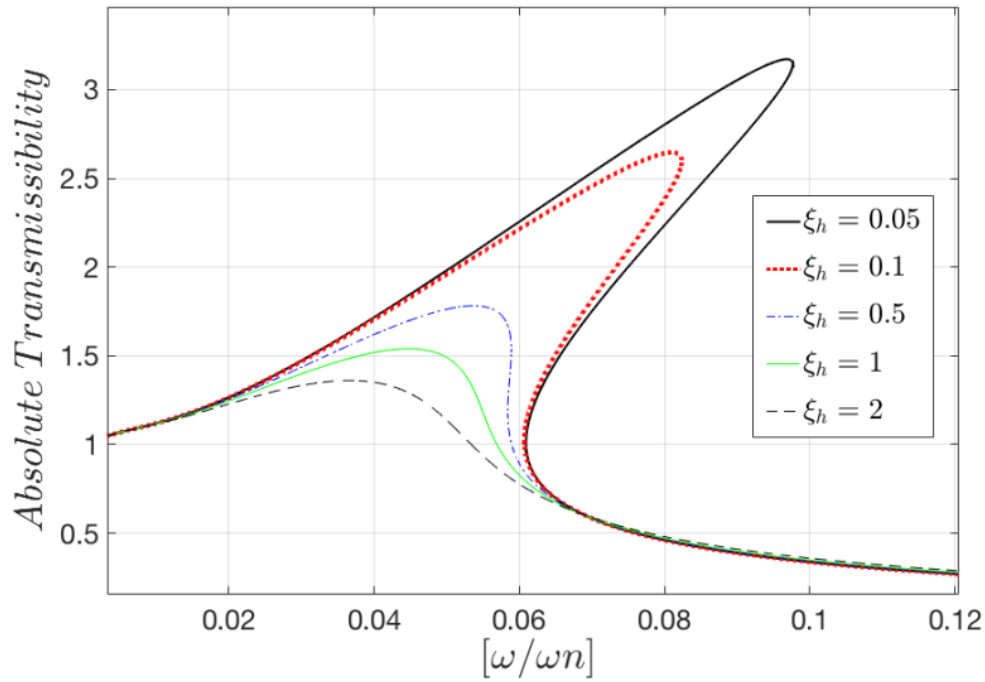


Figure 3-17 Effect of nonlinear damping $\delta = 2, \gamma = 1, \xi_v = 0.015, Z/a = 0.035$

3.2.3 Validation of Single Harmonic Solution Method

In order to validate the results obtained by harmonic balance method, solution of the case with base input of $Z/a = 0.035$ is obtained by time domain integration utilizing a 4th order Runge Kutha method and the comparison is given in Figure 3-18.

It can be seen that results obtained by HBM and time integration method agree well with each other; therefore, it can be concluded that a single harmonic representation is sufficient for this problem.

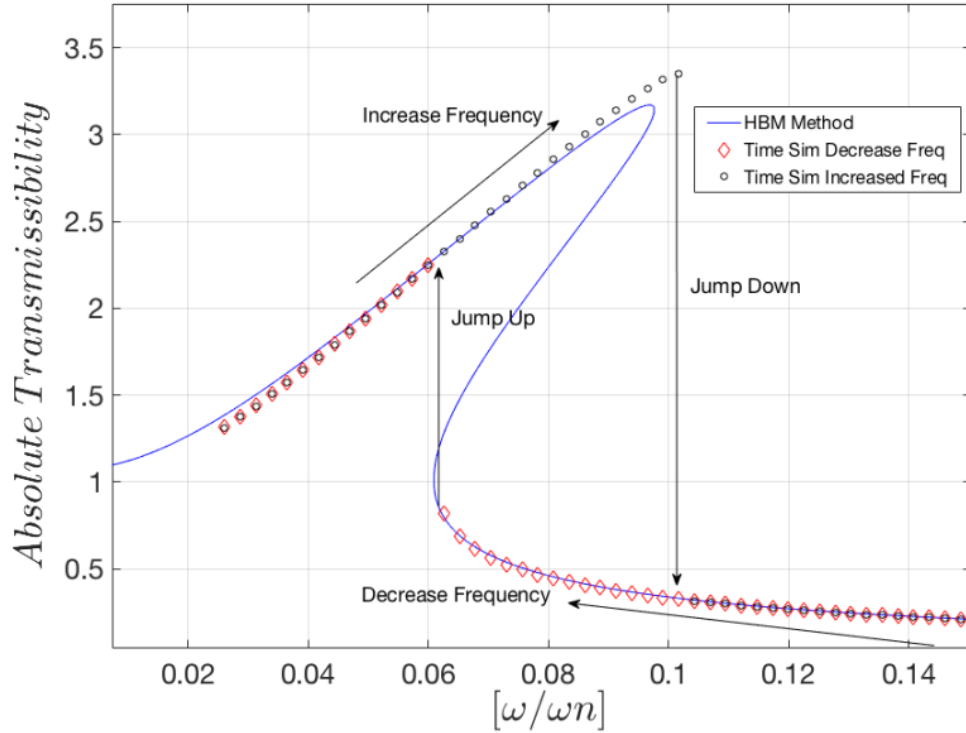


Figure 3-18 Comparison of Time Domain and HBM $Z/a = 0.035$, $\delta = 2$, $\gamma = 1$,
 $\xi_v = 0.015$, $\xi_h = 0.05$

3.2.4 Conclusion

A nonlinear isolation system with quasi-zero stiffness and geometrically nonlinear damping is considered in Section 3.1 and Section 3.2. The nonlinear differential equations of the system are converted into a set of nonlinear algebraic equations by using Single Harmonic Balance Method (SHBM). The resulting set of nonlinear algebraic equations are solved by using Newton's method with arc-length continuation. In order to validate the results obtained by SHBM, solution of the same system is obtained by using time integration and the results obtained are compared with each other which verifies the solutions obtained by HBM. Several case studies are performed in order to investigate the effect of certain system parameters. As the input motion amplitude increases, the use of only QZS has issues due to increased vibration amplitude and resonance frequency. This problem is overcome by the use of geometrically nonlinear damping which decreases both

the vibration amplitude and resonance frequency without affecting the isolation performance of the system.

In addition to these, the effect of variations in isolator stiffness and load are studied. As the deviations increases the amplitude of the vibrations increase and the resonance frequency of the system shifts towards higher frequencies. Therefore, possible deviations of these parameters need to be considered in the design of such nonlinear isolation systems in order to eliminate the adverse effects due to uncertainties.

3.3 Dry Friction-Isolator 1

To increase the effectiveness of the isolation region for different excitation levels, nonlinear damping is introduced in Section 3.2. In this chapter, dry friction, another nonlinear damping mechanism, is implemented to HSLDS isolation system. Hysteresis loop of dry friction combined with QZS is obtained and mathematical model is introduced. Harmonic balance method is used to convert nonlinear differential equations to set of nonlinear algebraic equations. Analytical approximate solution of harmonic balance methods is obtained for single harmonics. Isolation performance under base excitation is studied for different base excitation levels. Stability of the steady state solutions are also considered by Hill's method that is explained in Section 3.1.3.

3.3.1 Dry Friction Model

Dry Friction implemented system can be seen in Figure 3-19. As can be seen from Section 3.1.1, the stiffness of the overall system is cubic like and the effective range of the isolation system is limited. Unstable solutions can be obtained due to cubic like stiffness behavior. However, proposed isolator system starts to slip when stiffness force exceeds the slip force. Therefore, additional damping is introduced in the system and nonlinear behavior can be limited. As can be seen from Figure 3-19, k_h is the parameter of horizontal spring, k_v and c_v are the parameter of vertical spring and viscous damper. As stated in Section 3.1.1, the overall vertical stiffness is nonlinear and dependent on the position. Therefore, overall stiffness can be

defined as a position dependent nonlinear stiffness element as shown in Figure 3-19 (b).

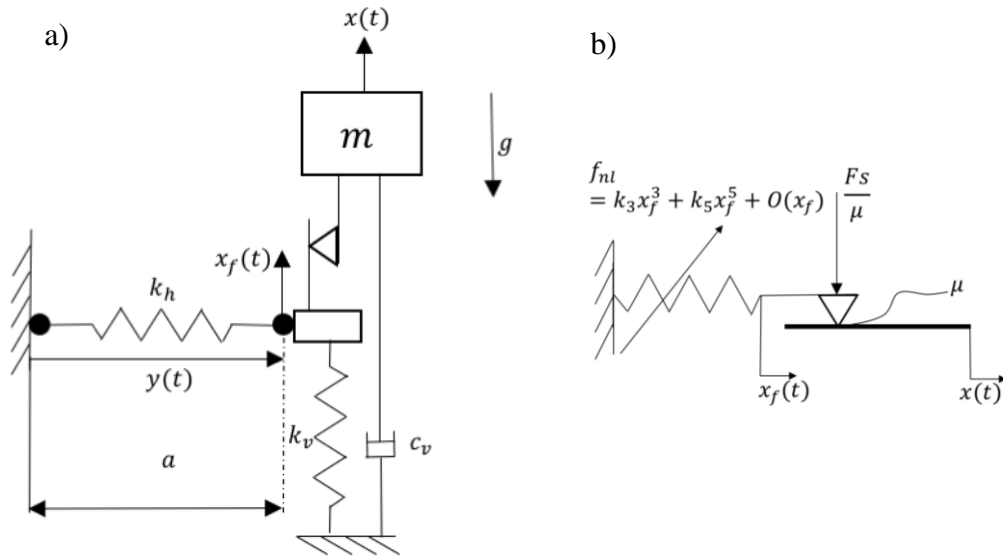


Figure 3-19 QZS Isolation system with dry friction (a) schematic drawing (b) equivalent dry friction model

Friction force, f_{dry} , can be obtained as Equation (3-40) assuming that it is elasto-perfectly plastic,

$$f_{dry} = \begin{cases} f_{nl}(x_f) & \text{stick condition,} \\ \text{sgn}(\dot{x})Fs & \text{slip condition.} \end{cases} \quad (3-40)$$

where $f_{nl}(x_f)$ is the nonlinear stiffness force, Fs is the slip force, x is the absolute displacement of the mass. The displacement x_f is defined in Figure 3-19. Hysteresis loop for this isolator can be seen in Figure 3-20 for the sinusoidal input. For the ease of calculations ωt is taken as ψ .

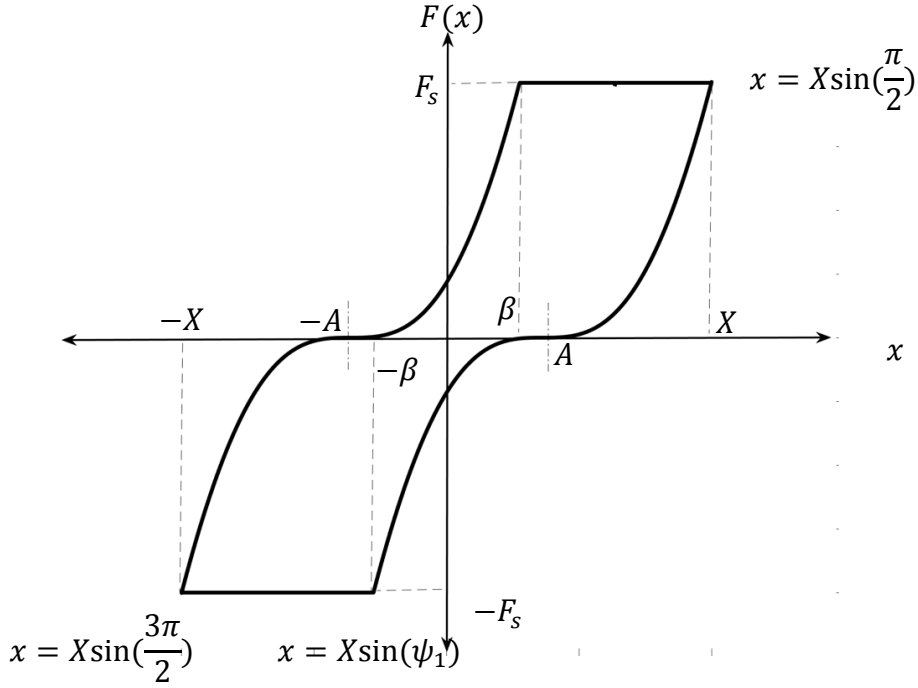


Figure 3-20 Hysteresis loop for the proposed isolator

For sinusoidal input $x = X \sin \psi$, dry friction, f_{dry} can be written as

$$f_{dry} = \begin{cases} f_{nl}(x_f) & , \frac{\pi}{2} < \psi < \psi_1 \\ -F_s & \psi_1 < \psi < \frac{3\pi}{2} \end{cases} \quad (3-41)$$

where,

$$\psi_1 = \text{asin}\left(-\frac{\beta}{X}\right), \quad (3-42)$$

and $f_{nl}(x_f)$ is the nonlinear stiffness force. For the complete stuck mode, the forcing is nonlinear due to the kinematic relationship between the vertical component of the horizontal spring force and the displacement vector. The same mechanism, i.e. negative stiffness mechanism, is studied in Section 3.1 in detail. Based on the static and dynamic analyses performed in Section 3.1, exact formulation of the nonlinear stiffness force at the complete stuck mode can be written as

$$f_{nl}(x_f) = k_h \left(1 - \frac{L_o}{\sqrt{x_f^2 + a^2}} \right) x_f + k_v x_f. \quad (3-43)$$

Referring the hysteresis loop shown in Figure 3-20, x_f can be taken as $(X \sin \psi - A)$ where $\frac{\pi}{2} < \psi < \psi_1$. Therefore, for the complete stuck mode, dry friction force f_{dry} can be rewritten following as

$$f_{dry} = \begin{cases} k_h \left(1 - \frac{L_o}{\sqrt{(X \sin \psi - A)^2 + a^2}} \right) (X \sin \psi - A) + k_v (X \sin \psi - A), & \frac{\pi}{2} < \psi < \psi_1 \\ -F_s & \psi_1 < \psi < \frac{3\pi}{2} \end{cases} \quad (3-44)$$

To calculate the nonlinear forcing angle transition angle ψ_1 , two unknowns β where the slip starts and A where the force equals to zero must be found. These unknowns can be found by solving Equation (3-45) and (3-46).

$$F_s = k_h \left(1 - \frac{L_o}{\sqrt{(X - A)^2 + a^2}} \right) (X - A) + k_v (X - A), \quad x = X, \quad (3-45)$$

$$F_s = k_h \left(1 - \frac{L_o}{\sqrt{(\beta + A)^2 + a^2}} \right) (\beta + A) + k_v (\beta + A), \quad x = -\beta. \quad (3-46)$$

In Equation (3-45) and (3-46), nonlinear stiffness force is written by using exact formulation. Assuming relatively small oscillations around the equilibrium point, 5th order Taylor Series Expansion which is obtained in Sec.3.1.1 can be used. Then equations can be written in the following form

$$F_s = k_3(X - A)^3 + k_5(X - A)^5, \quad (3-47)$$

$$F_s = k_3(\beta + A)^3 + k_5(\beta + A)^5. \quad (3-48)$$

where $k_3 = \frac{1}{2} \frac{k_h L_o}{a^3}$, $k_5 = -\frac{3}{8} \frac{k_h L_o}{a^5}$.

Two unknowns β and A are calculated from the solution of nonlinear algebraic equations (Equation (3-49) to (3-52))

$$k_5 \varphi^5 + (-5X k_5) \varphi^4 + (k_3 + 10X^2 k_5) \varphi^3 + (-3X k_3 - 10X^3 k_5) \varphi^2 + (3X^2 k_3 + 5X^4 k_5) \varphi - X^3 k_3 + F_s - X^5 k_5 = 0, \quad (3-49)$$

$$A = \text{Real Root}(\varphi_i), \dots, i = 1..7, \quad (3-50)$$

$$k_5\varphi^5 + 5Ak_5\varphi^4 + (k_3 + 10A^2k_5)\varphi^3 + (3Ak_3 + 10A^3k_5)\varphi^2 + (3A^2k_3 + 5A^4k_5)\varphi + A^3k_3 - Fs + A^5k_5 = 0, \quad (3-51)$$

$$\beta = \text{Real Root}(\varphi_i), \dots, i = 1..7. \quad (3-52)$$

3.3.2 Response to Base Excitation

For a single mass isolated by a nonlinear isolator the equation of motion can be obtained as

$$m\ddot{x} + c\dot{x} + f_n(u, Fs) = c\dot{z}(t). \quad (3-53)$$

where $u(t)$ is the relative displacement defined as $u(t) = x(t) - z(t)$. The isolator model for the base excitation is shown in Figure 3-21.

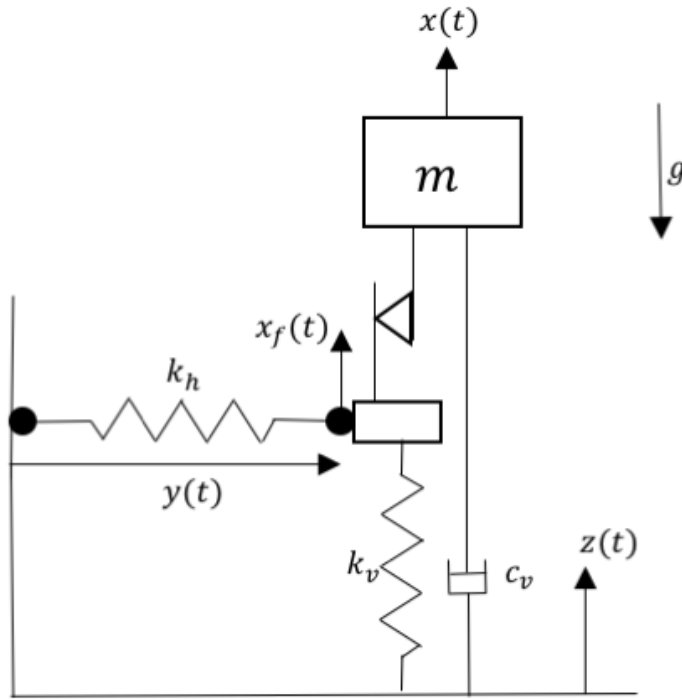


Figure 3-21 Base excitation model of the nonlinear isolator

For a single harmonic base input as $z(t) = Z \sin(\omega t)$, the response of the mass can as well be assumed harmonic in the following form $x(t) = X_s \sin(\omega t) + X_c \cos(\omega t)$ utilizing a single harmonic representation. Similarly, the relative motion can be written in the following form

$$u(t) = U \sin(\omega t + \phi) = U \sin(\psi). \quad (3-54)$$

Equation of motion can be studied under two conditions; complete stick condition and stick-slip condition.

3.3.2.1 Stick-Slip Mode

For complete stick condition where $(k_3 U^3 + k_5 U^5) > F_s$, nonlinear forcing f_n is given by

$$f_{dry} = \begin{cases} k_3(U \sin(\psi) - A)^3 + k_5(U \sin(\psi) - A)^5 & , \frac{\pi}{2} < \psi < \psi_1 \\ -F_s & \psi_1 < \psi < \frac{3\pi}{2} \end{cases} \quad (3-55)$$

By using a single harmonic Fourier Series representation as Section 3.1, the nonlinear forcing can be written as follows

$$f_n = f_{ns} \sin(\omega t + \phi) + f_{nc} \cos(\omega t + \phi), \quad (3-56)$$

$$f_n = (f_{ns} \cos \phi + f_{nc} \sin \phi) \sin(\omega t) + (f_{nc} \cos \phi + f_{ns} \sin \phi) \cos(\omega t). \quad (3-57)$$

where f_{ns} and f_{nc} are the sine and cosine Fourier coefficients, f_n is the nonlinear forcing. Fourier coefficients can be calculated as given in Equation (3-58) and (3-59) for the case where stick slip condition i.e. $(k_3 U^3 + k_5 U^5) > F_s$ is satisfied,

$$f_{nc} = \frac{2}{\pi} \left(\int_{\frac{\pi}{2}}^{\psi_1} (k_3(U \sin(\psi) - A)^3 + k_5(U \sin(\psi) - A)^5) \cos(\psi) d\psi + \int_{\psi_1}^{\frac{3\pi}{2}} -F_s \cos(\psi) d\psi \right), \quad (3-58)$$

$$f_{ns} = \frac{2}{\pi} \left(\int_{\frac{\pi}{2}}^{\psi_1} (k_3(U \sin(\psi) - A)^3 + k_5(U \sin(\psi) - A)^5) \sin(\psi) d\psi + \int_{\psi_1}^{\frac{3\pi}{2}} -F_s \sin(\psi) d\psi \right). \quad (3-59)$$

Then, Fourier coefficients can be written as,

$$f_{nc} = \frac{2}{\pi} \left(B_o + \sum_{n=1}^7 B_n U^n + F_s(1 + \sin(\psi_1)) \right), \quad (3-60)$$

$$f_{ns} = \frac{2}{\pi} \left(C_0 + \sum_{n=1}^7 C_n U^n - Fs \cos(\psi_1) \right). \quad (3-61)$$

Coefficients defined in Equation (3-60) and (3-61) can be calculated as

$$B_0 = -\sin(\psi_1) A^5 k_5 + k_5 A^5 - \sin(\psi_1) A^3 k_3 + k_3 A^3, \quad (3-62)$$

$$B_1 = \frac{3}{2} \sin(\psi_1)^2 A^2 k_3 - \frac{5}{2} A^4 k_5 + \frac{5}{2} \sin(\psi_1)^2 A^4 k_5 - \frac{3}{2} A^2 k_3, \quad (3-63)$$

$$B_2 = -\frac{10}{3} \sin(\psi_1)^3 A^3 k_5 + A k_3 - \sin(\psi_1)^3 A k_3 + \frac{10}{3} A^3 k_5, \quad (3-64)$$

$$B_3 = -\frac{1}{4} k_3 + \frac{5}{2} \sin(\psi_1)^4 k_5 A^2 + \frac{1}{4} \sin(\psi_1)^4 k_3 - \frac{5}{2} A^2 k_5, \quad (3-65)$$

$$B_4 = k_5 A - \sin(\psi_1)^5 k_5 A, \quad (3-66)$$

$$B_5 = -\frac{1}{6} k_5 + \frac{1}{6} \sin(\psi_1)^6 k_5, \quad (3-67)$$

$$C_0 = k_3 A^3 \cos(\psi_1) + k_5 A^5 \cos(\psi_1), \quad (3-68)$$

$$C_1 = -\frac{3}{2} A^2 k_3 \cos(\psi_1) \sin(\psi_1) + \frac{3}{2} A^2 k_3 \psi_1 - \frac{5}{2} A^4 k_5 \cos(\psi_1) \sin(\psi_1) - \frac{3}{4} A^2 k_3 \pi - \frac{5}{4} A^4 k_5 \pi + \frac{5}{2} A^4 k_5 \psi_1, \quad (3-69)$$

$$C_2 = A k_3 \sin(\psi_1)^2 \cos(\psi_1) + \frac{10}{3} A^3 k_5 \sin(\psi_1)^2 \cos(\psi_1) + \frac{20}{3} A^3 k_5 \cos(\psi_1) + 2 A k_3 \cos(\psi_1), \quad (3-70)$$

$$C_3 = \frac{15}{4} k_5 A^2 \psi_1 - \frac{5}{2} k_5 A^2 \sin(\psi_1)^3 \cos(\psi_1) - \frac{1}{4} k_3 \sin(\psi_1)^3 \cos(\psi_1) + \frac{3}{8} k_3 \psi_1 - \frac{15}{4} k_5 A^2 \cos(\psi_1) \sin(\psi_1) - \frac{3}{16} k_3 \pi - \frac{15}{8} k_5 A^2 \psi - \frac{3}{8} k_3 \cos(\psi_1) \sin(\psi_1), \quad (3-71)$$

$$C_4 = k_5 A \sin(\psi_1)^4 \cos(\psi_1) + \frac{8}{3} k_5 A \cos(\psi_1) + \frac{4}{3} k_5 A \sin(\psi_1)^2 \cos(\psi_1), \quad (3-72)$$

$$C_5 = -\frac{5}{16}k_5 \cos(\psi_1) \sin(\psi_1) - \frac{5}{24}k_5 \sin(\psi_1)^3 \cos(\psi_1) + \frac{5}{16}k_5 \psi_1 - \frac{5}{32}k_5 \pi - \frac{1}{6}k_5 \sin(\psi_1)^5 \cos(\psi_1), \quad (3-73)$$

3.3.2.2 Complete Stuck Mode

For complete stuck condition where $(k_3 U^3 + k_5 U^5) \leq Fs$, nonlinear forcing is given by

$$f_{dry} = k_3 (U \sin(\psi))^3 + k_5 (U \sin(\psi))^5. \quad (3-74)$$

Fourier coefficients can be calculated as given in Equation (3-75) and (3-76) where $(k_3 U^3 + k_5 U^5) \leq Fs$,

$$f_{nc} = \frac{2}{\pi} \int_0^\pi (k_3 (U \sin(\psi))^3 + k_5 (U \sin(\psi))^5) \cos(\psi) d\psi, \quad (3-75)$$

$$f_{ns} = \frac{2}{\pi} \int_0^\pi (k_3 (U \sin(\psi))^3 + k_5 (U \sin(\psi))^5) \sin(\psi) d\psi. \quad (3-76)$$

Integrals can be evaluated as follows:

$$f_{nc} = 0, \quad (3-77)$$

$$f_{ns} = \frac{3}{4}k_3 U^3 + \frac{5}{16}k_5 U^5. \quad (3-78)$$

3.3.2.3 Solution

After obtaining Fourier Coefficients for complete stuck and stick-slip conditions, nonlinear differential equation of motion Equation (3-106) can be converted in to set of nonlinear algebraic equation. Using Harmonic Balance Method (HBM), the resulting nonlinear algebraic equations of motion can be obtained as follows for stick-slip mode,

$$-m\omega^2 U \sin(\psi) + c\omega \cos(\psi) + f_{ns} \sin(\psi) + f_{nc} \cos(\psi) = \omega^2 mZ \sin(\omega t). \quad (3-79)$$

where ω is the excitation frequency, Z is the base excitation amplitude. Balancing sine and cosine harmonics and introducing the phase,

$$\left(\frac{f_{ns}}{U} - m\omega^2\right)U \cos(\phi) - (f_{nc} + c\omega U) \sin(\phi) = \omega^2 mZ, \quad (3-80)$$

$$\left(\frac{f_{ns}}{U} - m\omega^2\right)U \sin(\phi) + (f_{nc} + c\omega U) \cos(\phi) = 0. \quad (3-81)$$

Using $\sin(\phi)^2 + \cos(\phi)^2 = 1$,

$$\left(\frac{f_{ns}}{U} - m\omega^2\right)^2 U^2 + (f_{nc} + c\omega)^2 = \omega^4 m^2 Z^2. \quad (3-82)$$

To find ω from this 4th order polynomial,

$$a_4 \omega^4 + a_2 \omega^2 + a_1 \omega + a_0 = 0, \quad (3-83)$$

where $a_4 = (U^2 - Z^2)m^2$, $a_2 = U^2 c^2 - 2f_{ns}mU - 2mU$, $a_1 = 2cUf_{nc}$, $a_0 = f_{nc}^2 + f_{ns}^2 + 2f_{ns}$. Solution of quadric equation is given by

$$\omega_{1,2} = -\frac{p_4}{2} \pm \frac{\sqrt{p_5 - p_6}}{2}, \quad (3-84)$$

$$\omega_{3,4} = \frac{p_4}{2} \pm \frac{\sqrt{p_5 - p_6}}{2}, \quad (3-85)$$

where,

$$p_1 = 2a_2 + 27a_4a_1 - 72a_4a_2a_0, \quad (3-86)$$

$$p_2 = p_1 + \sqrt{-4(a_2 + 12a_4a_0) + p_1^2}, \quad (3-87)$$

$$p_3 = \frac{a_2^2 + 12a_4a_0}{3a_4 \sqrt[3]{\frac{p_2}{2}}} + \frac{\sqrt[3]{\frac{p_2}{2}}}{3a_4}, \quad (3-88)$$

$$p_4 = \sqrt{-\frac{2a_2}{3a_4} + p_3}, \quad (3-89)$$

$$p_5 = -\frac{4a_2}{3a_4} - p_3, \quad (3-90)$$

$$p_6 = -\frac{2a_1}{a_4 p_4}. \quad (3-91)$$

For complete stuck mode, since $f_{nc} = 0$ the equation can be reduced to quadratic equation by replacing ω^2 in Equation (41) by λ .

$$a_4\omega^4 + a_2\omega^2 + a_0 = 0. \quad (3-92)$$

Then,

$$\omega_{1,2} = \sqrt{\frac{-a_2 \pm \sqrt{a_2^2 - 4a_4a_0}}{2a_4}}. \quad (3-93)$$

3.3.2.4 Absolute and Relative Transmissibility

For solution of absolute displacement which is defined as

$$x(t) = U \sin(\omega t + \phi) + Z \sin(\omega t). \quad (3-94)$$

phase ϕ shall be found from Equation (3-81). Then the magnitude of the absolute transmissibility is given by

$$\frac{X}{Z} = \frac{\sqrt{(U \cos(\phi) + Z)^2 + (U \sin(\phi))^2}}{Z}. \quad (3-95)$$

The relative transmissibility is defined as U/Z .

3.3.3 Validation of the Solution Method

To validate the results obtained by harmonic balance method, solution of the case with $\hat{Z} = 0.035$ and $\xi_v = 0.015$ by Hybrid Dynamical System Simulation utilizing ODE45 solver. To determine the slip-stick states, zero-crossing detection (ZCD) method explained in [89] is used. ZCD algorithms employ a discrete state, which remembers the most recent sign of the $F_{nl} - Fs$ and $\dot{x}(t)$ and is updated when these values cross zero. Zero-crossing events are defined as follows

$$\begin{cases} |f_n(u, Fs)| - Fs & \text{stick to slip,} \\ \dot{x}(t) & \text{slip to stick.} \end{cases} \quad (3-96)$$

When zero-crossing events are detected, transition equations are written as follows

$$\begin{cases} \dot{x}_f(t) = \dot{z}(t) & \text{stick to slip,} \\ \dot{x}_f(t) = \dot{x}(t) & \text{slip to stick.} \end{cases} \quad (3-97)$$

Displacements x_f and x are defined in Figure 3-19. Comparison of single harmonic assumption and hybrid dynamical system simulation results is given by Figure 3-22.

As can be seen Figure 3-22, the steady state solutions and time simulation response are agreed well except small deviations around the resonance where relative displacement has its peak value. Therefore, it can be concluded that single harmonic balance method can be used to represent the dynamics of the isolator.

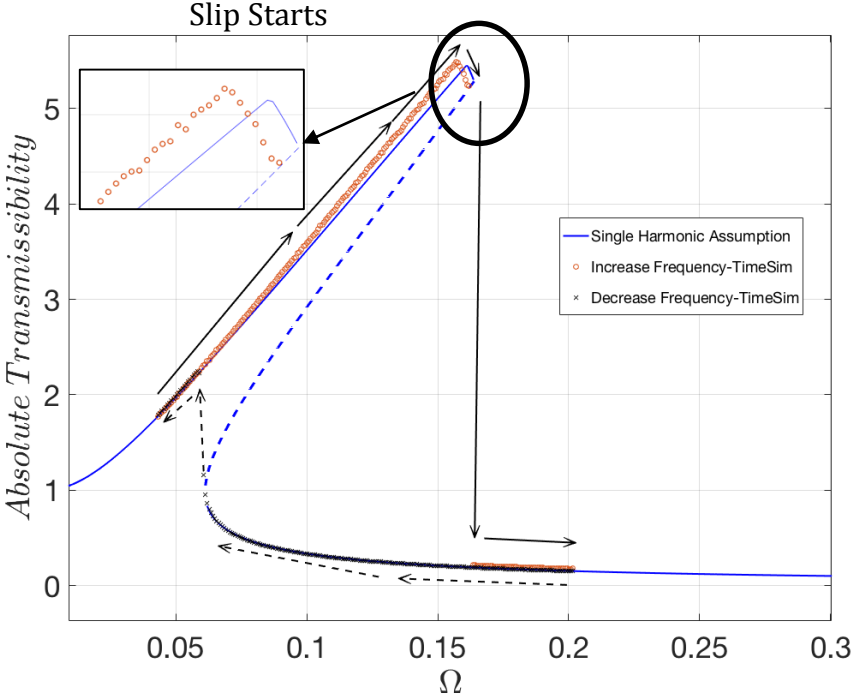


Figure 3-22 Time Simulation Results, ‘- -’:unstable solutions

Jump down phenomena can be seen in Figure 3-23 which is HDSS result in time domain. When the slip force is exceeded by the nonlinear stiffness force, system is translated from complete stick mode to stick-slip mode and jump down to another solution.

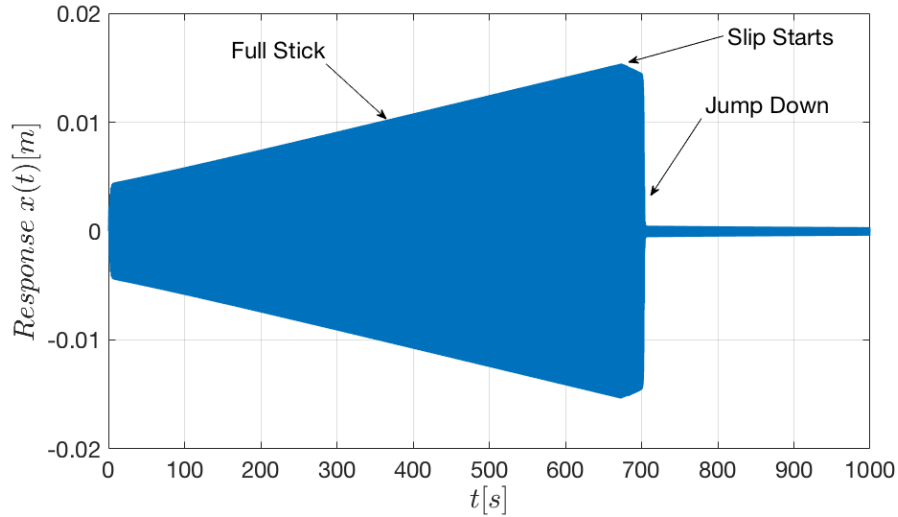


Figure 3-23 Jump down phenomena

3.3.4 Comparison of the Proposed Isolator with QZS vibration isolation system

The non-dimensional parameters are taken as $\delta = 2$, $\gamma = 1$, $\xi_v = 0.015$. Different base excitations with different excitation amplitudes are applied to the nonlinear isolator which satisfies the quasi-zero-stiffness condition. The frequency response function (FRF) is given in Figure 3-24. As the base excitation amplitude increases, the FRF bends towards higher frequencies due to the cubic stiffness effect of the QZS mechanism. It can be observed that the resonance amplitudes are reduced thanks to damping that is introduced by dry friction damper. When slip starts, damping is introduced in the system and resonance amplitudes are thus reduced. Stability of the steady state solutions are obtained by the procedure explained in Section 3.1.3

Table 3-5 Parameter Set

$m = 1 \text{ kg}$	$k_v = 20\,000 \text{ N/m}$
$k_h = 20\,000 \text{ N/m}$	$a = 0.08 \text{ m}$
$L_o = 0.016 \text{ m}$	$\xi_v = 0.015$
$\Omega = \frac{\omega}{\omega_n}$	$\omega_n = \sqrt{\frac{k_v}{m}}$

3.3.5 Effect of Slip Force Amplitude

The effect of the increased slip force is studied for normalized base excitation amplitude of $Z/a = 0.035$. Absolute and relative transmissibility curves are given in Figure 3-25. It can be clearly seen that as slip force decreases resonance amplitudes decreases and resonance frequency shifts towards lower frequencies while the isolation performance of the system at higher frequencies is not affected. However, the slip force is limited by the deadweight. Slip force must be greater than the deadweight. Even if, the case where $F_s = 5\text{ N}$ provides enhanced isolation performance, it is not possible to obtain this system practically since deadweight $mg = 9.81\text{ N}$ for this particular example.

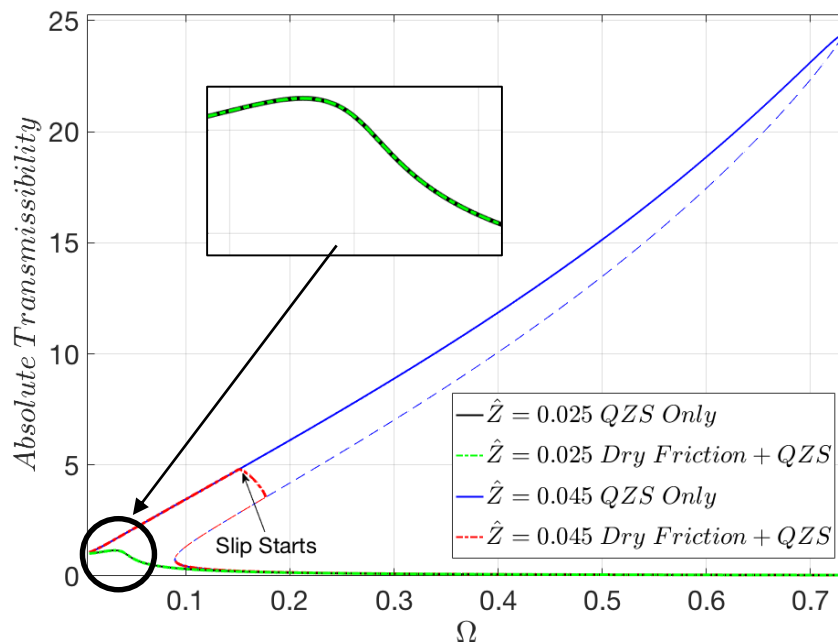


Figure 3-24 Effect of QZS Mechanism and dry friction $\delta = 2, \gamma = 1, \xi_v = 0.015$, '-':unstable solutions

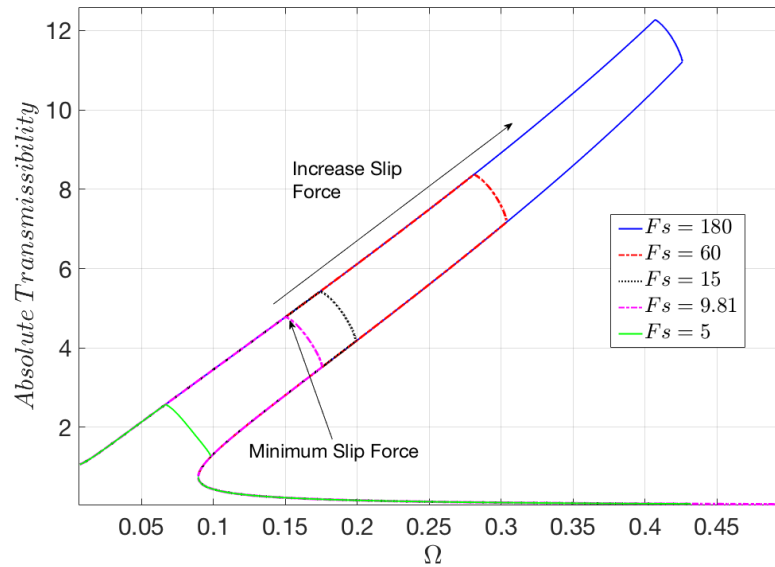


Figure 3-25 Effect of slip force $\delta = 2$, $\gamma = 1$, $\xi_v = 0.015$, $Z/a = 0.045$
 ‘- -’ :unstable solutions

3.3.6 Performance Comparison of Linear Viscous Damper and Dry Friction Damper

As stated in Section 1.4.6.2., increasing linear viscous damping also provides the reduced resonance amplitudes and unstable steady state solutions can be eliminated. However, it effects non-resonance regions adversely [64, 70]. This effect can be seen in Figure 3-26. Two responses having the same resonance amplitude are compared. One of them has dry friction and linear damping coefficient equals to zero. Other response contains only linear damping mechanism and QZS, i.e., $F_s = \infty$. It can be said that resonance amplitude can be reduced without effecting the non-resonance regions by means of dry friction. Since dry friction is in complete stuck mode at higher frequencies, it acts as only stiffness element. Thus, there is no energy dissipation from dry friction damper.

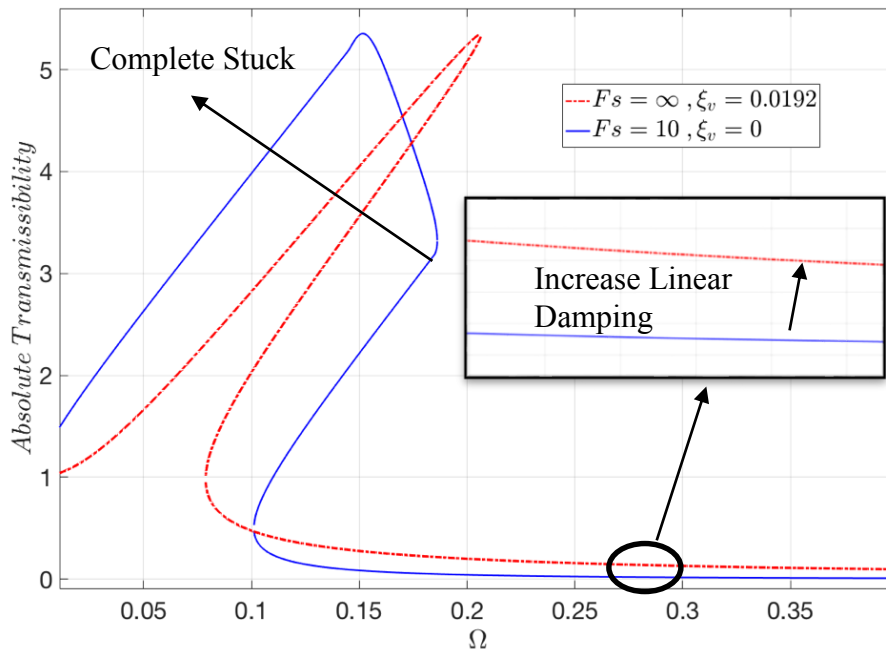


Figure 3-26 Comparison with dry friction and linear viscous damping
 $\delta = 2, \gamma = 1, Z/a = 0.045$, '- -': unstable solutions

In physical system, obtaining viscous damping in the Figure 3-19 may not be practical. Therefore, the effect of viscous damping coefficient in response is studied. Absolute and relative transmissibility for different damping ratios graphs are given in Figure 3-27 and Figure 3-28 respectively. Since the dry friction provides damping in stick slip mode, it is possible to have bounded and stable solutions around resonance region without linear viscous damper.

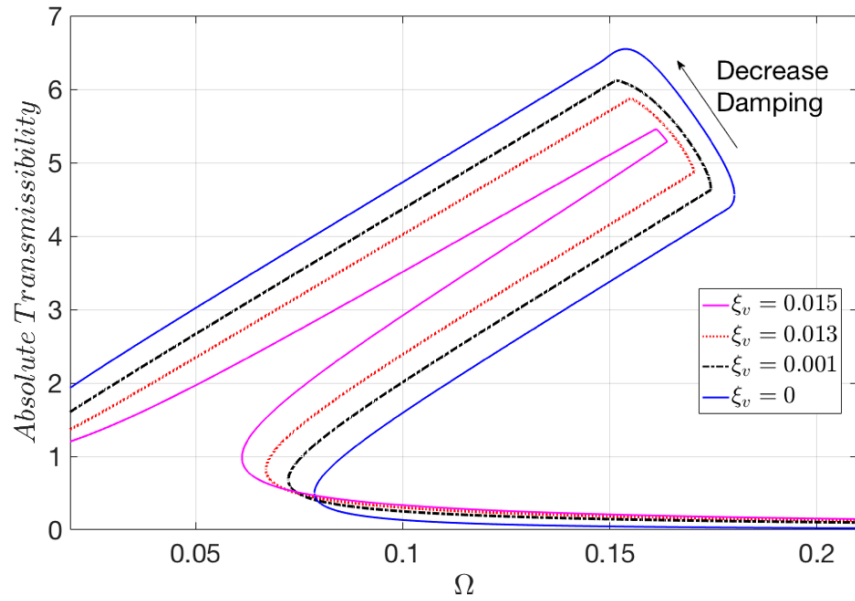


Figure 3-27 Effect of viscous damping coefficient, $Z/a = 0.035$

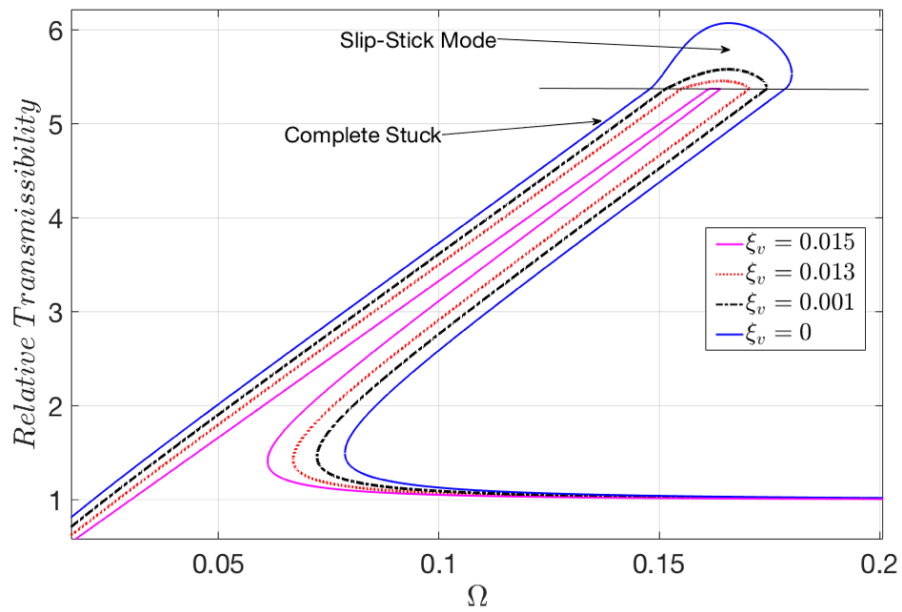


Figure 3-28 Effect of viscous damping coefficient, $Z/a = 0.035$

3.3.7 Conclusion

In this section, a nonlinear isolator having combination of QZS and dry friction damper is studied. Using single harmonic balance method, nonlinear differential

equations are converted into set of nonlinear algebraic equations. Fourier coefficients are obtained analytically for full stuck and stick-slip modes and stability of the steady state solutions are observed. From time simulation analysis, it can be said that single harmonic balance is sufficient to represent response of the system. Isolation performance of the isolator is compared to classical QZS isolation systems. It is observed that, input dependency of isolator can be eliminated by integrating dry friction damper. Since dry friction damping force only effective at resonance region, it does not affect the isolation region transmissibility. Thus, adverse effect of linear viscous damper is eliminated. Decreasing slip force reduces the resonance amplitudes. However, dry friction shall carry deadweight of the system. Therefore, minimum dry friction should be greater than the deadweight of the system to be isolated. Since system has damping mechanism due to dry friction, viscous damper can be removed from the isolator.

3.4 Dry Friction-Isolator 2

Although Dry Friction Isolator - 1 provides low frequency isolation and nonlinear damping, QZS mechanism may not be an alternative since it reduces the oscillations in working frequency range. Therefore, HSLDS systems can be considered and resonance frequency can be set according to cut-off frequency of the IMU. In this section, a nonlinear isolator having dry friction and HSLDS is considered. The unloaded and loaded condition of the proposed isolator can be seen in Figure 3-29. At the equilibrium point, horizontal spring is in compress and its vertical component is zero. However, this compressed spring starts to soften the total vertical stiffness when the system oscillates around the equilibrium point. In the equilibrium point, dry friction is in full stuck. Therefore, stiffness of the dry friction contributes to total vertical stiffness. When slip force exceeds by the stiffness force of the dry friction, system starts to slip, and damping is introduced in the system.

Unlike the “Dry Friction Isolator-1”, this system does not have any slip force limit since the weight is carried by total vertical stiffness.

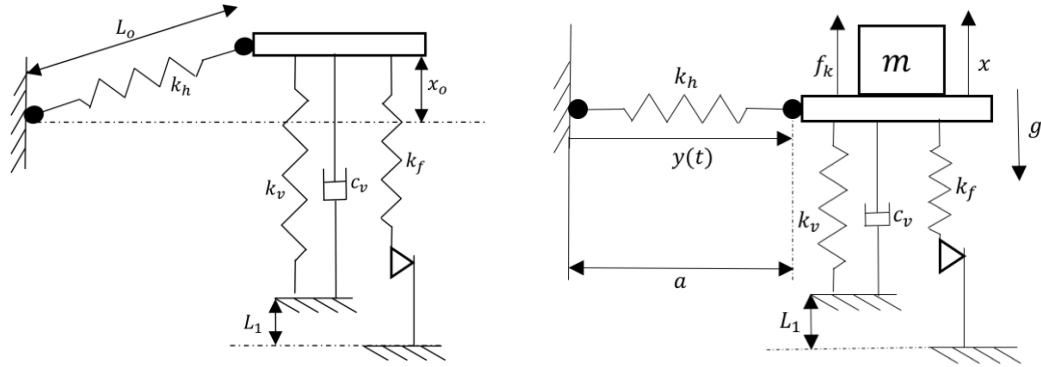


Figure 3-29 HSLDS and Dry Friction Vibration Isolation System

Referring isolator proposed in Figure 3-29, k_h is the stiffness of the horizontal spring and k_v, c_v are the parameters of the vertical dashpot, k_f is the parameters of the spring of the friction element. The distance between the two ends of the horizontal spring is $y(t)$; the free length of the horizontal spring is L_0 . When loading f_k is applied to the mass, it will deflect from its equilibrium point. The amount of deflection is defined as x . L_1 is defined in Figure 3-29. Then the vertical component of the horizontal springs can be found as stated in Equation (3-1). Total stiffness force for full stuck condition is given by

$$f_k - mg = k_h \left(1 - \frac{L_0}{\sqrt{x^2 + a^2}} \right) x + k_v(x - x_o) + k_f(x - x_o + L_1), \quad (3-98)$$

where $x_0 = \sqrt{L_0^2 + a^2}$. To satisfy the equilibrium point without slipping, slip force, F_s , must be greater than the spring preload yielding

$$F_s > k_f(L_1 - x_o). \quad (3-99)$$

Other condition for the equilibrium point follows that

$$mg = k_v x_o + k_f(L_1 - x_o). \quad (3-100)$$

Slip force and the friction stiffness are important parameters for the isolation performance. After obtaining optimum values for slip force and stiffness of dry friction, equilibrium point can be adjusted by considering Equation(3-99) and

(3-100). Assuming that equilibrium and complete stuck conditions are satisfied, total stiffness force takes the form

$$f_k = k_h \left(1 - \frac{L_0}{\sqrt{x^2 + a^2}} \right) x + (k_v + k_f)x. \quad (3-101)$$

The non-dimensional form of the stiffness force is given by

$$\frac{f}{(k_v + k_f)a} = \left(\gamma \left(1 - \frac{\delta}{\sqrt{\hat{x}^2 + 1}} \right) + 1 \right) \hat{x}. \quad (3-102)$$

where $\delta = L_0/a$, $\gamma = k_h/(k_v + k_f)$. From Equation (3-104), it can be seen that non-dimensional total stiffness force is same with the Equation (3-4). Therefore, effects of non-dimensional parameters on stiffness can be seen in Figure 3-3 and Figure 3-4. Increasing the ratio of horizontal stiffness to total vertical stiffness, including dry friction spring and vertical spring, results in negative stiffness around equilibrium point and quasi-zero-stiffness can be achieved. As can be seen in Figure 3-3 and Figure 3-4, the effect of δ and γ are similar to each other. If one tries to decrease stiffness around the equilibrium point, it can be achieved by increasing δ and/or γ according to design limitations. It can be concluded that total vertical stiffness, horizontal stiffness and ratio off free-length of horizontal spring to link length are basic parameters to define stiffness characteristic of isolator.

3.4.1 Dynamic analysis of Proposed Isolator

Dry Friction implemented to system can be seen in Figure 3-30. As stated in Section 3.1.1, the stiffness of the overall system is cubic like and the effective range of the isolation system is limited. Unstable solutions can be obtained due to cubic like stiffness behavior. However, proposed isolator system starts to slip when stiffness force exceeds the slip force. Therefore, additional damping is introduced in the system and nonlinear behavior can be limited. In the dynamic analysis of the dry friction damper, macro-slip model is used, in which the normal load, F_s/μ , is constant and the damper is either full stuck or stick-slip.

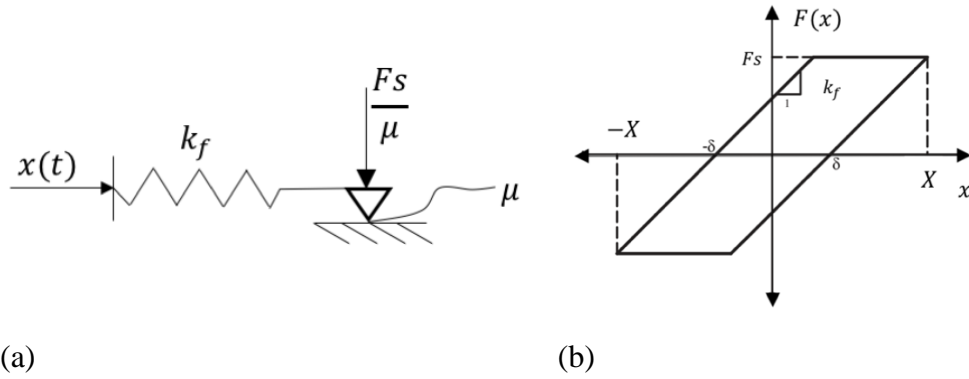


Figure 3-30 Dry Friction Damper (a) schematic drawing (b) Hysteresis Loop

Hysteresis loop for this isolator can be seen in Figure 3-30 b for a sinusoidal displacement input $x(t) = X \sin \omega t$, where F_s is the slip force, X is the amplitude of the oscillation and μ is the friction coefficient between the surfaces. The force across the two ends of the dry friction damper for a sinusoidal excitation of $x(t)$ can be expressed as

$$f_{dry} = \begin{cases} -F_s + k_f(x + \delta) & , \frac{\pi}{2} < \omega t < \psi_1 \\ -F_s & \psi_1 < \omega t < \frac{3\pi}{2} \end{cases} \quad (3-103)$$

where,

$$\delta = \frac{2F_s - k_f X}{k_f}, \quad (3-104)$$

$$\psi_1 = \text{asin}\left(-\frac{\delta}{X}\right). \quad (3-105)$$

3.4.2 Response to Base Excitation

For a single mass isolated by a nonlinear isolator, the equation of motion can be obtained as

$$m\ddot{x} + c\dot{x} + k_h \left(1 - \frac{L_o}{\sqrt{x^2 + a^2}}\right) x + k_v(x - x_o) + f_{dry} = k_v z + c\dot{z}(t) - mg, \quad (3-106)$$

where $u(t)$ is the relative displacement defined as $u(t) = x(t) - z(t)$. The isolator model for the base excitation is shown in Figure 3-31.

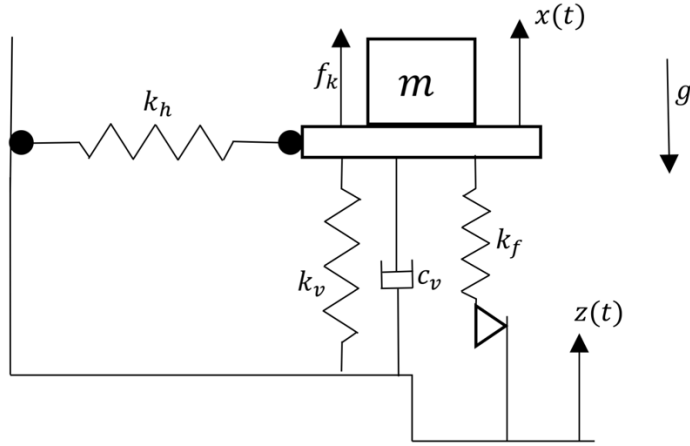


Figure 3-31 Base excitation model of the nonlinear isolator

For a single harmonic base input as $z(t) = Z \sin(\omega t)$, the response of the mass can as well be assumed harmonic in the following form $x(t) = X_s \sin(\omega t) + X_c \cos(\omega t)$ utilizing a single harmonic representation. Similarly, the relative motion, $u(t) = x(t) - z(t)$ can be written in the following form

$$u(t) = U \sin(\omega t + \phi) = U \sin(\psi). \quad (3-107)$$

Since macro-slip model is used to model dynamic behavior of the dry friction damper, the dry friction element undergoes complete stuck motion or alternating stick slip motion. Therefore, equation of motion is examined according to which state the dry friction undergoes and it is solved for full stuck motion and stick-slip motion.

By using a single harmonic Fourier Series representation, the nonlinear forcing can be written as follows

$$f_n = f_{ns} \sin(\omega t + \phi) + f_{nc} \cos(\omega t + \phi), \quad (3-108)$$

$$f_n = (f_{ns} \cos \phi + f_{nc} \sin \phi) \sin(\omega t) + (f_{nc} \cos \phi + f_{ns} \sin \phi) \cos(\omega t). \quad (3-109)$$

where f_{ns} and f_{nc} are the sine and cosine Fourier Coefficients

3.4.2.1 Complete Stuck Motion

When the dry friction damper in complete stuck condition, i.e. the maximum spring force does not exceed the slip force ($k_f U < F_s$), force across to the two ends of the damper is given by

$$f_{dry} = k_f U. \quad (3-110)$$

For both cases, the vertical component of the horizontal spring, f_s , follows that

$$f_s = \left(k_h \left(1 - \frac{L_o}{\sqrt{x^2 + a^2}} \right) \right) x. \quad (3-111)$$

Then, total nonlinear forcing can be written as sum of the horizontal spring force and force across the two ends of dry friction damper:

$$f_n = f_s + f_{dry}. \quad (3-112)$$

Fourier coefficients of nonlinear forcing can be given for complete stuck mode as follows:

$$f_{nc} = \frac{1}{\pi} \int_0^{2\pi} \left(k_h \left(1 - \frac{L_o}{\sqrt{(U \sin(\psi))^2 + a^2}} \right) + k_f \right) U \sin(\psi) \cos(\psi) d\psi, \quad (3-113)$$

$$f_{ns} = \frac{1}{\pi} \int_0^{2\pi} \left(k_h \left(1 - \frac{L_o}{\sqrt{(U \sin(\psi))^2 + a^2}} \right) + k_f \right) U \sin(\psi) \sin(\psi) d\psi. \quad (3-114)$$

After evaluating the integrals Fourier coefficients for complete stuck mode becomes,

$$f_{nc} = 0, \quad (3-115)$$

$$f_{ns} = \frac{2}{\pi} \left(\frac{1}{2} U \pi k_h + \frac{2k_h L_o a^2 \text{EllipticK}\left(\frac{U}{\sqrt{a^2 + U^2}}\right)}{U \sqrt{a^2 + U^2}} - \frac{2k_h L_o \sqrt{a^2 + U^2} \text{EllipticE}\left(\frac{U}{\sqrt{a^2 + U^2}}\right)}{U} \right) + k_f U. \quad (3-116)$$

3.4.2.2 Stick-Slip Motion

This motion is observed when the maximum spring force exceeds the slip force ($k_f U > Fs$). Then, force across to the two ends of the damper is given in Equation (3-103) by utilizing hysteresis loop. As can be seen from the hysteresis loop shown in Figure 3-30b, the stick slip motion is symmetric. Therefore, the Fourier coefficients are found by evaluating the integrals between $(\frac{\pi}{2}, \frac{3\pi}{2})$ as follows:

$$f_{nc} = \frac{2}{\pi} \left(\int_{\frac{\pi}{2}}^{\psi_1} (-Fs + k_f(U \sin(\psi) + \delta)) \cos(\psi) d\psi + \int_{\psi_1}^{\frac{3\pi}{2}} -Fs \cos(\psi) d\psi + \int_0^{\pi} k_h \left(1 - \frac{L_o}{\sqrt{(U \sin(\psi))^2 + a^2}} \right) U \sin(\psi) \cos(\psi) d\psi \right), \quad (3-117)$$

$$f_{ns} = \frac{2}{\pi} \left(\int_{\frac{\pi}{2}}^{\psi_1} (-Fs + k_f(U \sin(\psi) + \delta)) \sin(\psi) d\psi + \int_{\psi_1}^{\frac{3\pi}{2}} -Fs \sin(\psi) d\psi + \int_0^{\pi} k_h \left(1 - \frac{L_o}{\sqrt{(U \sin(\psi))^2 + a^2}} \right) U \sin(\psi) \sin(\psi) d\psi \right). \quad (3-118)$$

Evaluating the integrals analytically results in the following coefficients

$$f_{nc} = \frac{2}{\pi} \left(\delta \sin(\psi_1) - \frac{\cos(\psi_1)^2 U}{2} - \delta \right) + \frac{4Fs}{\pi}, \quad (3-119)$$

$$f_{ns} = \frac{2}{\pi} \left(\frac{1}{2} U \pi k_h + \frac{2k_h L_o a^2 \text{EllipticK}\left(\frac{U}{\sqrt{a^2 + U^2}}\right)}{U \sqrt{a^2 + U^2}} - \frac{2k_h L_o \sqrt{a^2 + U^2} \text{EllipticE}\left(\frac{U}{\sqrt{a^2 + U^2}}\right)}{U} - \frac{1}{4} k_f U \pi - \frac{1}{2} U \cos \psi_1 \sin \psi_1 + \frac{1}{2} k_f U \psi_1 - k_f \delta \cos \psi_1 \right). \quad (3-120)$$

3.4.2.3 Solution

For the solution of the equation of motion, the same procedure explained in Section 3.3.2.3 is used. Using Harmonic Balance Method (HBM), the resulting nonlinear algebraic equations of motion can be obtained as follows for stick-slip mode,

$$k_v - m\omega^2 U \sin(\psi) + c\omega \cos(\psi) + fns \sin(\psi) + fnc \cos(\psi) = \omega^2 mZ \sin(\omega t). \quad (3-121)$$

After evaluating the Fourier Coefficient of nonlinear forcing, equation is the same with (3-79). Therefore, the solution obtained by (3-93) is used. Moreover, absolute and relative transmissibility are obtained by (3-95).

3.4.3 Isolation Performance

Frequency response functions are plotted for different slip force values using the equations derived in Section 3.4.1. Below parameter set is used in calculations.

Table 3-6 Parameter Set

$m = 1 \text{ kg}$	$k_v = 18\,000 \text{ N/m}$
$k_h = 18\,000 \text{ N/m}$	$a = 0.08 \text{ m}$
$L_o = 0.015 \text{ m}$	$\xi_v = 0.02$
$k_f = 2\,000 \text{ N/m}$	$\omega_n = \sqrt{\frac{k_v + k_f}{m}}$
$\Omega = \frac{\omega}{\omega_n}$	

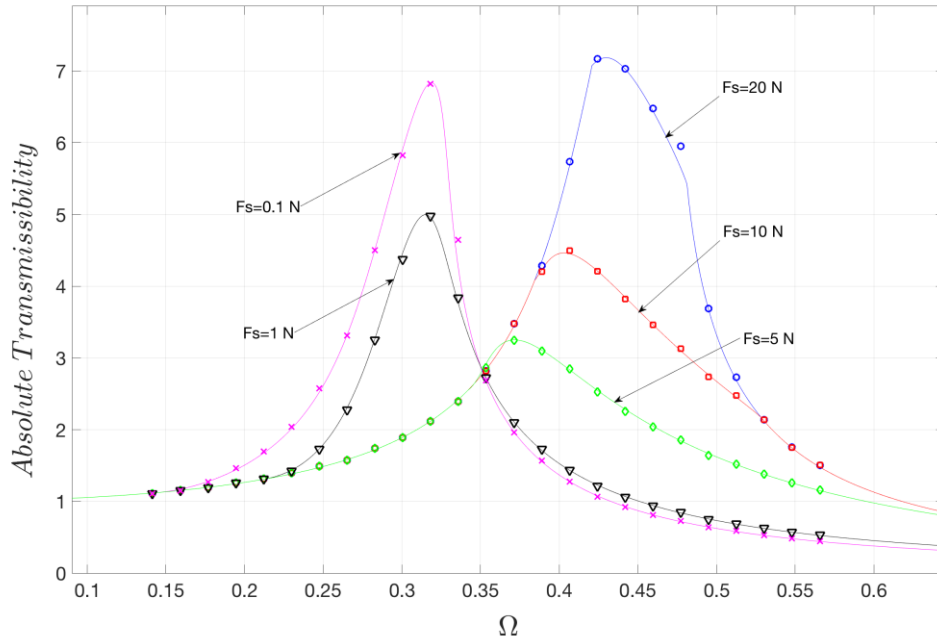


Figure 3-32 Frequency Response Functions for different sliding friction force values (discrete points are time simulations)

As it can be seen from Figure 3-32, time simulations and solutions that are obtained by utilizing single harmonic balance method are in agreement except small deviations around resonance where slip force equals to 20 N. Thus, it can be concluded that single harmonic balance method is sufficient to model dynamics of the problem. It should be noted that decrease sliding friction force results in decrease of resonance frequency and reduction of resonance amplitudes. However, after some point, resonance starts to increase and more sensitive to change of sliding friction force. Thus, it can be concluded that there is an optimum sliding friction force for reducing resonance amplitude.

Furthermore, it can be concluded that the low frequency isolation is obtained thanks to negative stiffness mechanism. Natural frequency of the system is reduced to approximately 0.35-0.45 of minimum possible natural frequency of the linear isolation system that can carry the deadweight of the mass. Since it enlarges the isolation frequency region, the performance is enhanced significantly.

Another important effect of dry friction on isolation performance is phase response of SDOF vibratory system. As stated in Section 1, while designing isolation system for measurement devices such as accelerometers and gyroscopes, both Frequency Response Functions (FRF) which indicates how vibration amplitudes effectively are reduced and phase response should be taken into account. Phase response of the isolation system is shown in Figure 3-33. Results show that damping introduced by dry friction is only effective when system in stick-slip mode. When vibration amplitudes are relatively small i.e. isolator in complete stuck mode, system phase response is same with the SDOF system having linear viscous damper. However, around resonance, phase response starts to bend due to the additional damping introduced by dry friction. Unless slip force is chosen carefully, both amplitude and phase response might be affected adversely. In addition, as can be seen from Figure 3-33, there is phase delay in even at low frequencies due to viscous damper in the isolator. Considering this and adverse effect of linear damping in isolation region, it can be advisable to have viscous damping as least as possible. Since dry friction introduce damping around resonance, there is no need to increase linear viscous damping to reduce the resonance amplitudes.

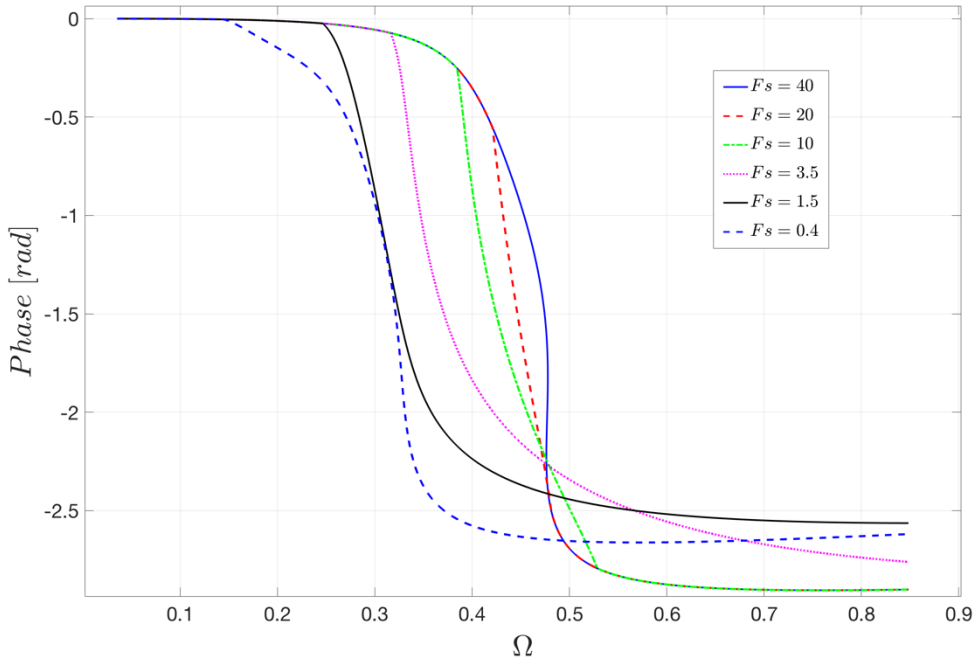


Figure 3-33 Phase response of dry friction isolator-2

Since the system performance is highly sensitive to slip force, performance plot is achieved for different slip force values and results are shown in Figure 3-34. Maximum response of FRF plot for each sliding friction force is obtained. For this particular problem, optimum sliding force can be chosen as 10 N considering Figure 3-33 and Figure 3-34 together. Even if, $F_s = 5 \text{ N}$ provides minimum resonance amplitude, system is very sensitive to variation of system parameters and phase delays increases at lower frequencies [77]

Designed isolator is analyzed under different excitation levels and results are compared with linear isolation system in Figure 3-35. Due to horizontal stiffness corrector, resonance frequency is reduced to 0.45 of linear system. Moreover, dry friction reduces the resonance amplitudes and adverse effect of nonlinear horizontal springs are eliminated.

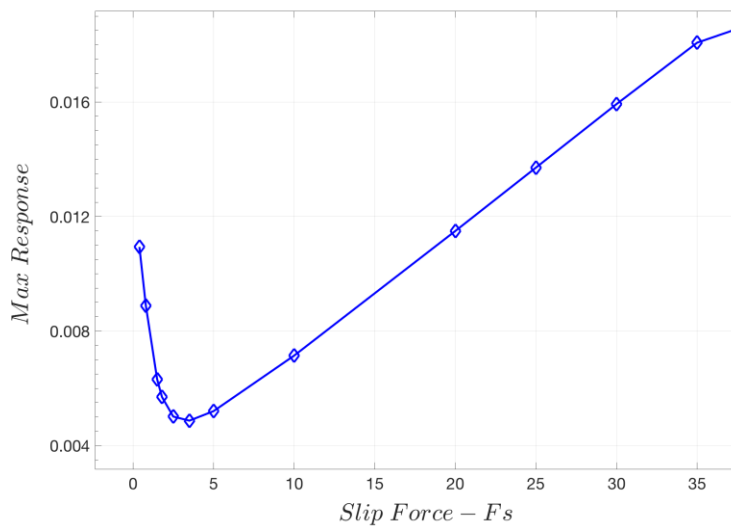


Figure 3-34 Performance plot of dry friction isolator

Maximum of FRFs for different excitation levels is shown in Figure 3-36. It can be concluded that isolation performance is affected adversely for less excitation levels than designed value since dry friction isolator starts to slip at higher frequencies. It should be noted that Figure 3-35 emphasizes the absolute transmissibility defined in Equation (3-94). In order to calculate the response, absolute transmissibility should be multiplied by base excitation amplitude.

After achieving optimum sliding friction force and δ and γ , dry friction stiffness and vertical spring stiffness and other design parameters can be determined by using equilibrium equations Equation (3-99) and (3-100).

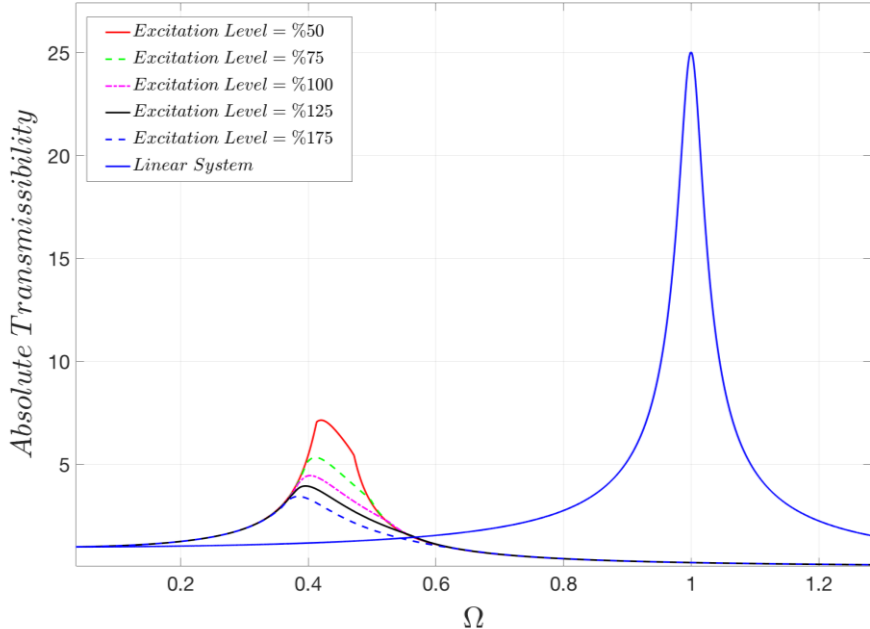


Figure 3-35 Designed isolator under different base excitation levels

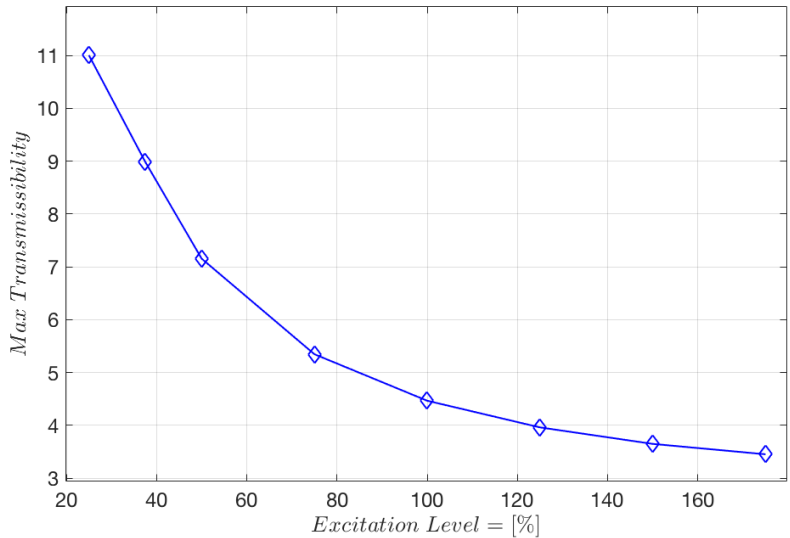


Figure 3-36 Maximum transmissibility vs excitation level

3.4.4 Conclusion

High-static-low-dynamic stiffness mechanism is combined with a dry friction damper. Equation of motion of the proposed isolator is obtained. Nonlinear differential equations are converted into a set of nonlinear algebraic equations for both complete stuck and slip-stick conditions by utilizing single harmonic balance method. The resulting quadric equation where the isolator undergoes stick slip mode and quadratic equation where isolator experiences complete stuck mode is solved analytically. Frequency response functions are obtained for different slip forces. It is observed that decrease in slip force reduces the resonance amplitude. However, after some point, resonance amplitude starts to increase since introduced damping due to dry friction decreases and amplitudes become more sensitive to deviation of slip force. Therefore, there is an optimum value which minimize the resonance amplitude. In addition, resonance frequency is decreased thanks to HSLD stiffness mechanism. The proposed isolator provides low-frequency isolation, less phase delay and limited resonance amplitude under different base excitation levels at the same time, each of which improves the isolation performance significantly and satisfies the requirements of vibration isolation problem of measurement devices. In addition, adverse effect of linear viscous damping on isolation region and highly nonlinear response of HSLD stiffness mechanism are eliminated.

CHAPTER 4

EXPERIMENTAL INVESTIGATION OF DYNAMICS OF THE GEOMETRICALLY NONLINEAR SHEAR ELASTOMER ISOLATOR

4.1 Dynamic Characterization of Rubber Isolator

The dynamic analysis of the High-Static-Low-Dynamic-Stiffness isolators are performed in Chapter 3. Their main advantage is that they lower the natural frequency of the system while providing relatively higher dead weight loading capacity. However, the system response is highly input depended due to its geometrically nonlinear dynamic characteristic. Though increasing linear damping eliminates these drawbacks of nonlinearity, it effects the isolation regions adversely and it may not even be applicable due to practical reasons. Since elastomers are widely used in the industry and easy to integrate into the isolation systems, a novel elastomer isolator, which has high static low dynamic stiffness and geometrically nonlinear damping, is designed. Dynamic behavior of this novel isolator is studied theoretically considering its physical nonlinearities such as loss factor and dynamic stiffness dependence on dynamic strain. Approximate analytical solutions are obtained by utilizing single harmonic balance method. Then, on a shear EPDM specimen, the displacement profile that the isolator experiences are applied, and force-displacement histories are recorded by using servo-position-control experiment setup. Damping and stiffness characteristics are achieved for different response amplitudes of the mass to be isolated.

4.2 Geometrically and Physically Nonlinear Rubber Isolator

The passive isolators, which are generally made up of rubber like materials, are widely used in the industry since it provides cost effective solutions and does not require any additional power supply and control electronics unlike active isolation systems [28].

However, the system parameters such as stiffness and loss factor are highly nonlinear, and they are dependent on environmental and operational conditions such as preload, dynamic strain, temperature, frequency [29]. Furthermore, the isolation performance is generally limited by the static loading capacity. Although decreasing stiffness of the isolator enlarges the isolation frequency range by decreasing natural frequency, the loading capacity decreases due to static deflections under the acting of gravitational forces [39].

Recently, geometrically nonlinear isolators, which enhance the isolation performance of passive isolators, have become a popular research area. Geometrically nonlinear isolators generally consist of pre-stressed horizontal springs. This geometric nonlinearity provides high static low dynamic stiffness characteristic which provides low frequency and relatively high loading capacity together. In literature, there are variety of study which analyze the dynamics of the passive nonlinear isolators both theoretically and experimentally. Furthermore, a lot of different design to obtain high static low dynamic stiffness are available. Ivana, in her study, considers the physical nonlinearities (softening behavior) in addition to geometrical studies as well [49]. Ivana states that softening behavior of oblique prestressed springs improves the isolation performance. However, the main drawback of passive nonlinear isolators is its input depended dynamics. Since the stiffness of QZS isolators is cubic like, increasing excitation adversely affects the isolation performance. Therefore, jumping phenomena may be observed due to unstable solutions

To eliminate drawback of input dependency, damping in the system, which is a vibration energy dissipation mechanism of the isolators, can be increased. As a result, resonance amplitudes are reduced, and stable solutions can be obtained for relatively larger excitation range. However, increasing damping adversely affect the isolation region and increase the transmissibility at the isolation frequency range. Therefore, an ideal damping mechanism should decrease the resonance amplitudes without effecting vibration transmissibility at isolation region. As stated in Section 3.2, cubic damping is only effective at resonance region and desired characteristic

can be obtained by means of cubic damping mechanism. Previous studies used linear viscous dampers with constant damping coefficients and only considers the geometrical nonlinearities.

Referring the advantages of the geometrically nonlinear isolators, it is aimed to achieve a rubber isolator having HSLDS and geometrically nonlinear damping. Furthermore, since viscoelastic materials are widely used in industry and it provides cost effective solutions, it is important to have a nonlinear isolator that is made up of viscoelastic materials and provides advantages of geometrically nonlinear isolators. This isolator is modeled so that nonlinear dynamics of rubber like materials are represented. Therefore, in this chapter, physical and geometrical nonlinearities of passive elastomer QZS isolator are studied both theoretically and experimentally. Since commercial test results are generally represented in structural damping model and it is mathematically useful in frequency analysis, complex stiffness model is used in the model. For different excitation levels, system parameters are obtained experimentally. Nonlinear displacement profile that isolator experiences is applied by servo position-controlled experiment setup. Then dynamics of the isolator is studied by utilizing harmonic balance method. Approximate analytical solutions are obtained.

4.3 Mathematical Development

4.3.1 Stiffness Model

The model of the proposed isolator can be seen in Figure 4-1. The horizontal rubber isolator has static-dynamic stiffnesses and loss factor which are function of dynamic strain. These system parameters are also function of frequency and temperature. Since experiments are conducted for a limited frequency range, effect of frequency is neglected, and temperature is assumed to be constant.

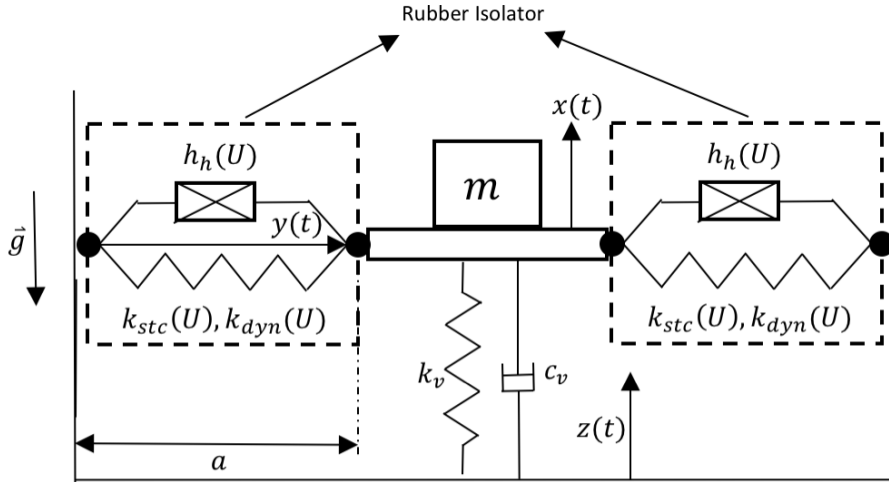


Figure 4-1 Geometrically and Physically Nonlinear Rubber Isolator

The relative displacement is defined as $u(t) = x(t) - z(t)$. Then, horizontal displacement can be written in following form

$$y(t) = \sqrt{u^2 + a^2} - Lo. \quad (4-1)$$

Equation (4-1) can be normalized as follows:

$$\hat{y}(t) = \sqrt{\hat{u}^2 + 1} - \delta, \quad (4-2)$$

where $\hat{u} = u/a$, $\delta = Lo/a$ and $\hat{y} = y/a$. Equation (4-2) can be approximated by using Taylor Series Expansion.

$$\hat{y}_{app}(t) = 1 - \delta + \frac{1}{2}\hat{u}^2 + H.O.T. \quad (4-3)$$

where \hat{y}_{app} is the Taylor Series expansion of horizontal displacement. Exact formulation and Taylor Series Expansion is compared in Figure 4-2. As expected, around the equilibrium point approximate horizontal displacement and exact expression agree with each other.

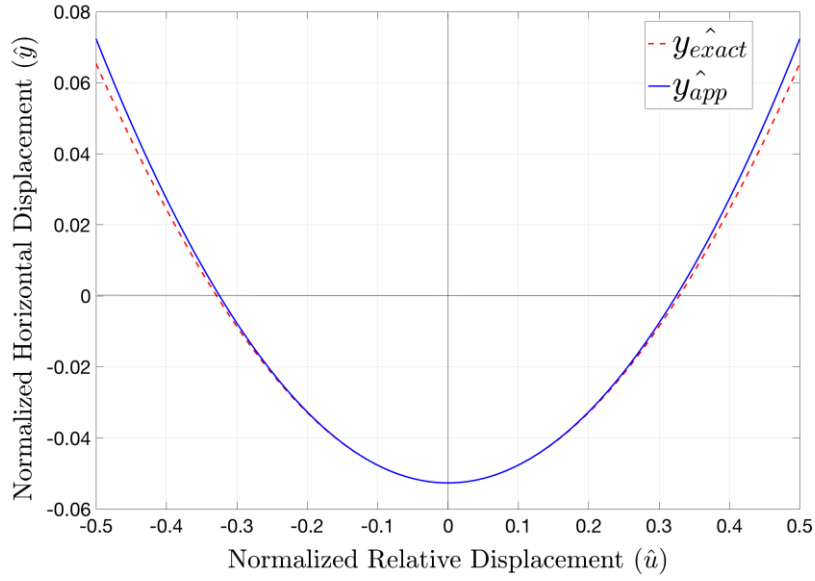


Figure 4-2 Taylor Series Expansion of Horizontal Displacement

For harmonic base excitation as $z(t) = Z \sin \omega t$, the normalized relative response of the mass can be assumed as $\hat{u}(t) = \hat{U} \sin(\omega t + \phi) = \hat{U} \sin(\psi)$ where $\hat{u} = u/a$. The Fourier coefficients of $\hat{y}(t)$ are given as

$$\hat{Y}_0 = \frac{1}{2\pi} \int_0^{2\pi} \hat{y} d\psi, \quad (4-4)$$

$$\hat{Y}_2 = \frac{1}{2\pi} \int_0^{2\pi} \hat{y} \cos(2\psi) d\psi. \quad (4-5)$$

Evaluating the integrals results in following form,

$$\hat{Y}_0 = 1 + \frac{1}{4} \hat{U}^2 - \delta, \quad (4-6)$$

$$\hat{Y}_2 = -\frac{1}{4} \hat{U}^2. \quad (4-7)$$

Fourier Coefficients of horizontal displacement function is plotted in Figure 4-3. As expected, the bias term (preload) decreases, and the amplitude of the first harmonic, (\hat{Y}_2) increases as normalized relative displacement increases. Since static and dynamic stiffnesses are different for viscoelastic materials, amplitudes of Fourier Coefficients are important to model nonlinear forcing [28].

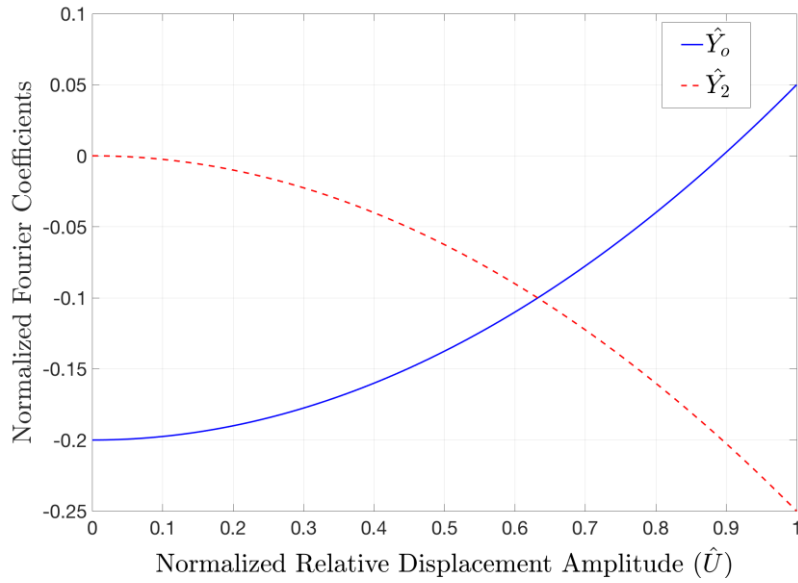


Figure 4-3 Fourier Coefficients of Horizontal Displacement Function

Forcing across the single elastomer isolator is shown in Figure 4-4. As can be seen from Figure 4-3, dynamic and stiffness are different and dependent on relative displacement amplitude. Loss factor is also dependent on relative displacement amplitude.

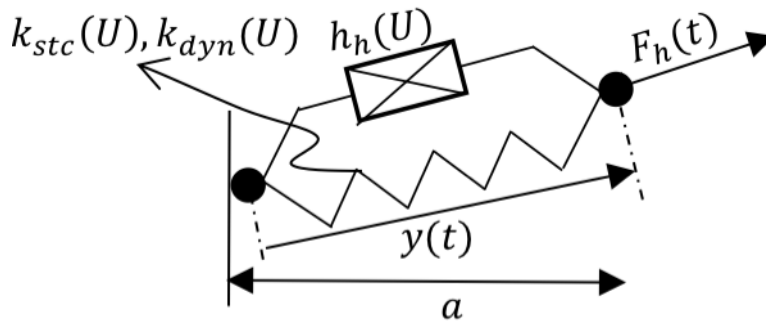


Figure 4-4 Forcing Across Elastomer

Forcing across the single elastomer isolator is given by

$$\frac{F_h}{a} = k_{stc} \hat{Y}_0 + k_{dyn} \hat{Y}_2 \cos 2\psi - h_h \hat{Y}_2 \sin 2\psi. \quad (4-8)$$

The vertical component of the forcing, F_v , can be calculated as

$$\frac{F_v}{a} = (k_{stc}\widehat{Y}_0 + k_{dyn}\widehat{Y}_2 \cos 2\psi - h_h\widehat{Y}_2 \sin 2\psi) \frac{\widehat{u}}{\sqrt{\widehat{u}^2 + 1}} \quad (4-9)$$

Then, normalized version of total vertical stiffness force including the vertical spring can written in the following form

$$\widehat{F}_v = \frac{F_v}{ak_v} = 2(\gamma_{stc}\widehat{Y}_0 + \gamma_{dyn}\widehat{Y}_2 \cos 2\psi) \frac{\widehat{u}}{\sqrt{\widehat{u}^2 + 1}} + \widehat{u}, \quad (4-10)$$

where $\gamma_{stc} = k_{stc}/k_v$ and $\gamma_{dyn} = k_{dyn}/k_v$, $\eta_v = h_h/k_v$.

The effect of non-dimensional parameters γ_{stc} and γ_{dyn} can be seen in Figure 4-5 and Figure 4-6. As can be seen from Figure 4-5, increase in γ_{stc} may result in negative stiffness around the static equilibrium point. Therefore, the ratio of static stiffness rate of the horizontal rubber isolator, k_{stc} , to vertical stiffness rate k_v should be determined carefully.

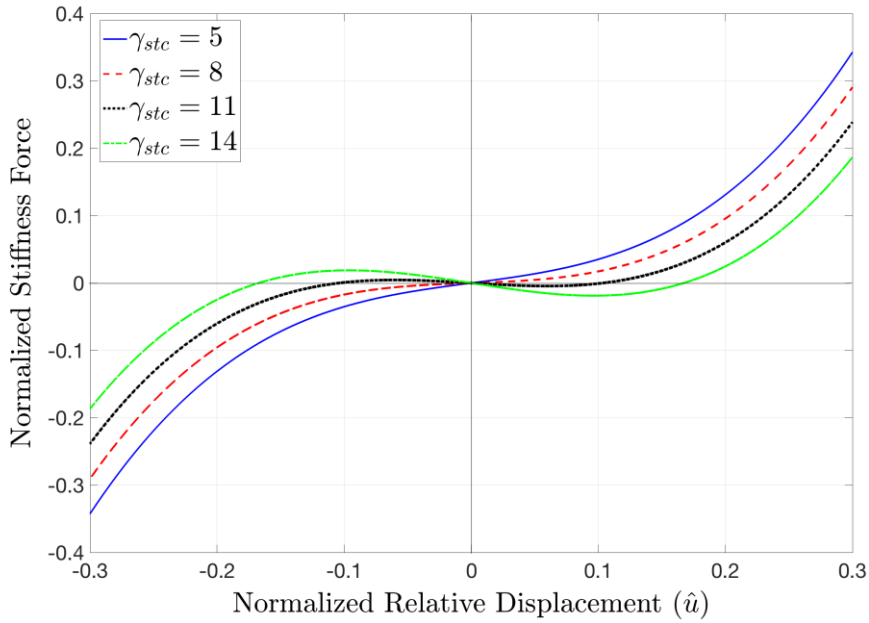


Figure 4-5 Effect of γ_{stc} on Normalized Force

Similarly, as the ratio of dynamic stiffness rate of the horizontal rubber isolator, k_{dyn} , to vertical stiffness rate k_v increases, total stiffness around the equilibrium decreases.

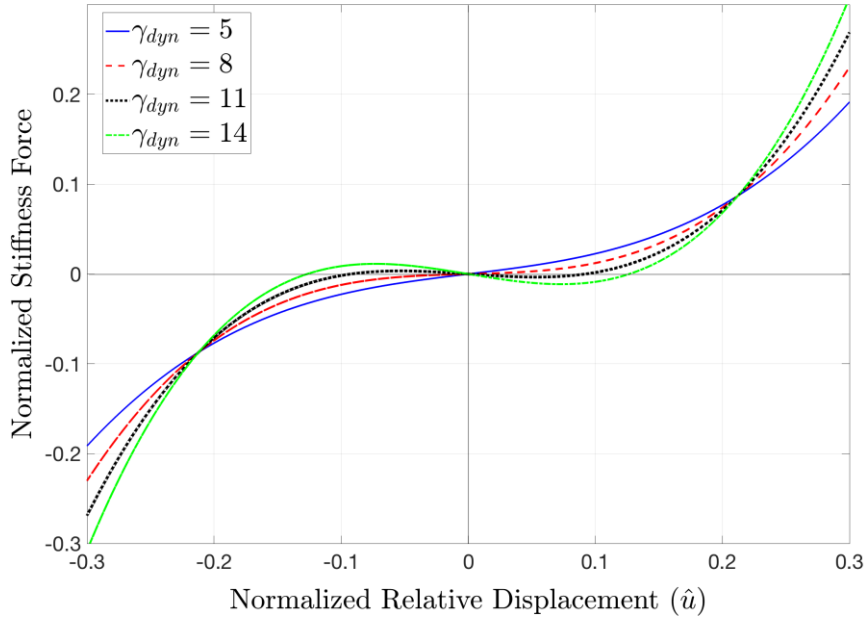


Figure 4-6 Effect of γ_{dyn} on Normalized Force

4.3.2 Damping Model

As stated before, damping characteristic of viscoelastic materials are physically nonlinear. In other words, loss factor is dependent on dynamic strain amplitude and frequency content of the excitation [28]. However, proposed isolator has geometrical nonlinearities as well. Therefore, the mathematical model is developed so that both geometrical and physical nonlinearities are taken into account. Since experiments were performed at limited frequency range, the frequency dependency is neglected in this study. Thus, the hysteric damping coefficient, h_h , is function of only relative displacement amplitude U .

The vertical component of the geometrically and physically nonlinear damping force for sinusoidal displacement of the rigid body is given by

$$\frac{F_{d_v}}{a} = 2(-h_h \hat{Y}_2 \cos 2\psi) \frac{\hat{u}}{\sqrt{\hat{u}^2 + 1}} \quad (4-11)$$

Equation (4-11) can be normalized as follows

$$\widehat{F}_{d_v} = \frac{F_{d_v}}{k_{dyn} a} = 2(-\eta \hat{Y}_2 \cos 2\psi) \frac{\hat{u}}{\sqrt{\hat{u}^2 + 1}} \quad (4-12)$$

where $\eta = h_h/k_{dyn}$. The effect of loss factor can be seen in Figure 4-7. In Figure 4-7, only geometrical nonlinearity is considered. Physical nonlinearity is considered after experimentally dynamic characterization of the viscoelastic material in Section 4.5. Due to the kinematic relationship between the force and displacement, damping force is equal to zero around the static equilibrium point. The advantages of the geometrically nonlinear dampers are discussed in Section 3.2. Moreover, increase in loss factor leads to increase in damping force, as expected.

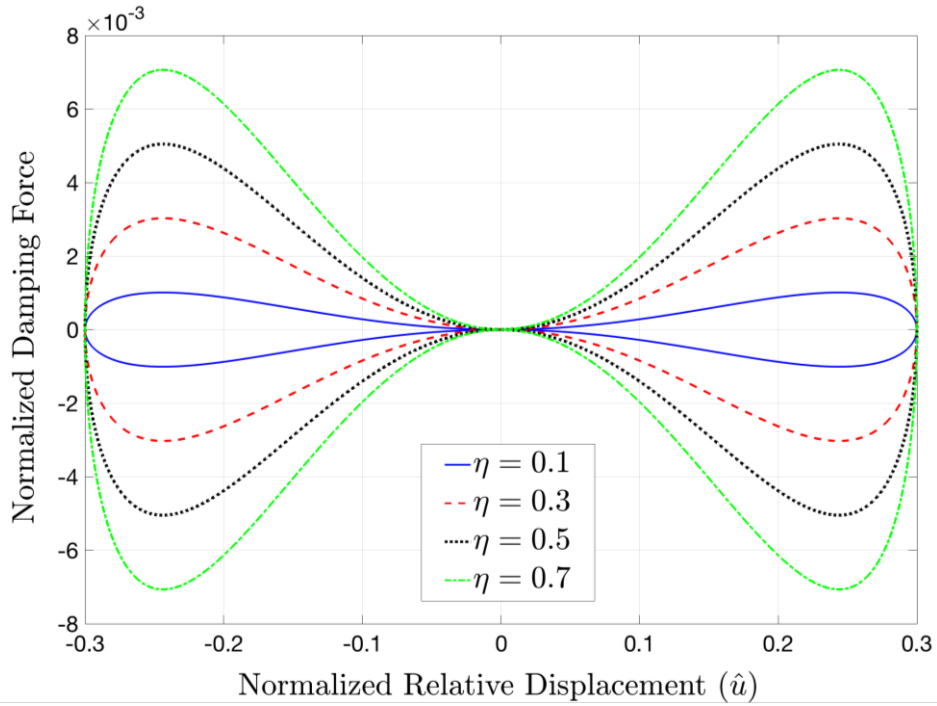


Figure 4-7 Effect of Loss Factor on Normalized Damping Force

4.3.3 Base Excitation and Approximate Analytical Solution

For a single mass the equation of motion can be written as

$$m\ddot{u} + k_v u + c_v \dot{u} + f_{ns} \sin \omega t + f_{nc} \cos \omega t = -m\ddot{z} + mg - k_v x_0. \quad (4-13)$$

where $x_0 = \sqrt{a^2 + L\omega^2}$.

By using a single harmonic Fourier series representation and the nonlinear stiffness and damping models, resultant nonlinear forcing can be written as follows

$$F_v = f_{ns} \sin(\psi) + f_{nc} \cos(\psi). \quad (4-14)$$

where $\psi = \omega t + \phi$. Fourier coefficient can be evaluated as

$$f_{ns} = \frac{1}{\pi} \int_0^{2\pi} \left(2(k_{stc}Y_0 + k_{dyn}Y_2 \cos 2\psi - h_h Y_2 \sin 2\psi) \frac{U \sin(\psi)}{\sqrt{a^2 + (U \sin(\psi))^2}} \right) \sin(\psi) d\psi, \quad (4-15)$$

$$f_{nc} = \frac{1}{\pi} \int_0^{2\pi} \left(2(k_{stc}Y_0 + k_{dyn}Y_2 \cos 2\psi - h_h Y_2 \sin 2\psi) \frac{U \sin(\psi)}{\sqrt{a^2 + (U \sin(\psi))^2}} \right) \cos(\psi) d\psi. \quad (4-16)$$

After evaluating the Fourier coefficients and assuming $mg = k_v x_0$, the nonlinear differential equation of motion can be transformed into set of nonlinear algebraic equations by utilizing single harmonic representation.

$$\begin{aligned} (k_v - m\omega^2)U \sin(\psi) \\ + c\omega U \cos(\psi) \\ + f_{ns} \sin(\psi) + f_{nc} \cos(\psi) = \omega^2 mZ \sin(\omega t). \end{aligned} \quad (4-17)$$

Balancing sine and cosine harmonics and introducing the phase,

$$\left(\frac{f_{ns}}{U} + k_v - m\omega^2 \right) U \cos(\phi) - (f_{nc} + c\omega U) \sin(\phi) = \omega^2 mZ, \quad (4-18)$$

$$\left(\frac{f_{ns}}{U} + k_v - m\omega^2 \right) U \sin(\phi) + (f_{nc} + c\omega U) \cos(\phi) = 0. \quad (4-19)$$

By using $\sin(\phi)^2 + \cos(\phi)^2 = 1$,

$$\left(\frac{f_{ns}}{U} + k_v - m\omega^2 \right)^2 U^2 + (f_{nc} + hU)^2 = \omega^4 m^2 Z^2. \quad (4-20)$$

To find ω from this 4th order polynomial,

$$a_4 \omega^4 + a_2 \omega^2 + a_1 \omega + a_0 = 0. \quad (4-21)$$

where $a_4 = (U^2 - Z^2)m^2$, $a_2 = U^2 c^2 - 2f_{ns}mU - 2k_v mU$, $a_1 = 2cUf_{nc}$, $a_0 = f_{nc}^2 + f_{ns}^2 + 2f_{ns}k_v + k_v^2$. Solution of quadric equation is given in Section 3.3.2.3.

4.4 Experimental Procedure

In dynamic characterization experiments, it was aimed to achieve a relationship between the vertical harmonic motion of the rigid mass and the dynamic properties of the rubber isolator such as stiffness and loss factor.

In order to conduct dynamic characterization of geometrically and physically nonlinear rubber isolator, a servo position controlled experiment setup was designed. In this experiment setup, preload and position is controlled dynamically. The horizontal displacement vector, $y(t)$, and the relative displacement vector $u(t)$ are shown in Figure 4-8. At the equilibrium point where horizontal springs are preloaded, horizontal displacement vector is equal to $a - L_o$ where L_o is the free length of the horizontal springs and a is the link length of the horizontal spring at equilibrium point.

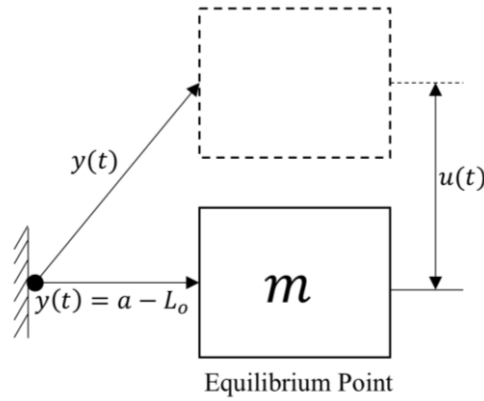


Figure 4-8 Horizontal Displacement Vector

An example of a displacement profile in time domain is shown in Figure 4-9. In Figure 4-9, the horizontal displacement vector is calculated for the case where $L_o = 0.5$, $a = 0.2$, $U = 0.5$. As expected, at the equilibrium point, horizontal displacement, $y(t)$ is equal to -0.3 , which is preload of the horizontal spring ($a - L_o$). For different relative displacement (U) amplitudes and frequencies, the displacement $y(t)$ is calculated by using Equation (4-22).

$$y(t) = \sqrt{u^2 + a^2} - L_o. \quad (4-22)$$

In the dynamic characterization experiments, horizontal displacement $y(t)$ is applied to a quad-lap shear rubber specimen and it is controlled by servo position control algorithm whose block diagram is shown in Figure 4-10. In other words, reference position signal defined in Figure 4-10 is equal to horizontal displacement $y(t)$.

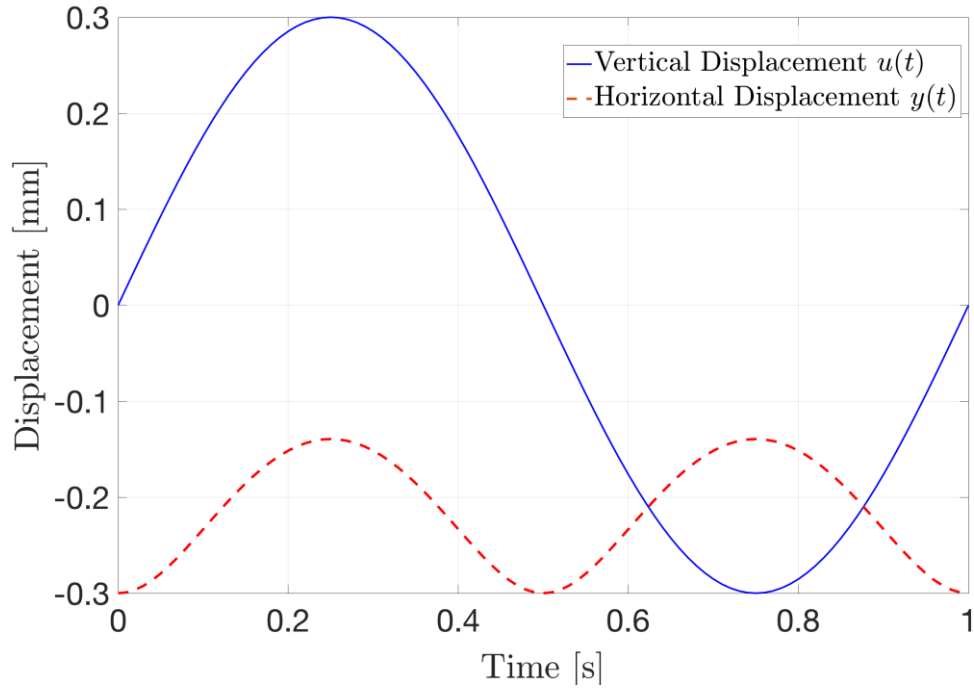


Figure 4-9 Displacement Profile in time domain, $L_o = 0.5$, $a = 0.2$, $U = 0.5$

The schematics of the servo position control loop and the experiment setup are shown in Figure 4-10 and Figure 4-11 respectively. As can be seen from Figure 4-10, there is a closed-loop control algorithm to control the displacement of the one end of the quad-lap isolator. The position feedback is supplied by motor encoder. The reference displacement $y(t)$, which is defined in Equation (4-22), is applied by servo position-controlled BLDC motor. The rotation of the BLDC motor is transformed to linear motion via ball screw mechanism (Figure 4-11). The displacement and force are measured by force transducer and laser displacement sensor synchronously.

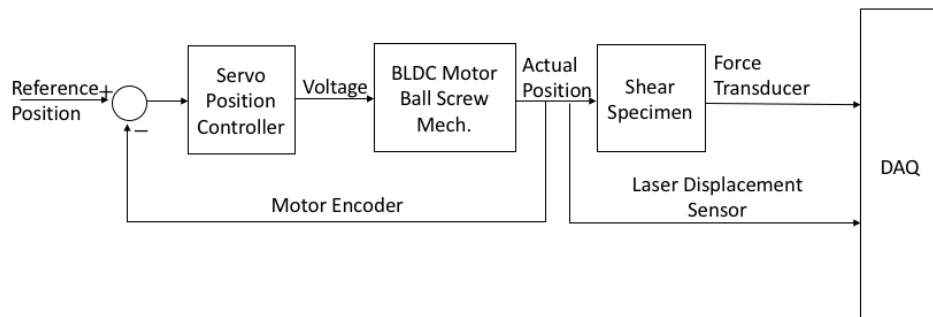


Figure 4-10 Experiment Setup Block Diagram

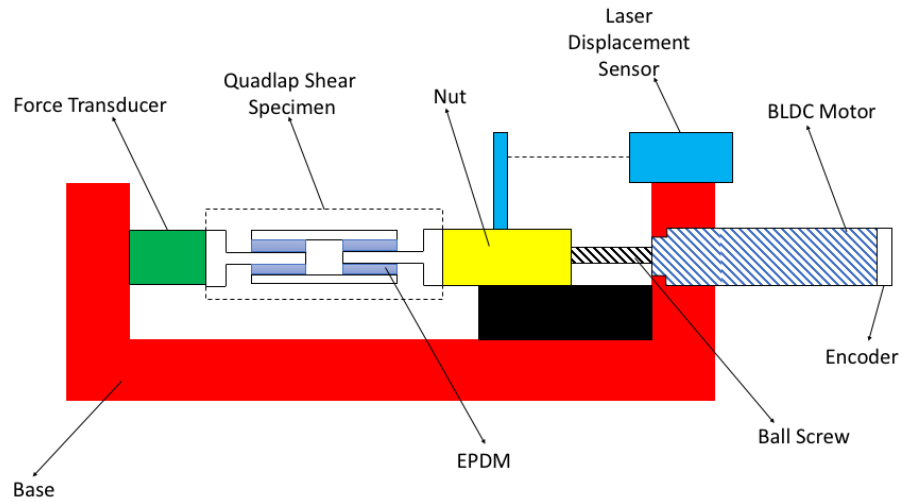


Figure 4-11 Experiment Setup Schematic

Prototype of the experimental setup can be seen in Figure 4-12. The control algorithm defined in Figure 4-10 runs at Servo Position Motor Driver. Target PC communicates with the Motor Driver via RS 485 serial communication protocol in order to feed reference position and acquire the force and displacement data.

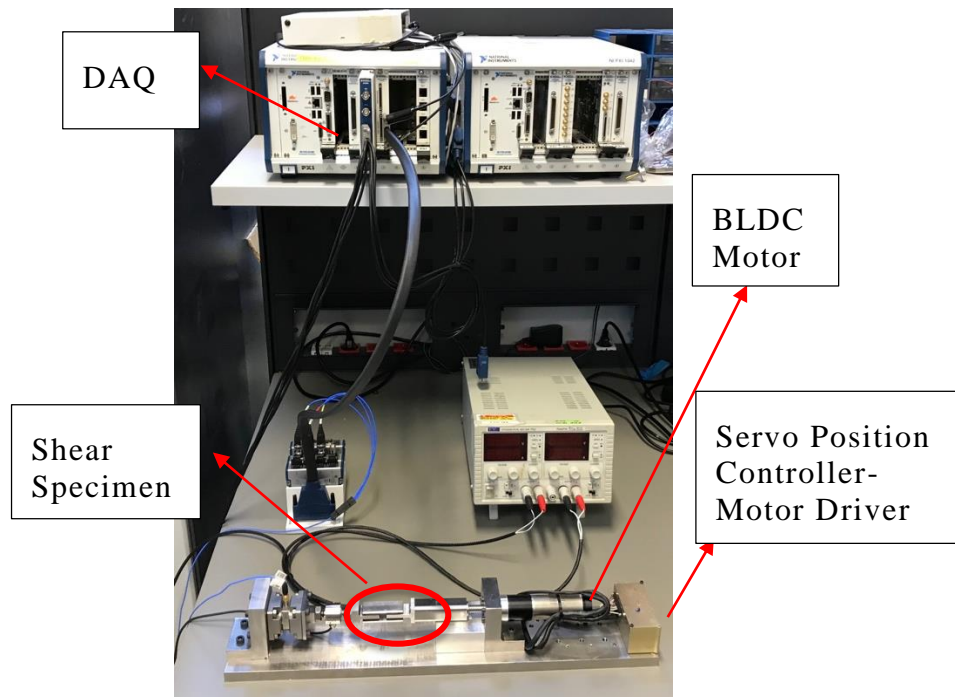


Figure 4-12 Experiment Setup

As a servo position controller, cascaded control strategy which is shown in Figure 4-13 is utilized. In the Figure 4-13, $\theta_{ref}, \dot{\theta}_{ref}, i_{ref}$ are the position, velocity and current references of the DC electric motor respectively. $\theta_{act}, \dot{\theta}_{act}, i_{act}$ defines the actual values of position, velocity and current. The controller of the outer loop, position control loop, is G_{C_p} . The inner loop is the velocity loop, and the controller is defined as G_{C_v} . The innermost loop is the current control loop and the controller is defined as G_{C_i} . V_m and G_m describes the voltage applied to electric motor and transfer function of the DC electric motor. The controller parameters are designed by considering the interested frequency range.

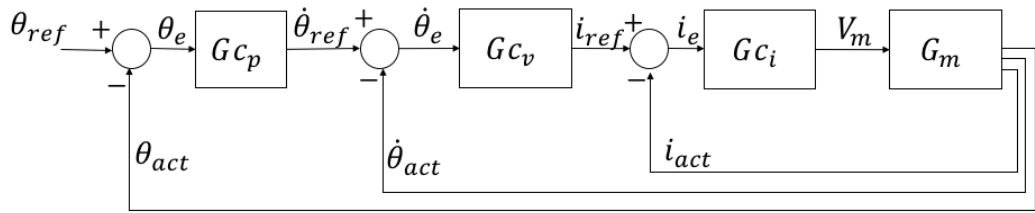


Figure 4-13 Servo Position Controller Block Diagram

The block diagram of DC motor mathematical model can be seen in Figure 4-14 where L is the inductance, R is the resistance, K_t is the torque constant, T_m is the torque at the output shaft of the motor, J is the total inertial load, K_b is the back EMF constant, T_d is the disturbance torque and C is the viscous damping coefficient.

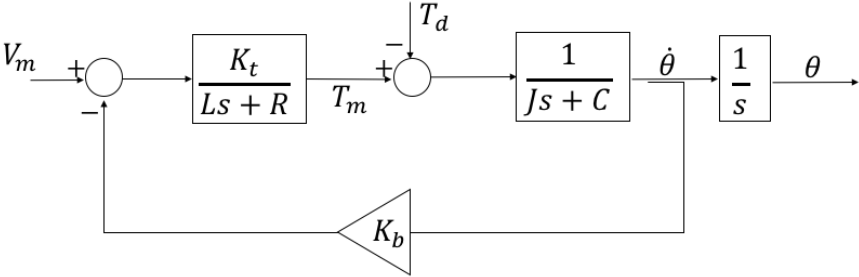


Figure 4-14 DC Motor Model

4.5 Dynamic Characterization of Elastomer

The basic dimensions of shear specimen can be seen in Figure 4-15. As an isolator, quad-lap shear configuration is preferred since it is symmetric in compression and tension directions.

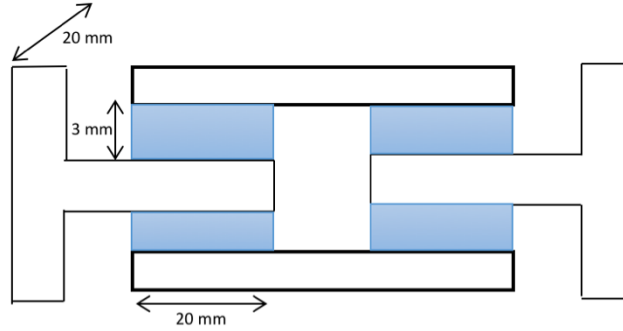


Figure 4-15 Rubber Specimen

For single harmonic oscillation of the rigid body, reference displacement is given as,

$$y(t) = \sqrt{(U \sin \omega t)^2 + a^2} - L_0, \quad (4-23)$$

where U is the relative displacement amplitude of the rigid mass, ω is the frequency of the single harmonic motion of the rigid mass, free length of the horizontal rubber isolator L_0 is equal to 50 mm and the length of the horizontal rubber isolator at equilibrium point a is taken as 47.50 mm considering the maximum allowable stress for shear specimen. The dynamic properties of the elastomer such as static-dynamic stiffness and loss factor are calculated by Equation(4-24) to (4-32) experimentally.

$$Y_o^{exp} = \frac{1}{2\pi} \int_0^{2\pi} y^{exp} d\psi, \quad (4-24)$$

$$Y_2^{exp} = \frac{1}{\pi} \int_0^{2\pi} y^{exp} \cos 2\psi d\psi, \quad (4-25)$$

$$F_o^{exp} = \frac{1}{2\pi} \int_0^{2\pi} F^{exp} d\psi, \quad (4-26)$$

$$F_{2c}^{exp} = \frac{1}{2\pi} \int_0^{2\pi} F^{exp} \cos 2\psi d\psi, \quad (4-27)$$

$$F_{2s}^{exp} = \frac{1}{2\pi} \int_0^{2\pi} F^{exp} \sin 2\psi d\psi, \quad (4-28)$$

$$k_{stc}^{exp} = \frac{F_o^{exp}}{Y_o^{exp}}, \quad (4-29)$$

$$k_{dyn}^{exp} = \frac{F_{2c}^{exp}}{Y_2^{exp}}, \quad (4-30)$$

$$h_h^{exp} = \frac{F_{2s}^{exp}}{Y_2^{exp}}, \quad (4-31)$$

$$\eta^{exp} = \frac{h_h^{exp}}{k_{dyn}^{exp}}, \quad (4-32)$$

where y^{exp}, F^{exp} are the time history of the experiment force data; Y_o^{exp} is the displacement due to the preload, $F_o^{exp}; Y_2^{exp}, F_{2c}^{exp}, F_{2s}^{exp}$ are the coefficients of the first harmonics of the displacement and force respectively; k_{stc}^{exp} is the ratio of the preload F_o^{exp} , and the bias term in the displacement Y_o^{exp} ; k_{dyn}^{exp} is the ratio of the first harmonic cosine term of the force F_{2c}^{exp} , to first harmonic term of the displacement Y_2^{exp} ; Structural damping coefficient is the ratio of the first harmonic sine term of the force F_{2s}^{exp} , to first harmonic term of the displacement Y_2^{exp} and loss factor η^{exp} is the ratio of structural damping coefficient, h_h^{exp} to dynamic stiffness, k_{dyn}^{exp} .

Dynamic stiffness characterization experiment results are shown in Figure 4-16 to Figure 4-18. The relative displacement level is increased gradually, and experiments are repeated for a frequency range 0.5 to 4 Hz. It should be noted that these frequencies are defined for $u(t) = U \sin \omega t$ while $y(t) = Y_o + Y_2 \cos 2\omega t$ as can be seen in Figure 4-9. From the Figure 4-16, it can be said that dynamic stiffness has logarithmic decrease with respect to relative displacement of single mass. Furthermore, increase in frequency results in increasing dynamic stiffness. Based on the experiment data, a logarithmic function whose parameters are defined in Equation (4-24) is fitted. The logarithmic function is saturated at 220 N/mm.

$$k_{dyn} = -67.39 \ln U + 321.93 \text{ N/mm}. \quad (4-33)$$

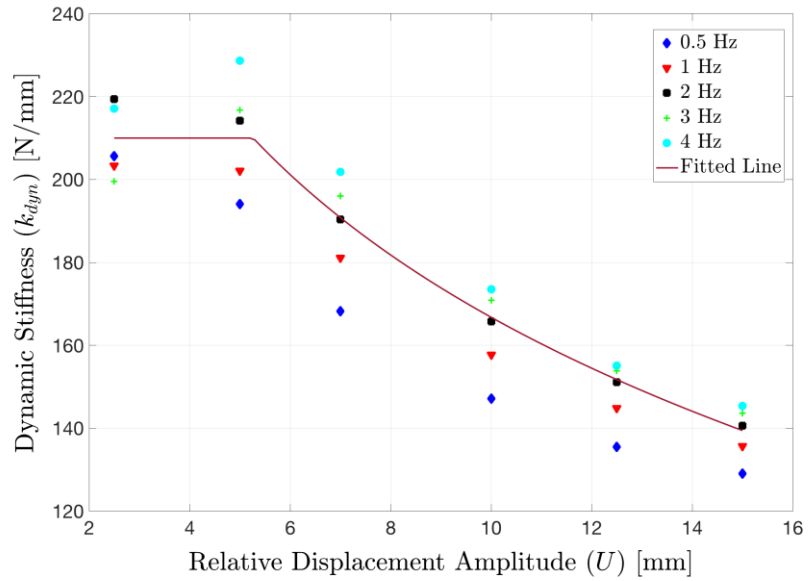


Figure 4-16 Effect of Relative Displacement Amplitude on Dynamic Stiffness

Static stiffness of the elastomer for different excitation levels and frequencies are shown in Figure 4-17. As can be seen in Figure 4-17, the static stiffness is almost constant. Therefore, it is taken following as

$$k_{stc} = 92 \text{ N/mm.} \quad (4-34)$$

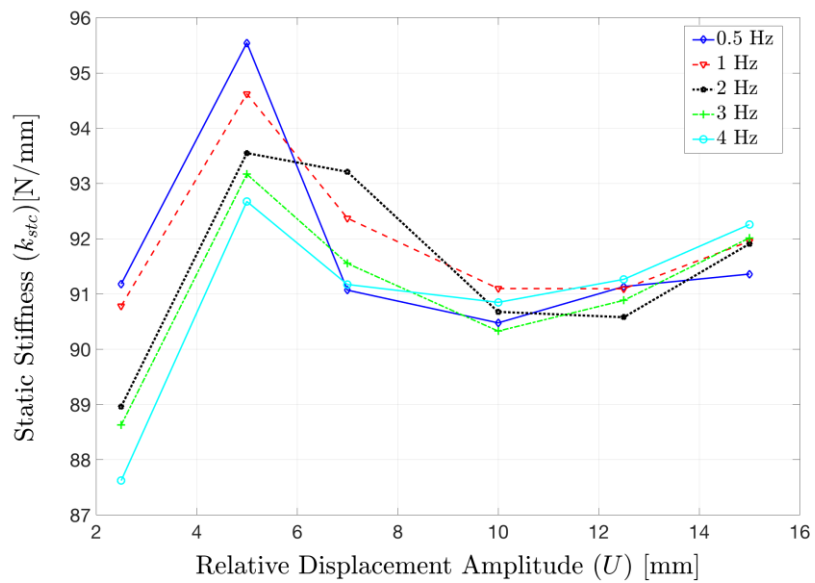


Figure 4-17 Effect of Relative Displacement Amplitude on Static Stiffness

To represent the relative displacement dependency, 4th order polynomial is placed as Equation (4-35). Referring the figures from Figure 4-18 to Figure 4-18, the frequency dependency can be neglected for the frequency range in which experiments are conducted.

$$\eta = -3.1 \cdot 10^{-5}U^4 + 0.0013U^3 - 0.021U^2 + 0.15U - 0.21. \quad (4-35)$$

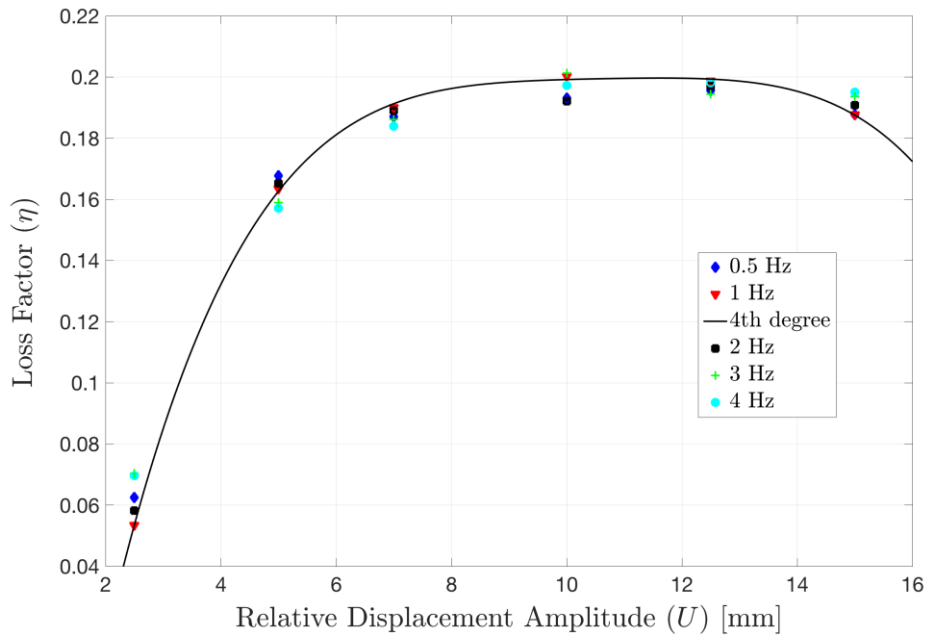


Figure 4-18 Effect of Relative Displacement Amplitude on Loss Factor

4.6 Isolation Performance

After obtaining elastomer dynamic properties such as k_{dyn} , k_{stc} , η experimentally isolation performance is investigated by analytical methods. The parameter set that is used in the dynamic analysis is given by Table 4-1.

Table 4-1 Parameter Set

$m = 7 \text{ kg}$	$k_v = 11.5 \text{ N/mm}$
$k_{stc} = 92 \text{ N/mm}$	$a = 47.5 \text{ mm}$
$L_o = 50 \text{ mm}$	$\xi_v = 0.01$
$k_{dyn} = -67.39 \ln U + 321.93 \text{ N/mm}$	$\omega_n = 6.45 \text{ Hz}$
$\eta = -3.1 \cdot 10^{-5}U^4 + 0.0013U^3 - 0.021U^2 + 0.15U - 0.21$	

The absolute transmissibility and relative displacement graphs for different base excitations can be seen in Figure 4-19 and Figure 4-20 respectively. The equation of motion of the linear isolation system is given by

$$m\ddot{u} + k_v u + c_v \dot{u} = -m\ddot{z}. \quad (4-36)$$

In Equation (4-37), it was assumed that vertical stiffness k_v is the softest spring that can be achieved by considering the static deflections. Then, nonlinear forcing terms obtained by Equation (4-15) and (4-16) are added and the results are compared. As can be seen from the Figure 4-19, the resonance frequency of the SDOF vibratory system is reduced to 0.4 of linear isolation system that has the lowest possible natural frequency. Moreover, as can be expected from Figure 4-5 and Figure 4-6, increase in base excitation results in increasing resonance frequency due to cubic like stiffness of the isolator.

Since the experiment is conducted for a relative displacement range, the analyses are performed in the same range as well. As can be seen from Figure 4-20, the maximum relative displacement amplitude is approximately 8 mm while experiments are performed up to 15 mm.

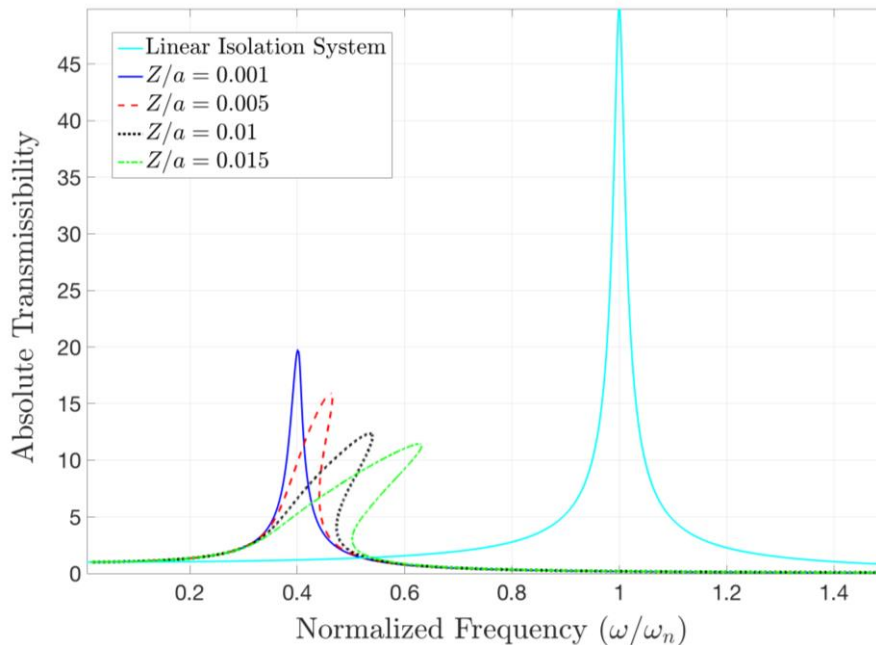


Figure 4-19 Absolute Transmissibility for Different Excitation Levels

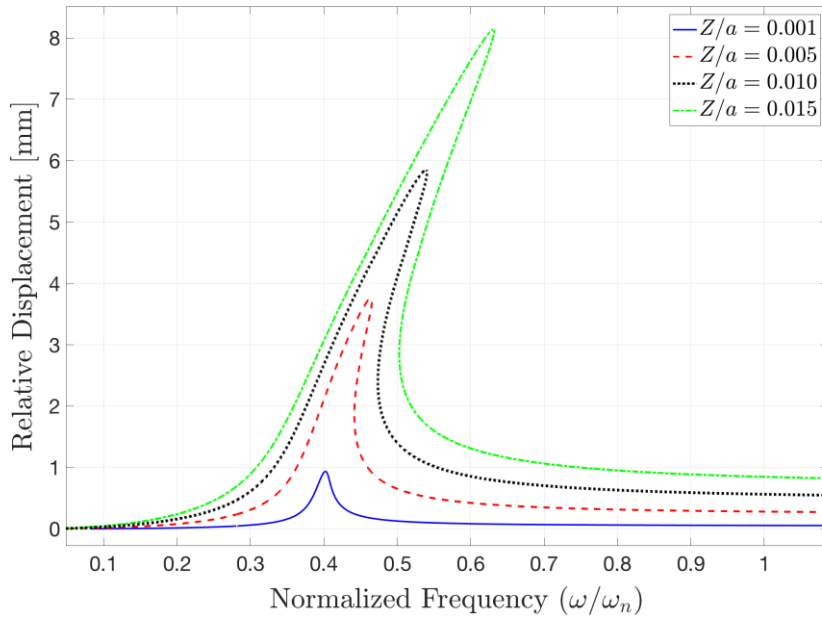


Figure 4-20 Relative Displacement Response for Different Excitation Levels

4.7 Performance Comparison of Proposed Isolator with QZS Isolator

In this section, the performance of geometrically nonlinear rubber isolator and QZS mechanism is compared. The quasi-zero-stiffness mechanism is shown in Figure 4-21 and this mechanism is studied in Section 3.1 in detail.

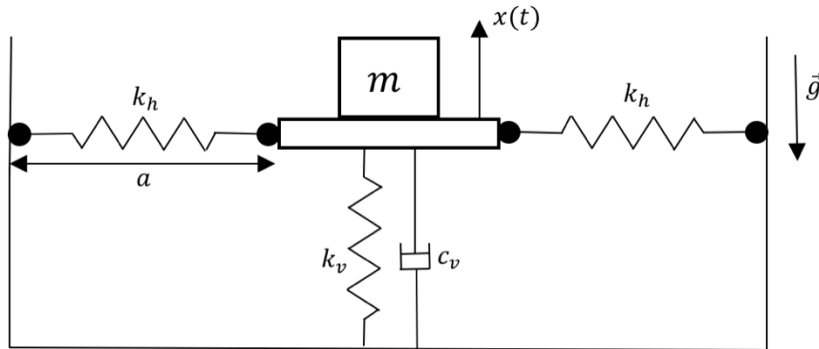


Figure 4-21 Quasi-Zero-Stiffness Isolator

To obtain quasi-zero-stiffness around the equilibrium point, Equation (4-37) should be satisfied.

$$\gamma = \frac{1}{\delta - 1} \quad (4-37)$$

Where $\gamma = 2k_h/k_v$ and $\delta = Lo/a$. To compare the performance of QZS mechanism consist of oblique spring and nonlinear elastomer isolator, Lo , a , ξ_v and k_v are taken as the values defined in Table 4-1. Horizontal stiffness is determined so that Equation (4-37) is satisfied. Then the peak absolute transmissibility and resonance frequencies are compared in Table 4-2 and Table 4-3. Normalized resonance frequency is defined as the ratio of the frequency, where the transmissibility has its peak value, to natural frequency of the linear isolation system.

Table 4-2 Peak Absolute Transmissibility Comparison

Excitation Level [Z/a]	Linear Isolation System	QZS Mechanism	Nonlinear Rubber Isolator
0.005	50	1	19.76
0.008	50	71.79	13.28
0.010	50	124.4	12.26
0.015	50	167.9	11.36

Table 4-3 Normalized Resonance Frequency Comparison

Excitation Level [Z/a]	Linear Isolation System	QZS Mechanism	Nonlinear Rubber Isolator
0.005	1	~0	0.402
0.008	1	1.436	0.506
0.010	1	2.487	0.539
0.015	1	3.358	0.631

As it can be seen from Table 4-2 and Table 4-3, nonlinear rubber isolator has enhanced isolation performance for wider excitation range with respect to Quasi-Zero-Stiffness Mechanism. The main reason is that nonlinear rubber isolator introduces damping around the resonance region where the relative displacement has its maximum value. Thus, it can be concluded that the drawback of the QZS isolator can be eliminated by utilizing geometrically nonlinear rubber isolator. As stated in the Section 3.2, geometrically nonlinear viscous damping provides the

same advantages. However, it might not be practical to design such a viscous damper physically by considering the cost, operational conditions and the size of the viscous damper.

4.8 Conclusion

In this chapter, dynamic model for geometrically nonlinear rubber isolator which provides high static low dynamic stiffness characteristic and nonlinear damping, is obtained. Unlike the previous studies, physical nonlinearities of the rubber material are also taken into account. It can be concluded that the dynamic stiffness and static stiffness are different for rubber materials, which changes the dynamics of the isolator considerably. These stiffnesses and damping properties are defined as the function of the relative displacement of the rigid mass. Furthermore, it is observed that physically more practical version of the geometrically nonlinear viscous damper defined in Section 3.2 can be obtained by means of rubber isolators. The performance of the isolator under different excitation levels is studied.

CHAPTER 5

DISCUSSION, CONCLUSION AND FUTURE WORK

5.1 Discussion on the Performance of Proposed Nonlinear Isolators

In this study, based on the goals that are defined in Section 3, four nonlinear isolators were proposed. Each of these four nonlinear isolators has different advantages and disadvantages which are explained in Chapters 3 and 4 based on the analytical performance investigation. These four nonlinear isolators are illustrated together in Figure 5-1.

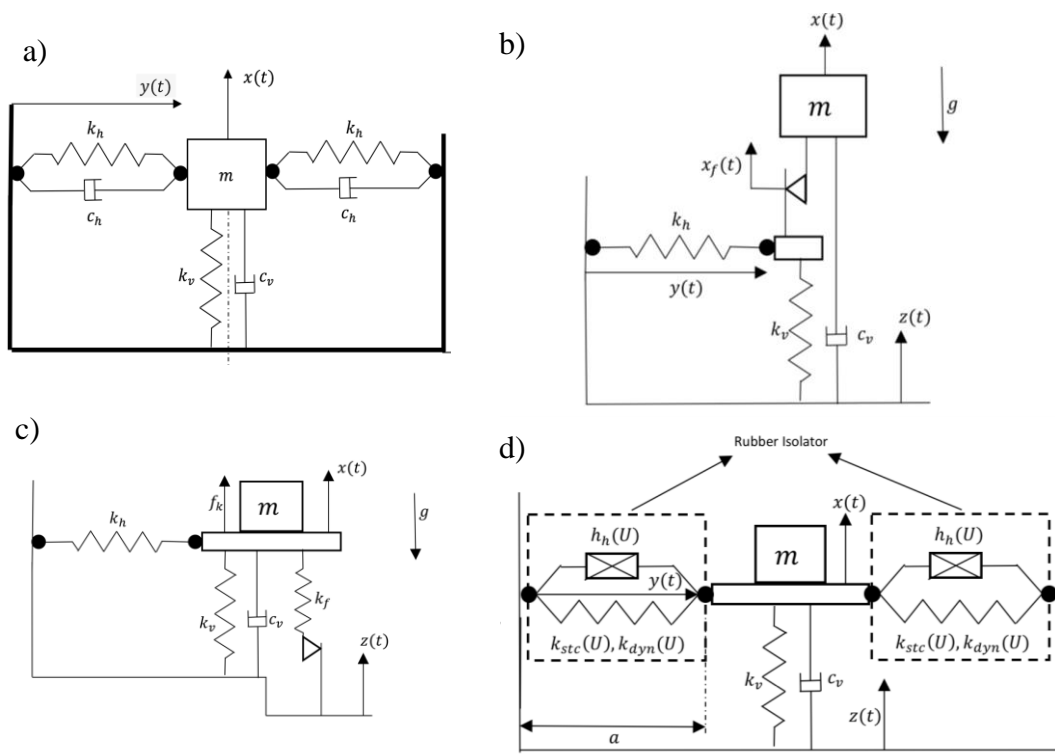


Figure 5-1 Proposed Isolators (a) Proposed Isolator-1, (b) Proposed Isolator-2,
(c) Proposed Isolator-3, (d) Proposed Isolator-4

Performance of them were investigated and presented in Chapters 3 and 4. In this chapter for the same excitation level, absolute transmissibilities of four nonlinear isolators were compared. As can be seen in Figure 5-2, Proposed Isolators 1 and 2 have the widest isolation region since their stiffness characteristic was adjusted so that around the equilibrium point stiffness is equal to zero. Although they might be preferable in other isolation applications, these isolators may not be useful for isolation of an IMU, since they do not provide measurement frequency range to the IMU. Furthermore, phase response starts to bend at very low frequencies which might be the measurement frequency range of the IMU.

Natural frequencies of the Proposed Isolator 3 and 4 were reduced to approximately 0.4 of the linear system containing vertical linear spring and viscous damper, in order to provide a measurement frequency range to IMU. Since Proposed Isolator-3 has dry friction element, nonlinear behavior was limited as can be seen in Figure 5-2. Due to the fact that damping elements are placed horizontally in Proposed Isolators 3 and 4, phase response starts to bend around the resonance region, which eliminates the drawback of the linear viscous damping.

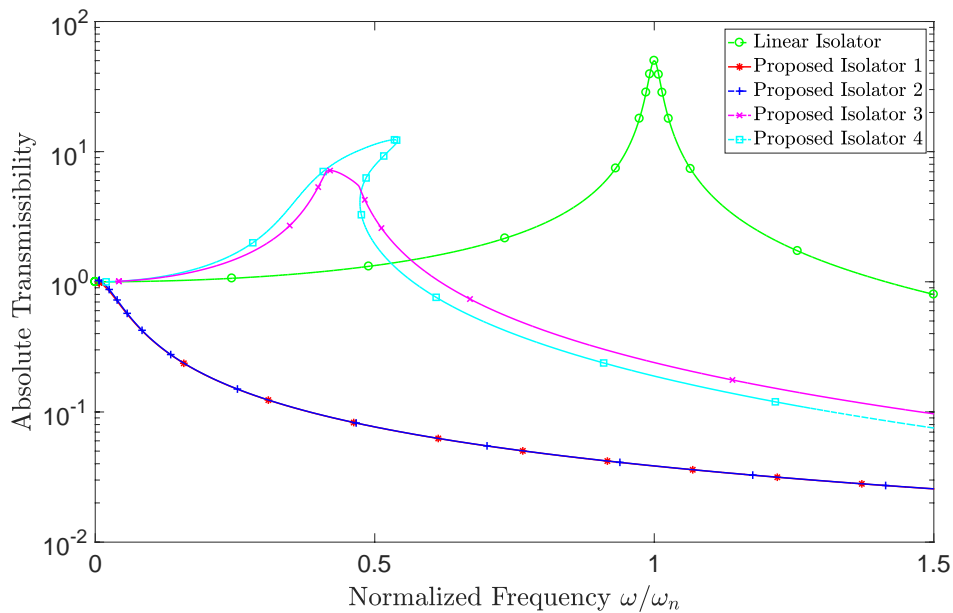


Figure 5-2 Absolute Transmissibility Comparison of the Proposed Isolators

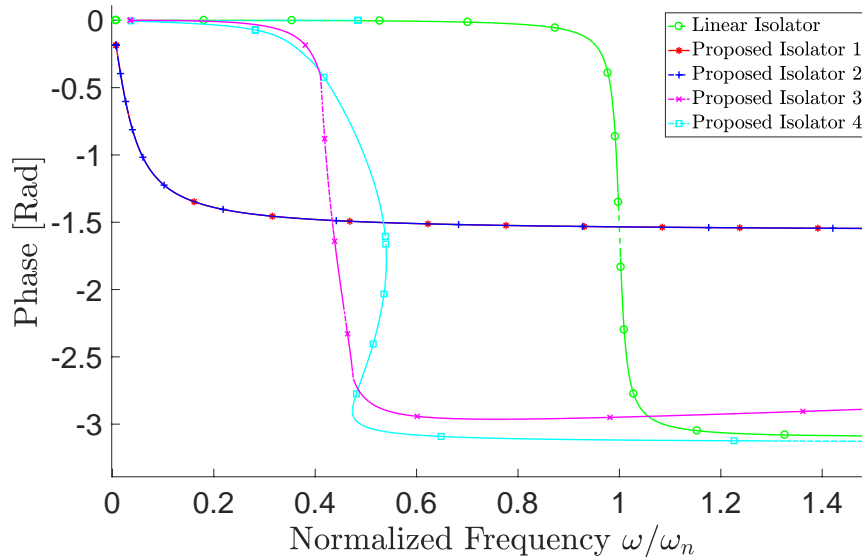


Figure 5-3 Phase Response of the Proposed Isolators

5.2 Conclusion

Passive isolation system can be designed and analyzed using the software and procedure developed in this study. Assuming that the dynamic behavior of vibration isolators is linear, required dynamic analyses can be achieved by Vibration Isolation Analysis Program VIASoft which utilizes six degrees of freedom mathematical model. User-friendly graphical user interface provides ease of analyzing 6 DOF vibration isolation system and reporting analysis results. The verification of the analysis software is conducted by shaker table experiments. The effect of dynamic strain amplitude on the dynamic properties of the rubber isolator are investigated. It is observed that as dynamic strain increases, stiffness of the viscoelastic isolator decreases and resonance frequencies shift towards lower frequencies.

The drawbacks and limitations of vibration isolation problem of inertial measurement unit with linear assumptions are discussed. Since IMUs measure the acceleration and the rotational rates, phase delays and the resonances in working frequency range should be also taken into account while designing isolation system of the IMU. Moreover, it should be noted that linear vibration isolation system has

limitations due to the fact that decreasing stiffness lowers natural frequency and increases the static deflections as well. Thus, there is a trade-off between the dead weight capacity and the natural frequency of the system, which determines the isolation region. Another important observation is that increasing linear viscous damping increases vibration transmissibility on the isolation region and it increases the phase delays at lower frequencies than the resonance frequency, which might be the working frequency range of the isolated inertial measurement unit. Therefore, although increasing damping in the system reduces the resonance amplitudes, it might cause phase delay issues.

Having these observations, it is aimed to enhance isolation performance by utilizing geometrically nonlinear isolators. Dynamic analysis of High-Static-Low-Dynamic-Stiffness mechanism is carried out. The nonlinear equation of motion is derived. By utilizing Singe Harmonic Balance Method, the nonlinear differential equation is converted into set of nonlinear algebraic equations and stability of the harmonic solutions is considered by Hill's Method. Moreover, excitation levels and viscous damping coefficient ranges, where Taylor Series expansion is valid, are determined. From the dynamic analyses, it is concluded that HSLDS mechanism reduces the natural frequency of the isolation system while providing the same dead load capacity thanks to its prestressed horizontal springs. However, this isolator response is highly nonlinear and thus the response is highly dependent on the excitation levels and the system parameters. The effect of stiffness and loading deviations on the system performance is also studied and it is observed that system performance is highly dependent on the static equilibrium point. Since these deviations introduce bias in the response, overall stiffness increases, and resonance frequencies and amplitudes increase. Therefore, combination of geometrically nonlinear stiffness mechanisms and geometrically nonlinear damping mechanisms is introduced.

Geometrically nonlinear damping mechanism which consists of oblique linear viscous dampers is studied. Due to geometry of the isolator, damping is only effective at the resonance region. Therefore, unlike the linear isolation systems, it does not affect the isolation region performance and it does not introduce phase

delay at lower frequencies while decreasing the resonance amplitudes. However, it may not be practically possible to have oblique viscous dampers considering the size of the viscous dampers. Therefore, combination of dry friction, which is another nonlinear damping element, and HSLDS mechanism is studied and improved results are obtained due to stick slip characteristic of the dry friction isolator. The validation of single harmonic solution assumption is conducted by time simulations. The isolation performance of the combination of nonlinear damping and nonlinear stiffness and performance of only nonlinear stiffness isolators are compared. It is observed that input dependency of the nonlinear isolators can be eliminated by integrating dry friction which is effective only at resonance regions.

Having observed the advantages of the geometrically nonlinear isolators, a mathematical model is derived for oblique pre-compressed rubber isolators since the rubber isolators are widely used in the industry as passive vibration isolator. Unlike the previous studies, this isolator has not only geometrical nonlinearities but also physical nonlinearity which is dynamic strain amplitude dependency of stiffness and loss factor of the rubber isolator. Furthermore, it is observed that the dynamic and static stiffnesses are different for the rubber isolators. After deriving a mathematical model which contains physical and geometrical nonlinearities, dynamic characterization of this isolator is conducted by experiments. A servo position control system is designed and multi harmonic displacements are applied to the quad-lap shear rubber specimen. Force and position are measured simultaneously. Damping and stiffness properties, which are function of vibration amplitude of the rigid mass, are derived. It is observed that dynamic stiffness of the elastomer specimen decreases logarithmically if dynamic strain amplitude increases. However, dynamic strain amplitude slightly affects the static stiffness of the rubber isolator, which might be neglected in the dynamic strain range applied during the experiments. Loss factor–dynamic strain relation is modeled as fourth order polynomial based on the experiment data. Isolation performance is investigated for the rubber isolator whose dynamic properties are obtained

experimentally. It is observed that combination of HSLDS mechanism and nonlinear damping can be achieved by rubber isolators which are the most common material for vibration isolators in the industry. The performance is compared with the QZS vibration isolation systems and it can be concluded that nonlinear rubber isolator has enhanced isolation performance due to its nonlinear damping characteristic.

5.3 Future Work

In the linear vibration analysis software, there were simplifications. Torsional stiffness and damping of the isolators were neglected. Moreover, only frequency dependency of the stiffness and loss factor of the isolators was considered. However, it is a well-known fact that the dynamic properties of the rubber isolators are dependent on the temperature and the dynamic strain amplitude. Therefore, in order to improve the vibration isolation analysis software, temperature and dynamic strain amplitude dependency of the isolators and torsional stiffnesses can be implemented to the software. Furthermore, the force and displacement curves of the rubber isolators are not symmetric based on the geometry of them. Thus, stiffness of the isolators is dependent on the payload, i.e. the static equilibrium point. Force and displacement curve of each isolator can be taken into account. Referring the shock analysis, only time simulations with viscous damper are available. Shock response spectrum analysis can be implemented to the analysis program and validation can be performed experimentally. Moreover, isolator dynamic properties can be added to the software by entering the material and dimensions. By utilizing a material library, dynamic properties can be calculated.

Referring the nonlinear isolators, the effect of system parameter deviations and static equilibrium point was only considered for HSLDS mechanism and geometrically nonlinear viscous damper. Dynamic analysis of dry friction isolators with bias term can be encountered. Furthermore, verification of the dynamic analysis of the nonlinear isolators having dry friction damper was conducted by time simulations. These analyses can be verified by experiments. Furthermore, in a

future study, these nonlinear isolators can be implemented to six-degree-of-freedom space and the performance in multi-degree-of-freedom model can be studied.

Finally, in this thesis, dynamic characterization of the nonlinear rubber isolator was studied and the response of the isolator under the multi-harmonic excitation was considered. In a future study, this isolator can be implemented to a single-degree-of-freedom system and the shaker experiments can be conducted to study the isolation performance of the isolators.

REFERENCES

- [1] D. J. Mead, *Passive Vibration Control*, John Wiley and Sons, 1999.
- [2] B. Tang and M. Brennan, "A Comparison of the Effects of Nonlinear Damping on the Free Vibration of a Single-Degree- of-Freedom System," *Journal of Vibration and Acoustics*, vol. 134, pp. 024501-1,5, 2012.
- [3] Ö. Ünlüsoy, *Reliability Analysis Process and Reliability Improvement of an Inertial Measurement Unit (IMU)*, Ankara: M.Sc. Thesis, Middle East Technical University, 2010.
- [4] C. Zaiss, *IMU Design for High Vibration Environments with Special Consideration for Vibration Rectification*, M.Sc. Thesis, University Of Calgary, 2012.
- [5] H. Naseri and M. Homaeinezhad, "Improving measurement quality of a MEMS-based gyro-free inertial navigation system," *Sensors and Actuators A: Physica*, vol. 207, pp. 10-19, 2014.
- [6] G. A. Aydemir and A. Saranlı, "Characterization and calibration of MEMS inertial sensors for state and parameter estimation applications," *Measurement*, vol. 45, no. 5, pp. 1210-225, 2012.
- [7] S. W. Yoon, *Vibration Isolation and Shock Protection for MEMS*, M.Sc. Thesis, The University of Michigan, 2009.
- [8] D. Çınarel, *Vibration Isolation of Inertial Measurement Unit*, M.Sc. Thesis, METU, 2012.
- [9] C. Harris and A. Piersol, *Shock and Vibration Handbook*, New York: McGraw-Hill, 2002.
- [10] C. Crede, *Vibration and Shock Isolation*, New York: Wiley, 1995.
- [11] J. Snowdon, "Vibration isolation use and characterization," *Journal of the*

Acoustical Society of America , vol. 66, pp. 1245-1279, 1979.

- [12] D. Çınarel and E. Ciğeroğlu, "Ataletsel Ölçüm Biriminin Titreşim Yalıtımı," in *SAVTEK 2012 6. Savunma Teknolojileri Kongresi*, Ankara.
- [13] B. Ravindra and A. K. Mallik, "Performance of non-linear vibration isolators under harmonic excitation," *Journal of Sound and Vibration*, vol. 170, pp. 325-337, 1994.
- [14] R. Dejong, G. Ermer, C. Paydenkar and T. Remtema, "High frequency dynamic properties of rubber isolation elements," in *Proceedings of Noise-Con '98*, 1998.
- [15] P. C. Painter, *Fundamentals of Polymer Science*, Taylor & Francis, 1998.
- [16] W. D. Callister, *Material Science Engineering*, John Wiley, 2011.
- [17] L.Meirovitch, *Fundamentals of Vibrations*, Mc Graw Hill, 2001.
- [18] O. Y. Baytemir, *Development of a Passive Vibration Isolation Analysis and Optimization Software for Mechanical Systems*, M.Sc. Thesis, METU, 2013.
- [19] O. Y. Baytemir, E. Ciğeroğlu and G. O. Özgen, "Hareketli Platforma Entegre Edilen Bir Mekanik Sistem İçin Optimum Pasif Titreşim İzolatörü Sayısının Belirlenmesi," in *SAVTEK 2012 6. Savunma Teknolojileri Kongresi*, ODTÜ, Ankara, 2012.
- [20] T. H. Vejsz, *Vibration Analysis of a Computer Hard Drive Subjected to a Random Vibration Input Using Integrated Solid Modeling and Simulation Software*, M.Sc. Thesis, Mechanical Engineering Department, California State University, 2002.
- [21] S. Chen, Q. Wei and J. Huang, "An Equivalent Model for Modal Analysis of Engine Mounting System," in *Proceedings of the 2nd International Conference on Electronic and Mechanical Engineering and Information Technology*, EMEIT 2012, 2012.
- [22] M. Zehsaz, M. Sadeghi, M. Etefagh and F. Shams, "Tractor Cabin's Passive Suspension Parameters Optimization," *Iran: Journal of Terramechanics*, 2011.

- [23] C. Silva, *Vibration Damping, Control and Design*, CRC Press, 2007.
- [24] F. Kerber, S. Hurlebaus and B. Beadle, "Control concepts for an active vibration isolation system," *Mechanical Systems and Signal Processing*, vol. 21, 2007.
- [25] D. H. Titterton and J. L. Weston, *Strapdown Inertial Navigation Technology*, The Institution of Electrical Engineers, 2004.
- [26] N. Barbour and N. Barbour, "Inertial MEMS Systems and Applications," RTO Lecture Series Supporting Papers, 2010.
- [27] G. Schmdt, "INS/GPS Technology Trends," "Low-Cost Navigation Sensors and Integration Technology," RTO Lecture Series Supporting Papers, 2010.
- [28] E. Rivin, *Passive Vibration Isolation*, New York: ASME Press, 2003.
- [29] A. D. Nashif, *Vibration Damping*, John Wiley&Sons, 1985.
- [30] D. Jones, *Handbook of Viscoelastic Vibration Damping*, John Wiley&Sons, 2001.
- [31] J. Zhang, *The Application of Maxwell Elements for Modeling, Identification and Analysis of Passive and Semi-Active Vibration Systems*, Department of Mechanical Engineering, University of Louisville,, 2006.
- [32] W. Flügge, *Viscoelasticity*, Second Revised Edition ed., 1975: Springer-Verlag, 1975.
- [33] T. Lin, N. Farag and J. Pan, "Evaluation of frequency dependent rubber mount stiffness and damping by impact test," *Applied Acoustics*, vol. 66, pp. 829-844, 2005.
- [34] P. Judson T. Bauman, *Fatigue, Stress, and Strain of Rubber Components*, Carl Hanser Verlag, 2008.
- [35] S. Kaul and A. K. Dhingra, "Engine mount optimisation for vibration isolation in motorcycles," *Vehicle System Dynamics*, vol. 47, no. 4, pp. 419-436, 2009.

- [36] Environmental Engineering Considerations and Laboratory Tests, Military Test method Standard-810 G, Department of Defense, 2008.
- [37] B. Tang, "On the shock performance of a nonlinear vibration isolator with high-static-low-dynamic-stiffness," *Journal of Mechanical Sciences*, 2014.
- [38] Diego Francisco Ledezma-Ramirez, "An experimental nonlinear low dynamic stiffness device for shock isolation," *Journal of Sound and Vibration*, vol. 347, pp. 1-13, 2015.
- [39] R. Ibrahim, "Recent Advances in Nonlinear Passive Vibration Isolators," *Journal of Sound and Vibration*, vol. 314, pp. 371-451, 2008.
- [40] A. Carrella, M. Brennan and T. Waters, "Static analysis of a passive vibration isolator with quasi-zero-stiffness characteristic," *Journal of Sound and Vibration*, vol. 301, pp. 678-689, 2007.
- [41] D. Platus, "Negative-stiffness-mechanism vibration isolation systems," *SPIE—Vibration Control in Microelectronics, Optics and Metrology*, pp. 44-54, 1991.
- [42] X. Huang, "Vibration isolation characteristics of a nonlinear isolator using Euler buckled beam as negative stiffness corrector: A theoretical and experimental study," *Journal of Sound and Vibration*, vol. 333, pp. 1132-1148, 2013.
- [43] J. Zhang, D. Li, M. J. Chen and S. Dong, "An ultra-low frequency parallel connection nonlinear isolator for precision instruments," *Key Engineering Materials*, pp. 231-238, 2004.
- [44] X. Huang, "Effects of stiffness and load imperfection on the isolation performance of a high- static-low-dynamic-stiffness non-linear isolator under base displacement excitation," *International Journal of Non-Linear Mechanics*, vol. 65, pp. 32-43, 2014.
- [45] A. Carrella, *Passive Vibration Isolators with High-Static-Low-Dynamic-Stiffness*, VDM Verlag Dr. Muller, 2010.
- [46] P. Alabuzhev and E. I. Riven, *Vibration Protecting and Measuring Systems with Quasi-Zero Stiffness*, Hemisphere, 1989.

- [47] W. Wu, "Analysis and experiment of a vibration isolator using a novel magnetic spring with negative stiffness," *Journal of Sound and Vibration*, vol. 333, pp. 2958-2970, 2013.
- [48] X. Liu, X. Huang and H. Hua, "On the characteristics of a quasi-zero stiffness isolator using Euler buckled beam as negative stiffness corrector," *Journal of Sound and Vibration*, vol. 332, no. 14, pp. 3359-3376, 2013.
- [49] I. Kovacic, M. Brennan and T. Waters, "A study of a nonlinear vibration isolator with a quasi-zero stiffness characteristic," *Journal of Sound and Vibration*, vol. 315, pp. 700-711, 2008.
- [50] T. Le and K. Ahn, "A vibration isolation system in low frequency excitation region using negative stiffness structure for vehicle seat," *Journal of Sound and Vibration*, vol. 330, pp. 6311-6335, 2011.
- [51] J. Zhou, X. Wang, D. Xu and S. Bishop, "Nonlinear dynamic characteristics of a quasi-zero stiffness vibration isolator with cam-roller-spring," *Journal of Sound and Vibration*, vol. 346, pp. 53-69, 2015.
- [52] X. X. L. a. H. H. Huang, "On the characteristics of an ultra-low frequency nonlinear isolator using sliding beam as negative stiffness," *Journal of Mechanical Science and Technology*, pp. 813-822, 2014.
- [53] A. Shaw, S. Neild and D. Wagg, "Dynamic analysis of high static low dynamic stiffness vibration isolation mounts," *Journal of Sound and Vibration*, pp. 1437-1455, 2013.
- [54] L. Meng, J. Sun and W. Wu, "Theoretical Design and Characteristics Analysis of a Quasi-Zero Stiffness Isolator Using a Disk Spring as Negative Stiffness Element," *Shock and Vibration*, pp. 1-19, 2015.
- [55] X. Sun, X. Jing and J. Xu, "Vibration isolation via a scissor-like structured platform," *Journal of Sound and Vibration*, pp. 2404-420, 2014.
- [56] X. Sun and X. Jing, "A nonlinear vibration isolator achieving high-static-low-dynamic stiffness and tunable anti-resonance frequency band," *Mechanical Systems and Signal Processing*, vol. 80, pp. 166-88, 2016.
- [57] X. Sun and X. Jing, "Multi-direction vibration isolation with quasi-zero stiffness by employing geometrical nonlinearity," *Mechanical Systems and*

Signal Processing, pp. 149-63, 2015.

- [58] Z. Lu, M. Brennan and T. Yang, "An investigation of a two-stage nonlinear vibration isolation system," *Journal of Sound and Vibration*, pp. 1456-464, 2013.
- [59] A. Carella and M. Brennan, "On the design of a high-static–low-dynamic stiffness isolator using linear mechanical springs and magnets," *Journal of Sound and Vibration*, vol. 315.3, pp. 712-20, 2008.
- [60] N. Zhou and K. Liu, "A tunable high-static–low-dynamic stiffness vibration isolator," *Journal of Sound and Vibration*, pp. 1251-273, 2010.
- [61] W. Robertson, M. Kidner and B. Cazzolato, "Theoretical design parameters for a quasi-zero stiffness magnetic spring for vibration isolation," *Journal of Sound and Vibration*, Vols. 326.1-2, pp. 88-103, 2009.
- [62] T. Zhu, B. Cazzolato and S. William, "Vibration isolation using six degree-of-freedom quasi-zero stiffness magnetic levitation," *Journal of Sound and Vibration*, vol. 358, pp. 48-73, 2015.
- [63] A. Carella, M. Brennan, T. Waters and J. V. Lopes, "Force and displacement transmissibility of a quasi-zero stiffness vibration isolator with high-static-low-dynamic-stiffness," *Int. J. Mech. Sci.*, vol. 55, pp. 22-29, 2012.
- [64] G. N. Jazar, R. Houim, A. Narimani and M. F. Golnaraghi, "Frequency Response and Jump Avoidance in a Nonlinear Passive Engine Mount," *J. Vib. Control*, pp. 1205-1237, 2006.
- [65] J. Xing and Q. Zi, "Frequency domain analysis of a dimensionless cubic nonlinear damping system subject to harmonic input," *Nonlinear Dynamics*, vol. 58, pp. 469-485, 2009.
- [66] X. Zhenlong and j. . Xing, "The transmissibility of vibration isolators with cubic nonlinear damping under both force and base excitations," *Journal of Sound and Vibration*, vol. 332, no. 5, pp. 1335-1354, 2013.
- [67] L. Qibao and Y. Zhiyuan, "Analysis of the effects of nonlinear viscous damping on vibration isolator," *Nonlinear Dynamics*, vol. 79, no. 4, pp. 2325-332, 2014.

- [68] Z. L. H. Laalej, "Application of nonlinear damping to vibration isolation: an experimental study," *Nonlinear Dynamics*, vol. 69, no. 1-2, pp. 409-421, 2011.
- [69] R. E. Mickens, "Analytical and Numerical Study of a Non-Standard Finite Difference Scheme for the Unplugged van der Pol Equation," *J. Sound Vib*, vol. 245, pp. 757-761, 2001.
- [70] B. T. M. J. Brennan, "A comparison of two nonlinear damping mechanisms in a vibration isolator," *Journal of Sound and Vibration*, vol. 332, no. 3, pp. 510-520, 2013.
- [71] C. Cheng, S. Li, Y. Wang and X. Jiang, "Force and displacement transmissibility of a quasi-zero stiffness vibration isolator with geometric nonlinear damping," *Nonlinear Dynamics*, vol. 87, no. 4, pp. 2267-2279, 2016.
- [72] E. Ciğeroğlu and H. N. Özgüven, "Nonlinear vibration analysis of bladed disks with dry friction dampers," *Journal of Sound and Vibration*, vol. 295, no. 3-5, pp. 1028-1043, 2006.
- [73] A. Srinivasan and D. Cutts, "Dry Friction Damping Mechanisms in Engine Blades," *Journal of Engineering for Power*, vol. 105, no. 2, p. 332, 1983.
- [74] K. Y. Şanlıtürk, M. İmregün and D. J. Ewins, "Harmonic balance vibration analysis of turbine blades with friction dampers," *Journal of Vibration and Acoustics*, vol. 119, pp. 96-103, 1997.
- [75] A. Ferri and E. Dowell, "Frequency domain solutions to multi-degree of freedom, dry friction damped systems," *Journal of Sound and Vibration*, vol. 124, no. 2, pp. 207-224, 1988.
- [76] H. Kashani, "Analytical parametric study of bi-linear hysteretic model of dry friction under harmonic, impulse and random excitations," *Nonlinear Dynamics*, vol. 89, no. 1, pp. 267-279, 2017.
- [77] E. Ciğeroğlu and N. Özgüven, "Nonlinear vibration analysis of bladed disks with dry friction dampers," *Journal of Sound and Vibration*, vol. 295, pp. 1028-1043, 2006.
- [78] J.-S. Bae, K. Moon and J. Daniel, "Vibration suppression of a cantilever beam using eddy current damper," *Journal of Sound and Vibration*, vol. 248, no. 3-5,

pp. 805-24, 2005.

- [79] H. A. Sodano and D. J. Inman, "Non-contact vibration control system employing an active eddy current damper," *Journal of Sound and Vibration*, vol. 305, no. 4-5, pp. 596-613, 2007.
- [80] H. A. Sodano, J.-S. Bae and D. J. Inman, "Modeling and Application of Eddy Current Damper for Suppression of Membrane Vibrations," *AIAA Journal*, vol. 44, no. 3, pp. 541-549, 2006.
- [81] H. A. Sodano, J.-S. Bae and D. J. Inman, "Improved Concept and Model of Eddy Current Damper," *Journal of Vibration and Acoustics*, vol. 128, no. 3, p. 294, 2006.
- [82] A. Dönmez, E. Ciğeroğlu and G. O. Özgen, "The Effect Of Stiffness And Loading Deviations In A Nonlinear Isolator Having Quasi Zero Stiffness And Geometrically Nonlinear Damping," in *Proceedings of the ASME 2017 International Mechanical Engineering Congress and Exposition*, Tampa, 2017.
- [83] O. Sert and E. Ciğeroğlu, "Adaptive Harmonic Balance Methods, A Comparison," in *Special Topics in Structural Dynamics Conference Proceedings of the Society for Experimental Mechanics Series*, 2016.
- [84] G. Orbay and H. N. Özgüven, "Non-linear Periodic Response Analysis of Mistuned Bladed Disk Assemblies in Modal Domain," in *Proceedings of 9th International Conference on Vibrations in Rotating Machinery*, 2008.
- [85] E. Ciğeroğlu and H. Samandari, "Nonlinear free vibration of double walled carbon nanotubes by using describing function method with multiple trial functions," *Physica E: Low-dimensional Systems and Nanostructures*, vol. 46, pp. 160-173, 2012.
- [86] M. & B. T. Hamdan, " On the Steady State Response and Stability of Non-Linear Oscillators Using Harmonic Balance," *Journal of Sound and Vibration*, vol. 166, no. 2, pp. 255-266, 1993.
- [87] G. V. & E. D. Groll, "The Harmonic Balance Method With Arc-Length Continuation In Rotor/stator Contact Problems," *Journal of Sound and Vibration*, vol. 241, no. 2, pp. 223-233, 2001.
- [88] L. Xie, S. Baguet and B. Prabel, "Bifurcation tracking by Harmonic Balance

Method for performance tuning of nonlinear dynamical systems," *Mechanical Systems and Signal Processing*, vol. 88, pp. 445-461, 2017.

[89] R. Goebel, R. Sanfalice and A. Teel, "Hybrid Dynamical Systems," *IEEE Control Systems Magazine*, vol. 29, no. 2, pp. 28-93, 2009.

[90] M. Friswell, "Vibration isolation using nonlinear springs," in *ISMA*, 2012.

[91] A. Valeev, R. Tashbulatov and Zotov, "Experimental Study Of Low Frequency Vibration Isolator With Quasi-Zero Stiffness," in *23. Internaional Congress on Sound & Vibration*, 2016.

[92] Q. C. Yang, J. Jing and M. D. Ai, "Study on the Application of Damping Control Method in Multi-Solution Interval of the QZS System," *Applied Mechanics and Materials*, pp. 457-458, 2013.